Light fermionic WIMP dark matter with light scalar mediator

Shigeki Matsumoto,[a] Yue-Lin Sming Tsai[b,c] and Po-Yan Tseng[a]

[a]*Kavli IPMU (WPI), UTIAS, University of Tokyo,*
Kashiwa, 277-8583, Japan

[b]*Institute of Physics, Academia Sinica,*
Nangang, Taipei 11529, Taiwan

[c]*Key Laboratory of Dark Matter and Space Astronomy,*
Purple Mountain Observatory, Chinese Academy of Sciences,
Nanjing 210008, China

E-mail: shigeki.matsumoto@ipmu.jp, smingtsai@gate.sinica.edu.tw,
poyen.tseng@ipmu.jp

ABSTRACT: A light fermionic weakly interacting massive particle (WIMP) dark matter is investigated by studying its minimal renormalizable model, where it requires a scalar mediator to have an interaction between the WIMP and standard model particles. We perform a comprehensive likelihood analysis of the model involving the latest but robust constraints and those will be obtained in the near future. In addition, we pay particular attention to properly take the kinematically equilibrium condition into account. It is shown that near-future experiments and observations such as low-mass direct dark matter detections, flavor experiments and CMB observations play important roles to test the model. Still, a wide parameter region will remain even if no WIMP and mediator signals are detected there. We also show that precise Higgs boson measurements at future lepton colliders will significantly test this remaining region.

Contents

1 Introduction

In past decades, people tried to develop particle physics based on the electroweak naturalness [1, 2], namely how the electroweak scale should be naturally explained. Many new physics scenarios such as supersymmetry, extra-dimension and composite Higgs have been proposed in this context, and those have been and still are being tested by various experiments including Large Hadron Collider (LHC). However, people recently start doubting this guiding principle, for new physics signals predicted by the scenarios have not been detected at all. In other words, though the electroweak scale should be naturally explained, it may be achieved by some other mechanisms (or ideas) which are totally different from what we have thought about so far. Particle physicists are seeking new mechanisms based on this consideration, but none of candidate models can successfully explain electroweak naturalness yet. Under this circumstance, one starts taking another strategy: developing particle physics by solving the dark matter problem. Once the nature of dark matter is clarified, it may launch out into the exploration of new physics beyond the standard model (SM).

The thermal dark matter, often called the weakly interacting massive particle (WIMP), is known to be one of influential dark matter candidates among others, for the dark matter abundance observed today is naturally explained by the so-called freeze-out mechanism [3, 4], which can also successfully explain the history of the Big Band Nucleosynthesis (BBN) and recombination in the early universe. Though the WIMP is in general predicted to be in the mass range between $\mathcal{O}(1)$ MeV [5, 6] and $\mathcal{O}(100)$ TeV [7–12], those with the mass around the electroweak scale have been intensively studied because of a possible connection to new physics models for the electroweak naturalness. However, present negative experimental results, not only from the LHC experiment but also from direct dark matter detection experiments, start eroding the parameter space of the WIMP with the electroweak mass. Thus, it motivates us to consider other WIMPs with a lighter ($\lesssim \mathcal{O}(10)$ GeV) or heavier ($\gtrsim \mathcal{O}(1)$ TeV) mass. We focus on the former case in this paper.

Light WIMP must be singlet under the SM gauge group, otherwise it would be discovered already. Concerning the spin of the WIMP, we take one-half, namely a light fermionic

WIMP in this paper.[1] In the minimal (renormalizable) model to describe such a light fermionic WIMP, a new additional particle called the mediator must be introduced to have an interaction between the WIMP and SM particles. In addition, such a mediator is required to be as light as the WIMP to explain the dark matter abundance observed today, to be singlet under the SM gauge group to avoid constraints from the current performed collider experiments, to be bosonic being consistent with the Lorentz symmetry, and to be even under the Z_2 symmetry in order to make the WIMP stable. Such a light fermionic dark matter with a light bosonic mediator recently receives many attentions, as it has a potential to have a large and velocity-dependent scattering cross section between WIMPs and solve the so-called small scale crisis of the universe [20–22]. Among two possibilities of the bosonic mediator, either a scalar or a vector [23–27], we take the scalar one in this paper.[2]

To investigate the present status and future prospects of a light fermionic WIMP with a light scalar mediator, we perform a comprehensive analysis of its minimal (renormalizable) model [13, 14, 30–40], where our likelihood involves all robust constraints obtained so far and those will be obtained in the near future (if no WIMP and mediator signals are detected) from particle physics experiments as well as cosmological and astrophysical observations. We carefully involve a kinematical equilibrium condition assuming that the freeze-out (chemical decoupling) of the WIMP occurs when it is in kinematically equilibrium with SM particles. We pay particular attention to a possible case that the light WIMP can be in the kinematical equilibrium via existent mediators at the freeze-out even if the WIMP does not have an interaction to SM particles with enough magnitude [41, 42]. We find that a very wide parameter region is surviving at present in the certain mass region of the WIMP. We also show quantitatively how near-future experiments and observations such as low-mass direct dark matter detections, flavor experiments and CMB observations play important roles, by comparing the results of analyses for the present status and future prospects of the model. Moreover, we see that a wide parameter region will still remain even if neither WIMP nor mediator signal is detected in the near future, and show that precise Higgs boson measurements at future lepton colliders will play a significant role to test the region. Such comprehensive analysis by the global scanning is a recent trend in WIMP studies [43–48].

The rest of the paper is organized as follow. In section 2, we show our setup, the minimal renormalizable model to describe a light fermionic WIMP with a scalar mediator. We will give all interactions predicted by the model and discuss physics of the mediator. All constraints that we have involved in our likelihood are discussed in section 3.[3] Results of our likelihood analysis are given and discussed in section 4, including several implications of the result to (near) future projects for the WIMP search. Section 5 is devoted to the

---

[1]Light scalar WIMP in its minimal model (Higgs-portal dark matter) is already excluded by the constraint from the invisible Higgs decay [13–17]. Light scalar WIMP still survives in next-to-minimal models [18, 19].

[2]A careful model-building is required to have a light fermionic WIMP with a light vector mediator [28], because such a WIMP has a s-wave annihilation and tends to be excluded by the cosmic microwave background (CMB) observation. Such a constraint can be avoided for the scalar mediator case [29], as seen in section 3.

[3]For readers who are not very much interested in the detail of the constraints and want to see the results of our analysis quickly, please skip this section (section 3) and go to the next section (section 4) directly.

summary of our discussion. There are several appendices at the end of this paper, where preselection criteria we have involved in our analysis (appendix A), the kinematical equilibrium condition (appendix B) and results of our analysis (appendix C) are shown in details.

2 The minimal model

2.1 Lagrangian

Two general properties of the WIMP field are considered before constructing a simplified model: the spin and weak-isospin(s) of the field(s).[4] Since we are interested in a light fermionic WIMP with its mass of $\mathcal{O}(1)\,\mathrm{GeV}$ or less, we focus on a Majorana WIMP, namely the simplest one among spin half WIMPs. On the other hand, the weak-isospin of the WIMP must be fixed to be zero, because a light WIMP carrying a non-zero weak-charge is excluded by collider experiments (LEP, etc.) performed so far. Such a singlet Majorana WIMP is well-motivated by e.g. a neutralino (Bino, Singlino, etc.) in supersymmetric models.

An additional new mediator has to be introduced, otherwise the WIMP cannot have any renormalizable interaction with SM particles due to SM gauge symmetry, Lorentz symmetry and Z_2 symmetry making the WIMP stable. The mediator is required to be as light as the WIMP to satisfy the relic abundance condition, as seen in following sections. If we consider a Z_2-odd mediator, it must be charged under the SM gauge interactions due to the SM gauge symmetry and such a light charged particle is also excluded by the collider experiments [50, 51]. Hence, the mediator must be even under the Z_2 symmetry. Moreover, the mediator is either a scalar or a vector boson, because it must have a renormalizable interaction with the WIMP (the WIMP-WIMP-mediator interaction). We consider the case of the scalar mediator in this paper, and leave the vector mediator case for future work.

We assume that the mediator is described by a real singlet from the viewpoint of minimality. Then, the Lagrangian involving all possible renormalizable interactions of the singlet Majorana WIMP χ, the mediator Φ and SM particles is given as follows [52]:

$$\mathcal{L} = \mathcal{L}_{\mathrm{SM}} + \frac{1}{2}\bar{\chi}(i\slashed{\partial} - m_\chi)\chi + \frac{1}{2}(\partial\Phi)^2 - \frac{c_s}{2}\Phi\bar{\chi}\chi - \frac{c_p}{2}\Phi\bar{\chi}i\gamma_5\chi - V(\Phi, H), \qquad (2.1)$$

with $\mathcal{L}_{\mathrm{SM}}$ and H being the SM Lagrangian and the SM Higgs doublet, respectively. In order to make the WIMP stable as mentioned above, a Z_2 symmetry is imposed, where χ is odd under the symmetry but other particles are charged even. The scalar potential of the model is composed of $V(\Phi, H) \equiv V_\Phi(\Phi) + V_{\Phi H}(\Phi, H)$ and $V_H(H)$, where $V_H(H)$ is the potential of the SM doublet H involved in $\mathcal{L}_{\mathrm{SM}}$. Its explicit form is written as follows:

$$V_H(H) = \mu_H^2 H^\dagger H + \frac{\lambda_H}{2}(H^\dagger H)^2,$$

$$V_\Phi(\Phi) = \mu_1^3 \Phi + \frac{\mu_\Phi^2}{2}\Phi^2 + \frac{\mu_3}{3!}\Phi^3 + \frac{\lambda_\Phi}{4!}\Phi^4,$$

$$V_{\Phi H}(\Phi, H) = A_{\Phi H}\Phi H^\dagger H + \frac{\lambda_{\Phi H}}{2}\Phi^2 H^\dagger H. \qquad (2.2)$$

---

[4]Several dark matter fields with a different weak-charge are introduced for the well-tempered WIMP [49].

Here λ_is are dimensionless coupling constants of quartic interactions, while others (μ_is and $A_{\Phi H}$) are mass dimension one coupling constants for cubic and quadratic interactions.

We take $v_H = (-2\mu_H^2/\lambda_H)^{1/2} \simeq 246\,\text{GeV}$ and v_Φ as vacuum expectation values of H and Φ. Taking the unitary gauge, the fields are expressed as $H = [0, (v_H + h')/\sqrt{2}]^T$ and $\Phi = v_\Phi + \phi'$, where v_Φ can be fixed to be zero without a loss of generality. Mass eigenstates of the scalars are then obtained by diagonalizing the quadratic terms of the potential,

$$\mathcal{L} \supset -\frac{1}{2}(h', \phi') \begin{pmatrix} m_{h'h'}^2 & m_{h'\phi'}^2 \\ m_{h'\phi'}^2 & m_{\phi'\phi'}^2 \end{pmatrix} \begin{pmatrix} h' \\ \phi' \end{pmatrix} = -\frac{1}{2}(h, \phi) \begin{pmatrix} m_h^2 & 0 \\ 0 & m_\phi^2 \end{pmatrix} \begin{pmatrix} h \\ \phi \end{pmatrix}, \qquad (2.3)$$

where $m_{h'h'}^2 = \lambda_H v_H^2$, $m_{h'\phi'}^2 = A_{\Phi H} v_H$ and $m_{\phi'\phi'}^2 = \mu_\Phi^2 + \lambda_{\Phi H} v_H^2/2$. The diagonalization matrix is described by the mixing angle θ, which controls the strength of interactions between ϕ and SM fermions or ϕ and SM gauge bosons. This angle is defined through the relation:

$$\begin{pmatrix} h \\ \phi \end{pmatrix} = \begin{pmatrix} \cos\theta & -\sin\theta \\ \sin\theta & \cos\theta \end{pmatrix} \begin{pmatrix} h' \\ \phi' \end{pmatrix}. \qquad (2.4)$$

Shown in following sections, the mixing angle $\sin\theta$ is severely constrained, and hence its absolute value is phenomenologically required to be much smaller than one, namely $|\theta| \ll 1$. As a result, the mass eigenstates and the mixing angle are expressed as

$$m_{h\,(\phi)}^2 = \frac{m_{h'h'}^2 + m_{\phi'\phi'}^2 \pm \sqrt{(m_{h'h'}^2 - m_{\phi'\phi'}^2)^2 + 4m_{h'\phi'}^4}}{2}, \qquad \tan 2\theta = -\frac{2m_{h'\phi'}^2}{(m_{h'h'}^2 - m_{\phi'\phi'}^2)}. \qquad (2.5)$$

Note that the solution of the second equation for the angle θ has a multi-fold ambiguity within the domain of definition, $-\pi \leq \theta \leq \pi$. However, we do not have to worry about this ambiguity because the angle is phenomenologically required to be suppressed as $|\theta| \ll 1$.

2.2 Interactions

Because of the mixing between the singlet Φ and the SM doublet H, the model predicts various interactions. First, interactions between the Higgs boson h and SM fermions & SM gauge bosons are suppressed slightly by $\cos\theta$ compared to the SM prediction. On the other hand, the mixing introduces interactions between the mediator ϕ and the SM particles, where ϕ behaves like a light Higgs boson with the couplings suppressed by $\sin\theta$ compared to the SM prediction. Both scalars have interactions with the WIMP as follows:

$$\mathcal{L}_{\text{int}} \supset -\frac{\cos\theta}{2}(c_s \phi \bar{\chi}\chi + c_p \phi \bar{\chi} i\gamma_5 \chi) + \frac{\sin\theta}{2}(c_s h \bar{\chi}\chi + c_p h \bar{\chi} i\gamma_5 \chi). \qquad (2.6)$$

Other interactions among SM fermions and SM gauge bosons in $\mathcal{L}_{\text{SM}}$ are not changed.

We next consider interactions among the scalars h and ϕ. From the scalar potential, four kinds of triple scalar interactions are obtained. Their explicit forms are given by

$$\mathcal{L} \supset -\frac{c_{hhh}}{3!}h^3 - \frac{c_{\phi hh}}{2}\phi h^2 - \frac{c_{\phi\phi h}}{2}\phi^2 h - \frac{c_{\phi\phi\phi}}{3!}\phi^3, \tag{2.7}$$

$$c_{hhh} = 3\lambda_H v_H c_\theta^3 - 3A_{\Phi H}c_\theta^2 s_\theta - \mu_3 s_\theta^3 + 3\lambda_{\Phi H}v_H s_\theta^2 c_\theta,$$

$$c_{\phi hh} = 3\lambda_H v_H c_\theta^2 s_\theta + A_{\Phi H}(c_\theta^3 - 2c_\theta s_\theta^2) + \mu_3 c_\theta s_\theta^2 + \lambda_{\Phi H}v_H(s_\theta^3 - 2c_\theta^2 s_\theta),$$

$$c_{\phi\phi h} = 3\lambda_H v_H c_\theta s_\theta^2 + A_{\Phi H}(2c_\theta^2 s_\theta - s_\theta^3) - \mu_3 c_\theta^2 s_\theta + \lambda_{\Phi H}v_H(c_\theta^3 - 2c_\theta s_\theta^2),$$

$$c_{\phi\phi\phi} = 3\lambda_H v_H s_\theta^3 + 3A_{\Phi H}c_\theta s_\theta^2 + \mu_3 c_\theta^3 + 3\lambda_{\Phi H}v_H c_\theta^2 s_\theta,$$

where we define $s_\theta \equiv \sin\theta$ and $c_\theta \equiv \cos\theta$, respectively. In addition to the cubic scalar interactions, the model predicts five quartic interactions from the scalar potential:

$$\mathcal{L} \supset -\frac{c_{hhhh}}{4!}h^4 - \frac{c_{\phi hhh}}{3!}\phi h^3 - \frac{c_{\phi\phi hh}}{4}\phi^2 h^2 - \frac{c_{\phi\phi\phi h}}{3!}\phi^3 h - \frac{c_{\phi\phi\phi\phi}}{4!}\phi^4, \tag{2.8}$$

$$c_{hhhh} = 3\lambda_H c_\theta^4 + 6\lambda_{\Phi H}c_\theta^2 s_\theta^2 + \lambda_\Phi s_\theta^4,$$

$$c_{\phi hhh} = 3\lambda_H c_\theta^3 s_\theta - 3\lambda_{\Phi H}(c_\theta^3 s_\theta - c_\theta s_\theta^3) - \lambda_\Phi c_\theta s_\theta^3,$$

$$c_{\phi\phi hh} = 3\lambda_H c_\theta^2 s_\theta^2 + \lambda_{\Phi H}(c_\theta^4 - 4c_\theta^2 s_\theta^2 + s_\theta^4) + \lambda_\Phi c_\theta^2 s_\theta^2,$$

$$c_{\phi\phi\phi h} = 3\lambda_H c_\theta s_\theta^3 + 3\lambda_{\Phi H}(c_\theta^3 s_\theta - c_\theta s_\theta^3) - \lambda_\Phi c_\theta^3 s_\theta,$$

$$c_{\phi\phi\phi\phi} = 3\lambda_H s_\theta^4 + 6\lambda_{\Phi H}c_\theta^2 s_\theta^2 + \lambda_\Phi c_\theta^4.$$

As seen from all interactions discussed in this subsection, when the mixing angle θ is very suppressed, the scalar h becomes almost the SM Higgs boson, and it couples to the WIMP weakly. On the other hand, ϕ couples to the WIMP without any suppression, while interacts with SM particles very weakly.[5] As a result, the WIMP χ and the mediator ϕ form a dark sector coupling to the SM sector weakly through the mixing between H and Φ. Hence, precision measurements of particle physics experiments are expected to play important roles to search for the dark sector particles, as we will see in following sections.

2.3 Model parameters

There are eight parameters in the scalar potential: μ_H^2, μ_1^3, μ_Φ^2, μ_3, λ_H λ_Φ, $\lambda_{\Phi H}$ and $A_{\Phi H}$. Since the two vacuum expectation values of the SM doublet H and the singlet Φ are fixed and the Higgs mass is determined to be $m_h \simeq 125\,\mathrm{GeV}$ thanks to the LHC experiment, the number of free parameters in the potential becomes five. Adding the WIMP mass m_χ as well as two couplings between the WIMP and the singlet Φ, namely c_s and c_p, the total number of free model parameters is then reduced to be eight in the end.

The condition of the two vacuum expectation values, $v_H \simeq 246\,\mathrm{GeV}$ and $v_\Phi = 0$, gives two relations among the model parameters, $\mu_H^2 + \lambda_H v_H^2/2 = 0$ and $\mu_1^3 + A_{\Phi H}v_H^2/2 = 0$, so that we can drop the two parameters μ_H^2 and μ_1^3 from the set of independent parameters.

---

[5]The mediator ϕ seems to have unsuppressed interactions with h through the couplings $A_{\phi H}$ and $\lambda_{\phi H}$ even if the mixing angle is very close to zero. The coupling $A_{\phi H}$ is, however, suppressed when the mixing angle is small, as can be deduced from eq. (2.5). On the other hand, the coupling $\lambda_{\Phi H}$ can be still large, though interactions between ϕ and SM fermions, which plays an important role in cosmology, are suppressed by small Yukawa couplings especially when the dark matter mass (hence, the freeze-out temperature) is small.

Moreover, as seen in eq. (2.3), the Higgs mass is determined mainly by the parameter λ_H when the mixing angle θ is suppressed, and hence it can also be dropped from the parameter set. On the other hand, when $\theta \ll 1$, the mediator mass m_ϕ is determined mainly by the combination of the two parameters μ_Φ^2 and $\lambda_{\Phi H}$, while the mixing angle is given mainly by the parameter $A_{\Phi H}$, as can be seen in eq. (2.3). Thus, we adopt m_ϕ and $\sin\theta$ as independent parameters instead of $\lambda_{\phi H}$ and $A_{\phi H}$. As a result, we have the following eight parameters, m_χ, c_s, c_p, m_ϕ, $\sin\theta$, μ_ϕ^2, μ_3 and λ_Φ, as free model input parameters.

2.4 Mediator decay

Because the decay of the mediator ϕ plays an important role in phenomenology of the model, we discuss some details of the decay in this subsection. As already mentioned in section 2.2, ϕ behaves like a light Higgs boson, and its decay into SM particles is from the mixing between H and Φ. Its partial decay width into a specific SM final state is

$$\Gamma(\phi \to \mathrm{SMs}) = \sin^2\theta \times \Gamma(h_{\mathrm{SM}} \to \mathrm{SMs})|_{m_{h_{\mathrm{SM}}}^2 \to m_\phi^2}. \tag{2.9}$$

We will discuss each decay mode below, and present how we estimate the decay width.

When the mediator is lighter than the electron-positron threshold, namely $m_\phi \leq 2m_e$, it decays mainly into two photons. We use the formula in ref. [53] to calculate its partial decay width. Above the threshold, though this channel is not a dominant one anymore, the same formula is still used up to $m_\phi = 0.6\,\mathrm{GeV}$. If $m_\phi \geq 2\,\mathrm{GeV}$, the decay width is computed by using the HDECAY code [54]. In the region of $0.6\,\mathrm{GeV} \leq m_\phi \leq 2\,\mathrm{GeV}$, the formula in ref. [55] is used to connect the regions $m_\phi \leq 0.6\,\mathrm{GeV}$ and $m_\phi \geq 2\,\mathrm{GeV}$ smoothly.

At the region of $2m_e \leq m_\phi \leq 2m_\mu$ with m_μ being the muon mass, it decays mainly into a electron and a positron. Its partial decay width is given by the following formula,

$$\Gamma(\phi \to e^+e^-) = \sin^2\theta \times \frac{m_e^2 m_\phi}{8\pi v_H^2} \left(1 - \frac{4m_e^2}{m_\phi^2}\right)^{3/2}. \tag{2.10}$$

When the mediator mass is above the muon threshold but below the pion threshold, namely $2m_\mu \leq m_\phi \leq 2m_\pi$, the mediator decays mainly into a muon pair. Its partial decay width is computed by the same formula as above with m_e being replaced by m_μ. The formulae for the two channels are used up to $m_\phi = 2\,\mathrm{GeV}$. In the mass region of $m_\phi \geq 2\,\mathrm{GeV}$, the HDECAY code is used to compute the partial decay widths of the two channels.

When ϕ is heavier than the pion threshold but lighter than a few GeV, it decays mainly into a pair of pions (and a pair of K mesons if $m_\phi \geq 2m_K$). Concerning the decay channel into $\pi\pi$, we use the result in ref. [56] to compute its partial decay width in the mass region of $2m_\pi \leq m_\phi \leq 1.4\,\mathrm{GeV}$, which is also consistent with the latest result in ref. [57]. On the other hand, the width becomes negligibly small compared to other channels when $m_\phi \geq 2\,\mathrm{GeV}$, so that we set $\Gamma(\phi \to \pi\pi) = 0$ in this region. The width is evaluated by a linear interpolation in the mass range of $1.4\,\mathrm{GeV} \leq m_\phi \leq 2\,\mathrm{GeV}$. On the other hand, the result in ref. [56] is used again to compute the partial decay width of the $\phi \to KK$ channel at $2m_K \leq m_\phi \leq 1.4\,\mathrm{GeV}$. Then, the width is evaluated using a linear interpolation at $1.4\,\mathrm{GeV} \leq m_\phi \leq 2\,\mathrm{GeV}$ by connecting the width to that of the $\phi \to s\bar{s}$ channel continuously, where

s is the strange quark. The partial decay width of the $\phi \to s\bar{s}$ channel is computed by the HDECAY code at $m_\phi \geq 2\,\mathrm{GeV}$.[6] Moreover, in order to take other hadronic decay channels into account, we also consider the $\phi \to gg$ channel with g being the gluon in the mass range of $m_\phi \geq 1.4\,\mathrm{GeV}$. When $m_\phi \geq 2\,\mathrm{GeV}$, we use the result in the HDECAY code to compute its partial decay width, while the width is evaluated at $1.4\,\mathrm{GeV} \leq m_\phi \leq 2\,\mathrm{GeV}$ by a linear interpolation with the boundary condition of $\Gamma(\phi \to gg) = 0$ at $m_\phi = 1.4\,\mathrm{GeV}$.

Other decay channels open in the mass range of $m_\phi \geq 2\,\mathrm{GeV}$ (e.g. decays into a tau lepton pair, a charm quark pair, a bottom quark pair, etc.). We consider all possible decay channels in this region and compute their partial decay widths using the HDECAY code.

Here, we consider the ϕ decay into $\pi\pi$ (KK) in more details, because it is known to have a large theoretical uncertainty in the range of $2m_\pi\,(2m_K) \leq m_\phi \leq 1.4\,\mathrm{GeV}$ [58] due to non-perturbative QCD effects. For instance, the total width of the SM Higgs boson in this mass range is predicted in other literature to be larger [59] or smaller [60] than what we have estimated based on ref. [56]. In order to make our analysis conservative, we introduce a nuisance parameter σ to take this uncertainty into account. Then, the partial decay widths of $\phi \to \pi\pi$ and $\phi \to KK$ channels are computed according to the equations

$$\Gamma(\phi \to \pi\pi) \equiv \frac{\Gamma_{\pi\pi}}{\Gamma_{\pi\pi} + \Gamma_{KK}} \left[\sigma\Gamma_+ + (1-\sigma)\Gamma_- \right],$$
$$\Gamma(\phi \to KK) \equiv \frac{\Gamma_{KK}}{\Gamma_{\pi\pi} + \Gamma_{KK}} \left[\sigma\Gamma_+ + (1-\sigma)\Gamma_- \right], \tag{2.11}$$

where $\Gamma_{\pi\pi}$ and Γ_{KK} are the partial decay widths into $\pi\pi$ and KK computed based on ref. [56]. On the other hand, Γ_+ and Γ_- are the sum of the widths computed based on ref. [59] and ref. [60], respectively. The nuisance parameter σ varies between $0 \leq \sigma \leq 1$.

In addition to the decay channels into various SM particles, the mediator particle ϕ can also decay into a pair of WIMPs when the mediator mass is larger than twice the WIMP mass, namely $m_\phi \geq 2m_\chi$. Its partial decay width is described by

$$\Gamma(\phi \to \chi\chi) = \cos^2\theta \frac{m_\phi}{16\pi} \left[c_s^2 \left(1 - \frac{4m_\chi^2}{m_\phi^2} \right)^{3/2} + c_p^2 \left(1 - \frac{4m_\chi^2}{m_\phi^2} \right)^{1/2} \right]. \tag{2.12}$$

All results obtained so far in this subsection are summarized in figure 1, where the total decay width of ϕ is shown in the left panel of the figure assuming that $\sin\theta = 1$ and ϕ does not decay into a pair of WIMPs. The gray band indicates the theoretical uncertainty due to non-perturbative QCD effects, which are taken into account by the nuisance parameter σ. In the right panel, the partial decay widths of several channels of ϕ are depicted.

2.5 Higgs decay

In this model, the partial decay width of the Higgs boson into SM particles is slightly modified from the SM prediction because of the mixing between H and Φ. Its partial

---

[6]In order to take the effect of the K meson threshold into account, we multiply the partial decay width of the $\phi \to s\bar{s}$ channel (computed in the HDECAY code) by the phase space factor of $(m_\phi^2 - 4m_K^2)^{3/2}/(m_\phi^2 - 4m_s^2)^{3/2}$. A similar prescription is also applied for the other channel $\phi \to c\bar{c}$ with c being the charm quark.
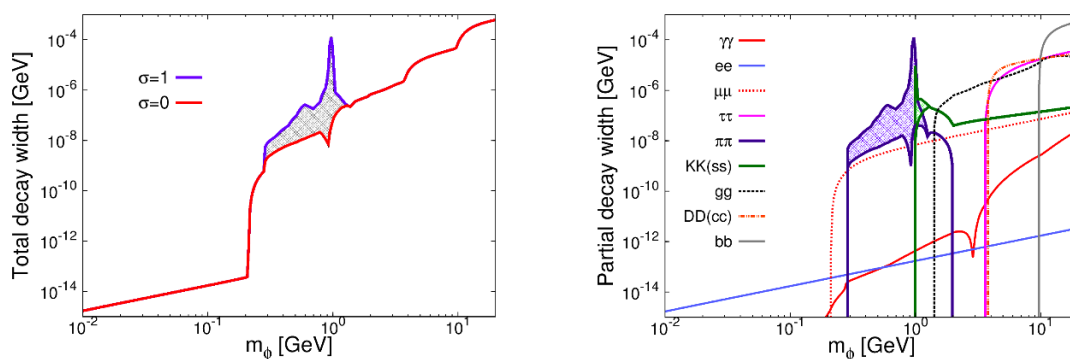
Figure 1. (Left panel) The total decay width of the mediator ϕ assuming that $\sin\theta = 1$ and ϕ does not decay into a WIMP pair. The gray band indicates the theoretical uncertainty due to non-perturbative QCD effects. (Right panel) Partial decay widths contributing to the total width.

decay width into a SM final state (a fermion or a gauge boson pair) is given by the following formula:

$$\Gamma(h \to \text{SMs}) = \cos^2\theta \times \Gamma(h_{\text{SM}} \to \text{SMs}), \tag{2.13}$$

where the Higgs mass is fixed to be $125\,\text{GeV}$. In addition to these channels, the Higgs boson decays into a pair of WIMPs, and its partial decay width is given by the same formula as the one shown in eq. (2.12) with $\cos\theta$ and m_ϕ replaced by $\sin\theta$ and m_h, respectively:

$$\Gamma(h \to \chi\chi) = \sin^2\theta \frac{m_h}{16\pi} \left[c_s^2 \left(1 - \frac{4m_\chi^2}{m_h^2} \right)^{3/2} + c_p^2 \left(1 - \frac{4m_\chi^2}{m_h^2} \right)^{1/2} \right]. \tag{2.14}$$

The Higgs boson can also decay into several mediators when the mediator ϕ is light enough. Considering the fact that the mixing angle θ is phenomenologically required to be much less than one and multi-ϕ channels are suppressed by their final state phase spaces, only the decay channel $h \to \phi\phi$ can be potentially comparable to the other decay channels into SM particles (and a WIMP pair). The explicit form of its partial decay width is

$$\Gamma(h \to \phi\phi) = \frac{c_{\phi\phi h}^2}{32\pi m_h} \left(1 - \frac{4m_\phi^2}{m_h^2} \right)^{1/2}, \tag{2.15}$$

where the coefficient $c_{\phi\phi h}$ is given in eq. (2.7). This decay channel gives distinctive signals at the LHC experiment, depending on the mass and the decay length of the mediator. For instance, when the mediator decays mainly into leptons and its decay length is enough shorter than $1\,\text{mm}$, this Higgs decay channel gives a signal of $h \to 4\ell$. On the other hand, if the decay length is much longer than the detector size, the channel gives a signal of the invisible h decay, regardless of the decay channel of the mediator. When the decay length is around the detector size, we can expect various signals at displaced vertex searches.

	Present	Future	Section
CMB distortion	Planck [61]	—	3.1.1
Higgcision	LHC [62]	—	3.1.2
Vacuum stability	See the text	—	3.1.3

Table 1. Preselection criteria that we have imposed in our analysis. The second and third columns are for present and near future experiments/observations used to apply the criteria. The last column is for the section where each criterion is discussed in detail. The third column is now blanked, as the preselection criteria are not stronger than other constraints we discuss in following subsections.

3 Constraints

We introduce all constraints used in our comprehensive analysis. The likelihood of the constraints will be modeled in various functions which will be further discussed in section 4.1. The usage and information of the constraints are discussed in the following in details.

3.1 Preselection criteria

Before performing the likelihood analysis, we apply preselection criteria on the model parameter space as one of our prior distribution. The following three criteria are imposed: CP conserving criterion, the criterion on the maximal value of the mixing angle, and the vacuum stability criterion. Those are implemented by a 1/0 logical cut in our analysis. All the preselection criteria involved in our analysis are summarized in table 1.

3.1.1 CP conserving criterion

The pseudo-scalar interaction between the WIMP χ and the singlet Φ in eq. (2.1) breaks the CP symmetry under the general scalar potential of $V(\Phi, H)$. Then, the existence of the non-zero pseudo-scalar coupling c_p induces the so-called s-wave WIMP annihilation into SM particles, namely the WIMP annihilates into SM particles without any velocity suppression at present universe. Moreover, when both the scalar and pseudo-scalar couplings, c_s and c_p, are non-zero, the WIMP annihilates into a pair of the mediators ϕ without the velocity suppression. In such cases, the WIMP annihilation cross section at present universe is almost the same as the one during the freeze-out process in the early universe, and this fact means that the cross section at present universe is expected to be about 1 pb.

WIMP annihilation cross section of $\mathcal{O}(1)$ pb at present universe is, however, not favored by the CMB observation, when the WIMP mass is less than $\mathcal{O}(1)$ GeV [61]. This is because the annihilation distorts the recombination history of the universe, while the observational result is consistent with the standard predication without the contribution from the WIMP. Thus, in order to avoid the CMB constraint, we set the pseudo-scalar coupling constant to be zero, namely $\boldsymbol{c_p = 0}$, in our analysis. In other words, we impose the CP symmetry on the interactions relevant to the WIMP. After switching off the coupling c_p, the WIMP annihilates into SM particles as well as a pair of the mediators with a velocity suppression at present universe, which enables us to avoid the CMB constraint easily.

3.1.2 Criterion on $|\theta|$

As already mentioned in previous section, the mixing angle θ is severely constrained by various experiments. In order to reduce a computational cost in our numerical analysis, we impose a condition on the angle as $|\theta| \leq \pi/6$, as a preselection criterion. This condition comes from the precision measurement of Higgs boson properties at the LHC experiment [62]. The measurement of the Higgs boson production process $gg \to h$ followed by its decay into a pair of gammas or W bosons gives a constraint on θ as $\cos\theta \geq 0.9$, which is translated into the constraint on the angle θ as above. On the other hand, much severe constraints are eventually obtained from other particle physics experiments and cosmological observations, and those are taken into account in the subsequent likelihood analysis.

3.1.3 Vacuum stability criterion

The minimal WIMP model in eq. (2.1) has an extended scalar sector composed of Φ and H. In order to guarantee the stability of our electroweak vacuum, we impose the following condition on the scalar potential. We first define the fields ξ and η as $\Phi = \eta$ and $H = (0, \xi/\sqrt{2})^T$, respectively, after taking the unitary gauge. Then, we impose a condition on the potential as $V(\eta, \xi) \geq V(v_\Phi, v_H)$ in the range of the fields $|\xi| \leq 1\,\mathrm{TeV}$ and $|\eta| \leq 1\,\mathrm{TeV}$. Philosophy behind the condition is as follows: we consider the minimal model as an effective theory of the WIMP defined at the energy scale of $1\,\mathrm{TeV}$, and require our electroweak vacuum to be absolutely stable within the range where the effective theory is applied. One might think that it is even possible to put a more conservative constraint on the potential by using the meta-stability condition, where our vacuum is required to be, at least, meta-stable with its lifetime much longer than the age of the universe. On the other hand, other constraints from particle physics experiments and cosmological observations give severer constraints on the potential, as we will see in the following subsections.[7] Hence, we adopt the absolute stable condition as a preselection criterion applied before the likelihood analysis.

3.1.4 Region of the parameters scanned

In addition to the preselection criteria mentioned above, we scan the parameter space (m_χ, c_s, m_ϕ, θ, μ_ϕ^2, μ_3 and λ_Φ) over the following ranges in our numerical analysis:

$$
\begin{aligned}
0 &\leq m_\chi \leq 30\,\mathrm{GeV}, \\
-1 &\leq c_s \leq 1, \\
0 &\leq m_\phi \leq 1\,\mathrm{TeV}, \\
-\pi/6 &\leq \theta \leq \pi/6, \\
-1\,\mathrm{TeV}^2 &\leq \mu_\Phi^2 \leq 1\,\mathrm{TeV}^2, \\
-1\,\mathrm{TeV} &\leq \mu_3 \leq 1\,\mathrm{TeV}, \\
-1 &\leq \lambda_\Phi \leq 1.
\end{aligned}
\tag{3.1}
$$

The dimensionless coupling constants c_s and λ_Φ vary between -1 to $+1$, assuming that UV completion behind the minimal WIMP model is described by a weak interacting theory.

---

[7]Radiative corrections to the potential are also not taken into account because of the same reason.

	Present	Future	Section
Relic abundance	Planck [63]	—	3.2.1
Equilibrium	See the text	—	3.2.2
Direct detection	XENON1T [64], CRESST [65],	NEWS-SNOLAB [66, 67],	3.2.3
	PANDAX [68], SuperCDMS [69],	SuperCDMS [70],	
	NEWS-G [71], Darkside-50 [72]	LZ [73, 74]	
DOF ($\Delta N_{\rm eff}$)	PLANCK [75]	CMB-S4 [76]	3.2.4
BBN	See the text	—	3.2.5

Table 2. Cosmological and astrophysical conditions/constraints imposed in our likelihood analysis. See the caption of table 1, for the meaning of all the columns are the same as those in the table.

On the other hand, dimensionful coupling constants basically vary within the energy scale of 1 TeV due to the validity of the minimal WIMP model. Upper limit on the WIMP mass m_χ is fixed to be 30 GeV, simply because we are interested in the light WIMP region.

The surviving parameter space after applying the three preselection criteria are shown in appendix A. Though the seven parameters in eq. (3.1) are used to put the preselection criteria,[8] two of them, μ_Φ^2 and λ_Φ, are not very much relevant to the result of our likelihood analysis. This is because the coupling constant of the quadratic term, μ_Φ^2, appears only in the mass matrix of eq. (2.3), but the mass matrix is already parameterized by two parameters, m_ϕ and θ.[9] The other parameter λ_Φ appears in scalar quartic interactions, however no significant constraints on the quartic interactions are obtained so far and even in the near future. As a result, we will present our results of the likelihood analysis in terms of the following five parameters $\boldsymbol{m_\chi}$, $\boldsymbol{c_s}$, $\boldsymbol{m_\phi}$, $\boldsymbol{\theta}$ and $\boldsymbol{\mu_3}$ in subsequent sections.

3.2 Conditions/constraints from cosmology and astrophysics

In this subsection, we summarize cosmological and astrophysical conditions/constraints used to figure out the present status and future prospects of the minimal WIMP model. Those are taken into account through the likelihood analysis, unless otherwise stated. All the conditions/constraints involved in our analysis are summarized in table 2.

3.2.1 Relic abundance condition

The WIMP should satisfy the so-called relic abundance condition. On observational side, the relic abundance of the WIMP, or in other words, the averaged mass density of the WIMP at present universe, is very precisely measured by the PLANCK collaboration [63]:

$$\Omega h^2 = 0.1193 \pm 0.0014, \tag{3.2}$$

with h being the normalized Hubble constant. The uncertainty of the observation is less than 2%, which is comparable to precise measurements at collider experiments.

---

[8]Five parameters (m_ϕ, θ, μ_ϕ^2, μ_3 and λ_ϕ) among seven parameters are relevant to the preselection criteria.
[9]Since μ_Φ^2 determines the value of the parameter $\lambda_{\Phi H}$ via eq. (2.3), it is scanned as a nuisance to be honest.

On theoretical side, we calculate the relic abundance using the `MicrOMEGAs` code [77] based on the minimal WIMP model. The code first calculates the (thermal-averaged) annihilation cross section of the WIMP, and next compute the abundance by solving the Boltzmann equation numerically. Concerning the cross section, when $m_\chi \geq m_\phi$, the WIMP annihilates mainly into a pair of the mediators, where the mediators eventually decay into SM particles. On the other hand, when $m_\chi \leq m_\phi$, the WIMP annihilates into SM particles through the exchange of the mediator (or the Higgs boson) in the s-channel. Because the process is suppressed by small Yukawa couplings and the mixing angle, only the resonant region with $m_\chi \sim m_\phi/2$ satisfies the relic abundance condition. Concerning the Boltzmann equation, it is known to have a theoretical uncertainty originating in the massless degrees of freedom of the universe during the freeze-out process. Since we are interested in the light WIMP scenario, the freeze-out temperature can be as low as the energy scale of the QCD phase transition, which makes the estimate of the massless degrees of freedom uncertain due to several non-perturbative QCD effects. Its uncertainty is reported to be at most 10% [78], and we adopt this maximum value to make our analysis conservative. Here, it is also worth mentioning that the mediator may contribute to the massless degrees of freedom and affect the Hubble expansion rate if it is light enough. However, we do not include this contribution in this analysis, because it is negligibly small compared to the above QCD uncertainty.

Note that it may have the Sommerfeld effect on the WIMP annihilation process [79–81], for the mediator is sometimes much lighter than the WIMP in our setup [82–86]. We found that the effect is not sizable for model parameter sets passing all conditions and constraints adopted in this paper. This is verified by computing the quantity, $c_s^2/(4\pi) \cdot (m_\chi/m_\phi)$, and confirmed that it is always enough smaller than one for the sets.[10] We therefore do not take the effect into account to calculate the WIMP annihilation cross section.

3.2.2 Kinematical equilibrium condition

We also impose the kinematical equilibrium condition on the model, where the WIMP and SM particles are required to be in thermal equilibrium during the freeze-out process. Though the condition is automatically satisfied for a typical WIMP with its mass of $\mathcal{O}(100)\,\text{GeV}$, it should be imposed independently for the light WIMP, because both WIMP and mediator connect to SM with small couplings, and the condition is not automatically satisfied. It is worth emphasizing that we adopt this condition to figure out a very conventional WIMP parameter region in our setup. On the other hand, the condition can be relaxed by requiring that the WIMP is in the equilibrium at some temperature of the universe before the freeze-out, because it still allows us to make a quantitative prediction on its abundance. We will discuss in appendix D how the result of our analysis alters by relaxing the condition.

The WIMP annihilates directly into SM particles when $m_\chi \leq m_\phi$. Its reaction rate at the freeze-out temperature T_f is estimated to be the product of the thermally averaged annihilation cross section (times the relative velocity) and the number density of the WIMP,

---

[10]This quantity is known to be the one for testing whether the Sommerfeld effect becomes sizable or not [80–82]. If it is smaller than one, the effect only gives a small correction to the thermally averaged cross section.

namely $\Gamma_{\chi\chi} \sim \langle \sigma_{\chi\chi} v \rangle_{T_f} n_{\text{WIMP}}(T_f)$. The reaction rate $\Gamma_{\chi\chi}$ becomes the same order as the expansion rate of the universe $H(T_f)$ due to the relic abundance condition. The existence of the annihilation process guarantees that of the scattering process between the WIMP and the SM particles because of the crossing symmetry, and its reaction rate is $\Gamma_{\chi\text{SM}} \sim \langle \sigma_{\chi\text{SM}} v \rangle_{T_f} n_{\text{SM}}(T_f)$ with $\sigma_{\chi\text{SM}}$ and $n_{\text{SM}}(T_f)$ being the scattering cross section and the number density of the SM particles, respectively. Since the number density of the SM particles is much larger than that of the WIMP at the freeze-out temperature, this fact gives $\Gamma_{\chi\text{SM}} \gg \Gamma_{\chi\chi} \sim H(T_f)$ unless the annihilation cross section is significantly boosted compared to the scattering cross section. Hence, the equilibrium condition is usually automatically satisfied as far as $m_\chi \leq m_\phi$.[11]

On the other hand, the WIMP annihilates mainly into two mediators when $m_\chi \geq m_\phi$, so that $\Gamma_{\chi\text{SM}} \geq H(T_f)$ is not always guaranteed. However, even if $\Gamma_{\chi\text{SM}} \leq H(T_f)$, the WIMP can be in the kinematical equilibrium with SM particles when the equilibrium is maintained between the WIMP and the mediator and between the mediator and the SM particles simultaneously. It means that, even if the reaction rate between the WIMP and SM particles is smaller than the expansion rate of the universe, the WIMP has a possibility to be in the kinematical equilibrium via the mediator in the universe. We thus take the following strategy to impose the kinematical equilibrium condition to the minimal WIMP model.

At each set of the input model parameters to define the model, we first calculate the freeze-out temperature T_f by the `MicrOMEGAs` code. We next calculate the reaction rate $\Gamma_{\chi\text{SM}}$ and compare it with the expansion rate of the universe $H(T_f)$. We accept the set if $\Gamma_{\chi\text{SM}} \geq H(T_f)$. If it is not, we further calculate two reaction rates between the WIMP and the mediator and between the mediator and SM particles. The former reaction rate is estimated to be $\Gamma_{\chi\phi} \sim \langle \sigma_{\chi\phi} v \rangle_{T_f} n_\phi(T_f)$ with $\sigma_{\chi\phi}$ and $n_\phi(T_f)$ being the scattering cross section and the number density of the mediator at the freeze-out temperature. The latter reaction rate has a more complicated form than the former one. In fact, three different processes contribute to the reaction rate; decay, scattering and absorption processes. The rate is estimated to be $\Gamma_{\phi\text{SM}} \sim \langle \Gamma_\phi \rangle_{T_f} + \langle \sigma_{\phi\text{SM}} v \rangle_{T_f} n_{\text{SM}}(T_f) + \langle \sigma'_{\phi\text{SM}} v \rangle_{T_f} n_\phi(T_f)$ with Γ_ϕ, $\sigma_{\phi\text{SM}}$ and $\sigma'_{\phi\text{SM}}$ being the total decay width, the scattering and absorption cross sections of ϕ, respectively. If both $\Gamma_{\chi\phi}$ and $\Gamma_{\phi\text{SM}}$ are larger than $H(T_f)$, we accept the set of the model parameters. Note that, unlike the relic abundance condition, the kinematical equilibrium condition that we have discussed above is implemented by a 1/0 logical cut in our likelihood analysis.

In figure 2, the reaction rates $\Gamma_{\chi\chi}$, $\Gamma_{\chi\text{SM}}$, $\Gamma_{\chi\phi}$ and $\Gamma_{\phi\text{SM}}$ as well as the expansion rate of the universe $H(T_f)$ are depicted as a function of the temperature of the universe in two cases; one is for the model parameter set that does not satisfy the kinematically equilibrium condition (left panel) and the other is for that satisfying the condition (right panel). The freeze-out temperature is shown as a vertical (orange) line in both panels. See also the figure caption for the model parameters used to calculate the reaction rates. As we can see from the comparison between the results in the two panels, the equilibrium condition gives

---

[11]When m_χ is very close to $m_\phi/2$ and the decay width of the mediator is very suppressed, $\langle \sigma_{\chi\chi} v \rangle_{T_f}$ is indeed significantly boosted, and it requires a special treatment to calculate the correct relic abundance [87].
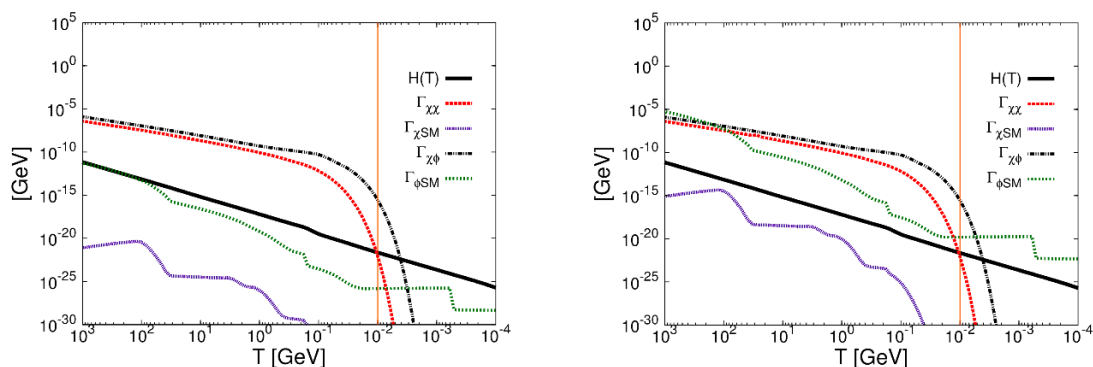
Figure 2. Reaction rates $\Gamma_{\chi\chi}$, $\Gamma_{\chi\mathrm{SM}}$, $\Gamma_{\chi\phi}$ and $\Gamma_{\phi\mathrm{SM}}$ as well as $H(T)$ as a function of the temperature of the universe. Model parameters are fixed to be $(m_\chi,\ c_s,\ m_\phi,\ \sin\theta,\ \mu_3) = (200\,\mathrm{MeV},\ 0.022,\ 100\,\mathrm{MeV},\ 10^{-6},\ 10\,\mathrm{MeV})$ in the left panel, showing that the equilibrium condition is not satisfied. On the other hand, those are fixed to be $(200\,\mathrm{MeV},\ 0.022,\ 100\,\mathrm{MeV},\ 10^{-3},\ 10\,\mathrm{MeV})$ in the right panel, satisfying the condition. The freeze-out temperature is shown as a vertical (orange) line in both panels.

the lower limit on the mixing angle $|\theta|$. In order to manifest how the equilibrium condition works for the minimal WIMP model, the parameter region survived after imposing the equilibrium condition as well as the preselection criteria and the relic abundance condition is presented in appendix B. All explicit forms of the reaction rates are also given there.

3.2.3 Constraint from direct dark matter detections

Direct dark matter detection is known to be a stringent constraint for the WIMP based on the scattering between the WIMP and a nucleon. In the minimal WIMP model, the scattering occurs through the exchange of the mediator or the Higgs boson in the t-channel, and it contributes to the spin-independent scattering [85]. In our analysis, the scattering cross section is computed by using `MicrOMEGAs` code, where its explicit form is given by

$$\sigma_{\mathrm{SI}} = c_s^2 \sin^2\theta \cos^2\theta \frac{m_\chi^2 m_N^4 f_N^2}{\pi v_H^2 (m_\chi + m_N)^2} \left(\frac{1}{m_\phi^2} - \frac{1}{m_h^2} \right)^2 . \tag{3.3}$$

Here, m_N is the mass of a nucleon and $f_N = f_{Tu} + f_{Td} + f_{Ts} + (2/9)f_{TG}$ with $f_{Tu} \simeq 0.0153$, $f_{Td} \simeq 0.0191$, $f_{Ts} \simeq 0.0447$ and $f_{TG} \simeq 0.921$, respectively. Since $m_\phi \ll m_h$ is required to satisfy the relic abundance condition, the scattering process through the exchange of the mediator, namely the first term in the parenthesis of eq. (3.3), dominates the cross section.

On experimental side, the most stringent constraint on the spin-independent scattering cross section is from XENON1T [64], PANDAX [68, 88], SuperCDMS [69], CRESST [65], Darkside-50 [72] and NEWS-G [71] experiments for the WIMP mass of our interest. On the other hand, in the near future, the constraint will be updated by LZ [73, 74], Super-CDMS/SNOLAB [70] and NEWS-SNOLAB [66][12] experiments, if no signal is detected. In particular, the NEWS experiment utilizes several gas detectors (e.g. Helium to Xenon)

---

[12]The limit is provided by the NEWS-G collaboration; see also ref. [67].

and will play an important role for the search with the mass less than a few GeV. For the present constraints (XENON1T, CRESST, and Darkside-50), we use the Poisson distribution likelihoods given by the `DDCalc` code [43]. On the other hand, we involve the future constraints (SuperCDMS(SNOLAB), LZ, and NEWS-SNOLAB) assuming a half-Gaussian [89] form with the central value being set to be zero to figure out the future prospects of the light WIMP.

3.2.4   Constraint from $N_{\rm eff}$ at $T_{\rm CMB}$

The mediator affects the expansion rate of the universe at the recombination era ($T_{\rm CMB} \simeq 4\,{\rm eV}$ [75]) when it is lighter than the neutrino decoupling temperature, namely $m_\phi \lesssim T_D \simeq \mathcal{O}(1)\,{\rm MeV}$ [90]. This is because neutrinos are already decoupled from the thermal bath composed of photons and electrons when the temperature of the universe is below T_D, while a part of the entropy of the universe is still being carried by the mediator at $T \sim T_D$ and it is eventually injected into the two systems (neutrino and photon+electron systems) asymmetrically before the recombination according to the interaction of the mediator.[13] In the minimal WIMP model, the mediator interacts only with electrons and photons when its mass is small enough, so that the entropy carried by the mediator goes into those particles. As a result, this injection contributes to the photon temperature of the universe, which makes the difference between the photon and neutrino temperatures larger, namely the expansion rate of the universe at the recombination era becomes smaller than usual.[14]

Such a contribution is severely constrained by the CMB observation, giving a lower limit on m_ϕ in order not to alter the effective number of relativistic degrees of freedom $N_{\rm eff}$ [75]. In the minimal WIMP model, the number $N_{\rm eff}$ at the recombination era is predicted as [91]

$$N_{\rm eff} \simeq 3 \left(1 + \frac{45}{11\pi^2} \frac{s_\phi(T_D)}{T_D^3}\right)^{-4/3}, \qquad s_\phi(T_D) \equiv h_\phi(T_D) \frac{2\pi^2}{45} T_D^3, \qquad (3.4)$$

where $h_\phi(T_D) = (15 x_\phi^4)/(4\pi^4) \int_1^\infty dy (4y^2 - 1)\sqrt{y^2 - 1}/(e^{x_\phi y} - 1)$ with $x_\phi \equiv m_\phi/T_D$ and T_D being $3\,{\rm MeV}$ [91]. Here, we have assumed that the mediator is never chemically and kinematically decoupled from the thermal bath, and it is indeed satisfied in most of the parameter region of the minimal WIMP model. This is because kinematical equilibrium is maintained among all species at the freeze-out temperature through the (inverse) decay process between the mediator and SM particles as well as the scattering process between the dark matter and the mediator, unless the mixing angle is vastly suppressed.[15] As a result, the mediator is in the equilibrium with SM particles below the freeze-out temperature.

---

[13]If the mediator is lighter than $T_{\rm CMB}$, it contributes directly to the expansion rate of the universe at the recombination era and this possibility is already excluded by the constraint on $N_{\rm eff}$ at the CMB observation.

[14]One may think that the WIMP also affects the expansion rate if it is light. The WIMP mass is, however, constrained to be more than $10\,{\rm MeV}$ due to the kinematical equilibrium condition and collider constraints as we will see later, so that the entropy carried by the WIMP is injected into the thermal bath at much above T_D.

[15]For instance, the mixing angle of $\mathcal{O}(10^{-5})$ is enough to maintain the kinematical equilibrium even if the mediator is lighter than $\mathcal{O}(100)\,{\rm MeV}$, and it is not excluded by collider constraints as seen in next section.

On the other hand, in other parameter regions, the mediator is chemically decoupled from (but still maintains the kinematical equilibrium with) the thermal bath before the freeze-out of the WIMP and/or kinematically decoupled from (and eventually recoupled with) the thermal bath after the freeze-out. In these cases, the mediator can contribute to $N_{\rm eff}$ more than that discussed in eq. (3.4) and receives a severer constraint from the observation. We, however, keep using the formula (3.4) as a conservative constraint obtained from the CMB observation, and leave those precise computations for a future study.

The effective number of relativistic degrees of freedom is observed to be $N_{\rm eff} = 2.99 \pm 0.17$ by the Planck collaboration [92]. The data could be improved by future observations, which resolves small angular scales (high multipole number ℓ) of CMB and allows a more precise measurement of $N_{\rm eff}$ by observing its damping tail at high-ℓ. According to their forecast, the measurement of $N_{\rm eff}$ can be improved by one order of magnitude at, for example, the CMB-S4 experiment [76], which leads to the expected limit of $\Delta N_{\rm eff} < 0.017$, if we do not see any deviation from the standard prediction. We involve these (expected) limits in our analysis for the present status and future prospects of the minimal WIMP model.

3.2.5 Constraint from BBN

If the mediator decays during or after the era of the Big Band Nuclear synthesis (BBN), it may spoil this successful scenario of generating light elements in the early universe. Hence, the mediator should be constrained so that it does not spoil the BBN scenario, which depends on its mass, lifetime, decay channels and abundance at the time that it is decaying.

For instance, if the mediator is heavier than $2m_\pi$ and mainly decays hadronically, it modifies the neutron-to-proton ratio and increases the primordial helium mass fraction, which gives a constraint on its lifetime as $\tau_\phi \lesssim \mathcal{O}(1)$ second [93]. On the other hand, the mediator also affects the BBN scenario even when its mass is in the range of $4\,{\rm MeV} \leq m_\phi \leq 2m_\pi$ and thus decays leptonically. This is because a few MeV-electrons pass their energies to CMB photons through the inverse Compton scattering and generate MeV gammas, which disintegrate ^{2}H and ^{7}Be (which eventually forms ^{7}Li). As a result, the leptonic decay produces less ^{7}Li and more ^{3}He/^{2}H than the usual case, leading to a constraint as $\tau_\phi \lesssim \mathcal{O}(10^5)$ seconds [93].[16] The mediator may affect the BBN scenario by other mechanisms if it is very light. For instance, when $m_\phi \lesssim T_{\rm BBN} \sim 0.1\,{\rm MeV}$, the mediator is relativistic during the BBN era and contributes to the expansion rate of the universe as an additional light degree of freedom. On the other hand, even when the mediator is in the mass range of $T_{\rm BBN} \lesssim m_\phi \lesssim T_D$, the mediator alters the expansion rate of the universe, because it changes the ratio between the photon and neutrino temperatures as discussed in section 3.2.4.

In order to impose the BBN constraint on the minimal WIMP model in a rigorous way, we have to consider the cosmology of the mediator at the late universe [94, 95][17] and implement all the decay channels of the mediator in an appropriate BBN code, which is beyond the scope of this paper. Instead, we impose the following two constraints, $\tau_\phi \leq 1$

---

[16]When the mediator is lighter than $4\,{\rm MeV}$, the energy of the electron produced by the mediator decay is not sufficient to photo-disintegrate nuclei, so that the constraint discussed here cannot be applied [94].

[17]In the references, $\sin\theta$ is assumed to be so small that the absorption and decay processes do not work to maintain the chemical equilibrium. Hence, constraints derived there cannot be directly applied to our case.

second when $m_\phi \geq 2m_\pi$ and $\tau_\phi \leq 10^5$ seconds when $4\,\text{MeV} \leq m_\phi \leq 2m_\pi$, by a simple 1/0 logical cut in the likelihood analysis, which is indeed a reference constraint adopted in many literature (see, e.g. ref. [52]).[18] We leave precise computations of the BBN constraints for a future study. On the other hand, we do not involve the BBN constraints concerning the expansion rate of the universe, for those in section 3.2.4, ΔN_{eff} had given severer constraint.

Let us briefly discuss how the BBN constraint works for the minimal WIMP model. The lifetime of the mediator is proportional to the mixing angle squared, and thus it gives the lower limit on the angle $\sin\theta$. As can be seen in figure 8 of appendix B.2, the result on the $(m_\phi, \sin\theta)$-plane, no lower limit on the mixing angle is obtained by imposing preselection criteria as well as relic abundance and kinematical equilibrium conditions, so that the BBN constraint plays an important role to make the allowed model parameter space finite.

3.2.6 Other constraints

It is also possible to impose further cosmological and astrophysical constraints on the minimal WIMP model in addition to those discussed above. One of such constraints is from the distortion of the CMB spectrum due to the late time decay of the mediator. When the lifetime of the mediator is longer than 10^6 seconds, where the double Compton scattering process ($\gamma\,e \to \gamma\,\gamma\,e$) is not active and the CMB cannot maintain the Planck distribution against an additional photon injection, the constraint on the so-called μ-distortion parameter put an upper limit on the lifetime [96]. When the lifetime is longer than 10^9 seconds, where the Compton process ($\gamma\,e \to \gamma\,e$) is also inactive and even the Bose-Einstein distribution cannot be maintained against the injection, the constraint on the y-distortion parameter put the upper limit on the lifetime [97]. These limits are, however, weaker than CMB and BBN constraints in section 3.2.4 and 3.2.5. Hence, we do not include the constraints from the distortion of the CMB spectrum due to the late time decay of the mediator in our analysis.

The other possible constraint can be obtained by the observation of neutrinos from the supernova (SN) 1987A [98]. Physics behind the constraint is as follows. The collapse at the SN heats up the core and its energy is estimated to be $\mathcal{O}(10^{59})\,\text{MeV}$, so that the cooling rate must be, at least, smaller than this value. The neutrino emission during a supernova explosion is known to be the only mechanism to cool down the core within the SM. On the other hand, the mediator can also contribute to the cooling in the minimal WIMP model. The dominant process is the nucleon scattering, $NN \to NN\phi$, followed by the ϕ decay into SM particles. It is then possible to put an upper limit on the mixing angle $\sin\theta$, such that the instantaneous luminosity in novel particles does not exceed the value $\mathcal{O}(10^{52})\,\text{erg/s}$. When $\sin\theta$ is too large, the parameter space is allowed because ϕ decays or is trapped inside the core and not contribute to the cooling. As a result, the SN physics has a potential to put a constraint on a certain region of m_ϕ and $\sin\theta$.

To include SN1987a cooling constraints into our analysis, it can be a highly non-trivial task because SN is a complicated physics system and the constraint from it suffers from several uncertainties [99–104]. For example, the nature of the core of protoneutron star to

---

[18]We would also like to thank Dr. Sebastian Wild for fruitful discussion for this BBN constraint [94].

the primary driver of the shock revival, the temperature, the density profiles, and equation of state of the progenitor star and the cross section of various QCD processes with soft radiations and environment effects to the process are known to give such uncertainties. Unfortunately, none of studies concerning the constraint is found to include all the uncertainties, and such a comprehensive study of the constraint is beyond the scope of our study. Hence, we did not include the constraint in our likelihood analysis, while we present the SN1987A exclusion contour on top of our result in the $(m_\phi, \sin\theta)$-plane in section 4.2.

Finally, we would like to comment on the cross section of the dark matter self-scattering process $(\chi\chi \to \chi\chi)$. Since the mediator ϕ in this model can be a thousand lighter than the dark matter and leads to an interesting enhancement of the dark matter self-scattering cross section. This enhancement becomes significant and velocity-dependent when the incident dark matter velocity is as small as 10^{-3} because of the diagram exchanging a light mediator in the t-channel. On the other hand, the velocity-dependence disappears when the velocity is larger than $\mathcal{O}(10^{-2})$ and the self-scattering cross section is approximately given as [83]

$$\sigma_T(\chi\chi \to \chi\chi) \simeq 5 \times 10^{-23} \left(\frac{c_s^2}{0.1}\right)^2 \left(\frac{m_\chi}{10\,\text{GeV}}\right)^2 \left(\frac{10\,\text{MeV}}{m_\phi}\right)^4 \text{cm}^2. \tag{3.5}$$

Phenomenologically, the velocity-dependent self-scattering at $v \sim \mathcal{O}(10^{-3})$ could provide a solution to the "small scale crisis" [105], namely the so-called core-cusp problem of dwarf galaxies can be solved by the self-scattering. On the other hand, a robust constraint on the self-scattering with $v \sim 10^{-2}$ is obtained from various clusters of galaxies (see, eg., ref. [106]). We have checked that all parameter points satisfying all conditions and constraints imposed in this paper are also consistent with the constraint on the self-scattering, and thus we do not include this self-scattering constraint in our likelihood analysis.

3.3 Constraints from collider experiments

In this subsection, we summarize collider constraints that we have considered for our likelihood analysis. Since the WIMP couples to SM particles mainly through the mediator while the mediator couples to several SM particles, the constraints on the minimal WIMP model are mostly from mediator productions at various colliders.[19] Collider signals then depend on how the mediator is produced and how it decays, depending on its mass m_ϕ and the mixing angle $\sin\theta$. We will discuss below the constraints based on the production processes. All the collider constraints that we have involved in our analysis are summarized in table 3.

3.3.1 Upsilon decay

Upsilons can produce the mediator through their decays. The most important decay channels are $\Upsilon(1S, 2S, 3S) \to \gamma\phi$ followed by the ϕ decay into a lepton pair such as $\mu^-\mu^+$ and $\tau^-\tau^+$. These upsilon decays allow us to detect the mediator through a narrow peak search in the di-lepton invariant mass spectrum at the mass region of $m_\phi < m_\Upsilon \simeq 10\,\text{GeV}$. These

---

[19]Only exception comes from the interaction between the WIMP and the Higgs boson. This interaction is constrained by observing the invisible decay width of the Higgs boson at colliders, as seen in section 3.3.4.

	Present	Future	Section
Υ decay	CLEO [107], BABAR [108, 109]	Belle II [21]	3.3.1
B decay	Belle [110, 111], LHCb [112–114],	Belle II [115, 116],	3.3.2
	BaBar [117–120]	LHCb [121]	
K decay	N48/2 [122], KTeV [123, 124], E949 [125],	NA62 [126, 127] ,	3.3.3
	CHARM [128, 129], KEK E391a [130]	SHiP [131], KOTO [132]	
H decay	LHC [133–136]	HL-LHC [137, 138]	3.3.4
Direct	LEP [139]	—	3.3.5

Table 3. Collider constraints that we have imposed in our analysis. See also the caption of table 1.

channels have been searched for by CLEO [107] and BaBar [108, 109] collaborations. Since no signal has been detected so far, they put an upper limit on the following quantity:

$$R_0 = \frac{\mathrm{Br}(\Upsilon \to \gamma\phi)\,\mathrm{Br}(\phi \to \ell\ell)}{\mathrm{Br}(\Upsilon \to \mu^-\mu^+)} = \sin^2\theta \frac{G_F m_b^2}{\sqrt{2}\pi\alpha} \left(1 - \frac{m_\phi^2}{m_\Upsilon^2}\right) \mathrm{Br}(\phi \to \ell\ell)\,\mathcal{F}_{\mathrm{QCD}}. \quad (3.6)$$

G_F, m_b and α are the Fermi constant, the bottom quark mass and the fine structure constant, respectively. The parameter $\mathcal{F}_{\mathrm{QCD}}$ takes a value between 0.5 to 1.5, originated from QCD bound state and relativistic corrections. The branching fraction of the decay channel $\Upsilon \to \mu^-\mu^+$ have been measured precisely [140]. Then, an upper limit on $\mathrm{Br}(\Upsilon \to \gamma\phi) \times \mathrm{Br}(\phi \to \ell\ell)$ is obtained at 90% confidence level, depending on the mediator mass m_ϕ [107–109]. For instance, an upper limit on $\mathrm{Br}(\Upsilon \to \gamma\phi) \times \mathrm{Br}(\phi \to \mu^-\mu^+) \lesssim 3 \times 10^{-6}$ is obtained in the mass region of $m_\phi \lesssim 3.5\,\mathrm{GeV}$, while $\mathrm{Br}(\Upsilon \to \gamma\phi) \times \mathrm{Br}(\phi \to \tau^-\tau^+) \lesssim 3 \times 10^{-5}$ is obtained for $4\,\mathrm{GeV} \lesssim m_\phi \lesssim 8.5\,\mathrm{GeV}$. The limit becomes weaker when m_ϕ approaches to m_Υ.

The mediator is assumed to promptly decay into a lepton pair in the above analysis. One might suspect that this method does not work because the mixing angle may become so small that the mediator is too long-lived. However, the method indeed works well but its reason is a bit complicated. We take the mediator mass to be $m_\phi = 220\,\mathrm{MeV}$ as an example, just above the $\mu^-\mu^+$ threshold giving the longest lifetime to make ϕ decay into $\mu^-\mu^+$ at each mixing angle.[20] The decay width of the mediator is then estimated to be $\Gamma_\phi \simeq 10^{-9} \times \sin^2\theta\,\mathrm{GeV}$. The constraint $\mathrm{Br}(\Upsilon \to \gamma\phi) \times \mathrm{Br}(\phi \to \mu^-\mu^+) \lesssim 3 \times 10^{-6}$ is then translated to $\sin\theta \lesssim 0.14$, so that the decay length of the mediator produced by the Υ decay is estimated to be $\gamma_\phi\,\tau_\phi\,c = \mathcal{O}(0.1)\,\mathrm{mm}$ with the speed of light c. Here, the so-called gamma factor is estimated to be $\gamma_\phi \simeq m_\Upsilon/(2m_\phi) \simeq 25$. This decay length is much shorter than the present sensitivity of displaced vertex searches, which requires $\mathcal{O}(1)\,\mathrm{cm}$ [117].

The Belle II experiment will update the constraints in the near future with the integrated luminosity about fifty times more than that of the BaBar experiment, if no signal is detected there.[21] The constraints on the branching fractions will be about six times more severer than the present ones. As a result, for instance, the constraints will be

---

[20]Needless to say, the lifetime (thus, the decay length) becomes shorter if the mediator mass is heavier.

[21]We thank prof. Akimasa Ishikawa for providing us fruitful information for the Belle II experiment.

$\text{Br}(\Upsilon \to \gamma\phi) \times \text{Br}(\phi \to \mu^-\mu^+) \lesssim 5 \times 10^{-7}$ and $\text{Br}(\Upsilon \to \gamma\phi) \times \text{Br}(\phi \to \tau^-\tau^+) \lesssim 5 \times 10^{-6}$. Note that the decay length of the mediator is, at most, $\mathcal{O}(1)$ mm even in the near future, so that its decay can be treated as a prompt one. We include all the constraints discussed here in our likelihood. It, however, turns out that the present constraints are not stronger than others. Those from $B(K)$ decays are more sensitive in the mass region of $m_\phi < m_B(m_K)$ with $m_B(m_K)$ being the $B(K)$ meson mass, while the LEP experiment gives a stronger constraint in $m_B < m_\phi < 9.2\,\text{GeV}$, as we will see in following discussions. On the other hand, the future constraints could play an important role to search for the mediator in a certain mass region of ϕ.

3.3.2 *B* meson decay

When the mediator ϕ is lighter than B mesons ($m_B \simeq 5.3\,\text{GeV}$), it can be produced by their decays through the sub-process $b \to s\phi$, where it is induced mainly from the one-loop diagram composed of weak bosons and various quarks in the loop [52]. Among various B meson decays, one of the efficient channels to search for the mediator at collider experiments is the charged B meson decay, $B^\pm \to K^\pm\phi$. Its decay width is estimated to be [141]:

$$\Gamma(B^\pm \to K^\pm\phi) = \frac{|C_{sb}|^2 F_K^2(m_\phi)}{16\pi m_B^3} \left(\frac{m_B^2 - m_K^2}{m_b - m_s}\right)^2 \sqrt{(m_B^2 - m_K^2 - m_\phi^2)^2 - 4m_K^2 m_\phi^2}, \quad (3.7)$$

where the scalar form factor of $K^\pm$ is estimated to be $F_K(q) \simeq 0.33\,(1 - q^2/38\,\text{GeV}^2)^{-1}$, while the coefficient of the FCNC effective interaction, $C_{sb}\,\bar{s}_L\,b_R\,\phi + h.c.$, is given by $|C_{sb}| \simeq |2g^2 m_b m_t^2 V_{ts}^* V_{tb} \sin\theta|/(64\pi^2 m_W^2 v_H) \simeq 6.4 \times 10^{-6} \sin\theta$ with V_{tb} and V_{ts} being the CKM matrix elements. Combined with the total decay width of the B meson, $\Gamma_{B^+} \simeq 4.1 \times 10^{-13}\,\text{GeV}$, the above formula allows us to compute the branching fraction of the decay channel $B^\pm \to K^\pm\phi$. It is also possible to consider other decay channels for the ϕ search such as $B^0 \to K^{*0}\phi$. Collider signals then depend on how the mediator decays and how long distance it travels before the decay. In this subsection, all experimental results of B meson decay at present and expected null signal results in the near future are discussed.

***B* meson decay with prompt ϕ decay.** When the decay length of the mediator is enough smaller than the detector size, its decay can be treated as a prompt one. In such a case, the decay channel $B^\pm \to K^\pm\phi \to K^\pm\mu^-\mu^+$ is frequently used to detect the mediator, as it gives a clean signal against backgrounds. At present, BaBar [118], Belle [110] and LHCb [112] collaborations give upper limits on its branching fraction as $P_p\,\text{Br}(B^\pm \to K^\pm\phi)\,\text{Br}(\phi \to \mu^-\mu^+) \lesssim 3 \times 10^{-7}$, accepting that the theoretical prediction of the SM contribution is $\text{Br}(B^\pm \to K^\pm\mu^-\mu^+)_{\text{SM}} = (3.5 \pm 1.2) \times 10^{-7}$ [142]. Here, the prefactor P_p is the probability that the mediator decays inside the detector,

$$P_p \equiv \frac{1}{2} \int_0^\pi d\theta_\phi \, \sin\theta_\phi \left(1 - \exp\left[-\frac{l_{xy}}{\sin\theta_\phi} \frac{1}{\gamma\beta c\tau_\phi}\right]\right), \quad (3.8)$$

where τ_ϕ is the lifetime of the mediator, while θ_ϕ is the angle between the direction of the mediator produced from the B decay and that of the beampipe. The boost factor is

estimated to be $\gamma\beta \simeq m_B/(2m_\phi)$, as the mediator is produced from the B decay. The size of the detector is set to be $l_{xy} \simeq 25\,\mathrm{cm}$ referencing to those of Belle and BaBar detectors [58].

The theoretical error on the SM contribution overwhelms the experimental errors due to the uncertainty of the form factor in eq. (3.7). Therefore, a significant improvement of the sensitivity is not expected even if more data is accumulated at e.g. the upcoming SuperKEKB experiment [115]. On the other hand, if the theoretical error is much reduced, thanks to the development of lattice QCD simulations and/or the use of the characteristic feature coming from the narrow dilepton invariant mass peak from the mediator decay, the analysis can have a further improvement. Since no convincing study on the issues has been performed yet, we do not involve the constraint from the prompt $B^\pm \to K^\pm \phi \to K^\pm \mu^- \mu^+$ decay to investigate the future prospects of the minimal WIMP model and involve it only for its present status.

B meson decay with displaced ϕ decay.   When the decay length of the mediator ϕ becomes comparable to the detector size, displaced vertex is the most powerful channel to search for ϕ. At present, BaBar [117] and LHCb [113, 114] collaborations give various stringent constraints. The BaBar collaboration has looked for the displaced vertex caused by decay channels $\phi \to e^- e^+$, $\mu^- \mu^+$, $\pi^- \pi^+$ and $K^- K^+$ by observing the invariant mass spectrum of the decay products, where the mediator is produced mainly from B decays, $B \to X_s \phi$ with X_s being a hadronic system with a strangeness. Since no excess over the SM prediction has been observed, they put a constraint on $\mathrm{Br}(B \to X_s \phi)\,\mathrm{Br}(\phi \to e^- e^+, \mu^- \mu^+, \pi^- \pi^+, K^- K^+)$, which is translated to that on the mixing angle, $\sin^2 \theta \gtrsim 2 \times 10^{-8}$ at 90% C.L., almost regardless of m_ϕ and τ_ϕ in the region of $0.5\,\mathrm{GeV} \leq m_\phi \leq 1.5\,\mathrm{GeV}$ and $1\,\mathrm{cm} \leq c\tau_\phi \leq 20\,\mathrm{cm}$. We adopt it in our likelihood analysis. More stringent limits on the mixing angle for regions $m_\phi \geq 1.5\,\mathrm{GeV}$ and $c\tau_\phi \geq 20\,\mathrm{cm}$ is obtained at LHCb (see below) and beam dump experiments, respectively.

On the other hand, the LHCb collaboration is recently searching for the mediator produced by both charged and neutral B-meson decays: $B^\pm \to K^\pm \phi \to K^\pm \mu^- \mu^+$ and $B^0 \to K^{*0} \phi \to K^{*0} \mu^- \mu^+$. Their latest report based on the negative result of the search using $3\,\mathrm{fb}^{-1}$ data at $7\,\mathrm{TeV}$ and $8\,\mathrm{TeV}$ running is found in ref. [114]. We also involve this result in our analysis, where it gives a stringent constraint in the region of $m_\phi \geq 1.5\,\mathrm{GeV}$.

In the near future, Belle II collaboration will update the constraint (given by the BaBar collaboration) with 100 times more data ($50\,\mathrm{ab}^{-1}$) [115], if no signal is detected. On the other hand, the LHCb collaboration will accumulate data during the $13\,\mathrm{TeV}$ running, where 300 times more B mesons will be in data compared to the present one [121]. For the near future prospects in our analysis, we therefore adopt the BaBar and LHCb constraints mentioned above with their sensitivities on the mediator searches increased 10 and 17 times.

B meson decay with very long-lived ϕ decay.   When the decay length of ϕ is much longer than the detector size, it is searched by utilizing the channel, $B^\pm \to K^\pm + \text{missing}$, where the SM process, $B^\pm \to K^\pm \nu\bar\nu$, is a background against the signal. This channel is also used to search for the mediator decaying invisibly, $B^\pm \to K^\pm \phi \to K^\pm \chi\chi$, even if it is short-lived. At present, Belle [111] and BaBar [119, 120] collaborations put a constraint

as $P_l \operatorname{Br}(B^\pm \to K^\pm \phi) + P_p \operatorname{Br}(B^\pm \to K^\pm \phi) \operatorname{Br}(\phi \to \chi\chi) \leq 1.6 \times 10^{-5}$. The factor P_l is the probability that ϕ decays outside the detector,

$$P_l \equiv \frac{1}{2} \int_0^\pi d\theta_\phi \, \sin\theta_\phi \exp\left[-\frac{l_{xy}}{\sin\theta_\phi} \frac{1}{\gamma\beta c\tau_\phi} \right], \tag{3.9}$$

where the values of l_{xy} and $\gamma\beta$ are the same as those in eq. (3.8). In future, the Belle II collaboration will update the sensitivity as $P_l \operatorname{Br}(B^\pm \to K^\pm \phi) + P_p \operatorname{Br}(B^\pm \to K^\pm \phi) \operatorname{Br}(\phi \to \chi\chi) \leq 5 \times 10^{-7}$ [116]. We include this constraint in our analysis for the near future prospects.

3.3.3 Kaon decay

The mediator is also produced from Kaon decays if it is lighter than Kaons ($m_K \simeq 0.5\,\text{GeV}$), which is induced from the sub-process $s \to d\,\phi$. The most efficient channels to search for ϕ are $K^\pm \to \pi^\pm + \phi$ and $K_L \to \pi^0 + \phi$, where their decay widths are given as follows [52]:

$$\Gamma(K^\pm \to \pi^\pm \phi) = \frac{|C_{ds}|^2}{16\pi m_{K^\pm}^3} \left(\frac{m_{K^\pm}^2 - m_{\pi^\pm}^2}{m_s - m_d} \right)^2 \sqrt{(m_{K^+}^2 - m_{\pi^+}^2 - m_\phi^2)^2 - 4m_{\pi^+}^2 m_\phi^2}, \tag{3.10}$$

$$\Gamma(K_L \to \pi^0 \phi) = \frac{(\operatorname{Im} C_{ds})^2}{16\pi m_{K_L}^3} \left(\frac{m_{K_L}^2 - m_{\pi^0}^2}{m_s - m_d} \right)^2 \sqrt{(m_{K_L}^2 - m_{\pi^0}^2 - m_\phi^2)^2 - 4m_{\pi^0}^2 m_\phi^2}. \tag{3.11}$$

Since scalar form factors for pions are close to unity [143], we neglect those in the above equations. On the other hand, the coefficient C_{ds} comes from the FCNC effective interaction, $C_{sd} \bar{s}_L d_R \phi + h.c.$, where $C_{sd} \simeq (2g_W^2 m_s m_t^2 V_{ts}^* V_{td} \sin\theta)/(64\pi^2 m_W^2 v_H) \simeq (1.2 + 0.5i) \times 10^{-9} \sin\theta$ with the CKM matrix elements V_{ts} and V_{td}. By given the total decay widths of the Kaons, $\Gamma_{K^\pm} = 5.3 \times 10^{-17}\,\text{GeV}$ and $\Gamma_{K_L} = 1.286 \times 10^{-17}\,\text{GeV}$, we can compute their branching fractions. The Kaon decays are then followed by the ϕ decay, and the decay channels $\phi \to \mu^- \mu^-$, $e^- e^+$ are used, as it gives a clean signal and has less theoretical uncertainties than others.

Kaon decay with prompt ϕ decay. When the mediator decays promptly, the most stringent limit on the branching fraction of the charged Kaon decay, $K^\pm \to \pi^\pm \phi \to \pi^\pm \mu^- \mu^+$, is put by the N48/2 collaboration [122]. Adopting the SM contribution, $\operatorname{Br}(K^+ \to \pi^+ \mu^- \mu^+)_{\text{SM}} \simeq (8.7 \pm 2.8) \times 10^{-8}$, they give a limit as $P_p' \operatorname{Br}(K^+ \to \pi^+ \phi) \operatorname{Br}(\phi \to \mu^- \mu^+) \leq 4 \times 10^{-8}$ at 90% C.L. with P_p' being the probability that the mediator decays within the range of the longitudinal vertex resolution $\sigma_z \simeq 100\,\text{cm}$ [58], namely $P_p' \equiv 1 - \exp[-\sigma_z/(\gamma\beta c\tau_\phi)]$. Here, the boost factor is estimated to be $\gamma\beta \simeq 120$, because the mediator is produced by the Kaon decay with its momentum of $60\,\text{GeV}$.

On the other hand, the KTeV collaboration [123, 124] put the other constraints using neutral Kaon decays as $P_p' \operatorname{Br}(K_L \to \pi^0 \phi) \operatorname{Br}(\phi \to e^- e^+, \mu^- \mu^+) \leq 2.8 \times 10^{-10}, 3.8 \times 10^{-10}$ at 90% C.L. with σ_z and $\gamma\beta$ in P_p' being replaced by those of the KTeV experiment, $\Delta l = 4\,\text{mm}$ and $\gamma\beta \simeq 1$ [141]. Since SM predictions are $\operatorname{Br}(K_L \to \pi^0 \mu^- \mu^+) \sim \operatorname{Br}(K_L \to \pi^0 e^- e^+) \sim 3 \times 10^{-11}$, those have not been observed at the experiment. We include all the above constraints in our likelihood analysis for the present status of the minimal WIMP model.

In the near future, an improvement of the sensitivity on the search with the $K^\pm$ decay is not expected, for the systematic error at the scalar form factor already dominates. Moreover, there is no successor of the KTeV experiment, so that the constraints from the neutral Kaon decays are not expected to have any improvement in the near future. We hence do not consider the constraints relevant to the above prompt Kaon decays in our likelihood analysis for the near future prospects of the minimal WIMP model.

Kaon decay with displaced ϕ decay. When ϕ decays with the decay length of $\mathcal{O}(100)\,\mathrm{m}$, it is efficiently searched at proton beam dump experiments. At present, the CHARM collaboration gives the stringent constraint on this search [128], where many Kaons and B mesons are produced from the $400\,\mathrm{GeV}$ proton beam which is dumped into the copper target. Then, the mediator is expected to be promptly produced from the channels, $K^\pm \to \pi^\pm \phi$, $K_L \to \pi^0 \phi$ and $B \to X_s \phi$. At the experiment, the detector is located at $480\,\mathrm{m}$ away from the target with its size of $35\,\mathrm{m}$, and ϕ penetrating the wall is searched for with leptonic decay channels $\phi \to e^- e^+$ and $\mu^- \mu^+$.

Since zero signal event was observed as expected by background, the collaboration put a constraint on the number of signal events as $N_{\mathrm{dec}} \leq 2.3$ at 90% C.L. [129]. The total number of signal events at the experiment is estimated by [57]

$$N_{\mathrm{dec}} = N_{\mathrm{p.o.t}} \left[P_{\mathrm{dec}}^K \frac{\ell_H}{c\gamma_K \tau_K} n_K \mathrm{Br}(K \to \pi\phi) + P_{\mathrm{dec}}^B n_B \mathrm{Br}(B \to X_s \phi) \right], \qquad (3.12)$$

where $N_{\mathrm{p.o.t}}$ is the number of protons on the target, and $n_{K(B)}$ is the number of $K(B)$ meson created per each incoming proton. Since Kaons are long-lived and absorbed in the target, the factor $\ell_H/(c\gamma_K \tau_K)$ is multiplied to its contribution with γ_K, τ_K and ℓ_H being the Lorentz factor, lifetime of the K meson and the hadronic absorption length, respectively. The factors P_{dec}^K and P_{dec}^B are probabilities that the mediator decays inside the detection region,

$$P_{\mathrm{dec}}^{K(B)} = \eta_{\mathrm{geom}}^{K(B)} \eta_{\mathrm{rec}}^{K(B)} \left(-\exp\left[-\frac{L_2}{\gamma\beta c\tau_\phi} \right] + \exp\left[-\frac{L_1}{\gamma\beta c\tau_\phi} \right] \right), \qquad (3.13)$$

with $\eta_{\mathrm{geom}}^{K(B)}$ and $\eta_{\mathrm{rec}}^{K(B)}$ are the geometric and reconstruction efficiencies, respectively, assuming those are independent along the beam line. In the CHARM experiment, the values of the above parameters are $N_{\mathrm{p.o.t}} = 2.4 \times 10^{18}$, $n_K = 0.9$, $n_B = 3.2 \times 10^{-7}$, $\ell_H = 15.3\,\mathrm{cm}$, $\eta_{\mathrm{geom}}^K \simeq 0.002$, $\eta_{\mathrm{geom}}^B \simeq 0.006$, $\eta_{\mathrm{rec}}^{K(B)} \simeq 0.5$, $\gamma_K \simeq 20\,\mathrm{GeV}/m_K$, $\gamma\beta m_\phi \simeq 10\,\mathrm{GeV}$ and $L_1 = L_2 - 35 = 480\,\mathrm{m}$ (the location of the detector), respectively. This constraint is included in our likelihood analysis to investigate the present status of the minimal WIMP model.

In the near future, the above constraint will be improved by the SHiP experiment at CERN SPS [131] if no signal is detected, where the $400\,\mathrm{GeV}$ proton beam is dumped to the fixed target and the expected number of protons on the target is $N_{\mathrm{p.o.t}} = 2 \times 10^{20}$. The SHiP detector is located at $69\,\mathrm{m}$ away from the target with its size of $51\,\mathrm{m}$, so that the probability that the mediator decays inside the detection region is given by P_{dec} in eq. (3.13) with $\eta_{\mathrm{geom}}^K \simeq 0.065$, $\eta_{\mathrm{geom}}^B \simeq 0.35$, $\gamma\beta m_\phi \simeq 25\,\mathrm{GeV}$ and $L_1 = L_2 - 51\,\mathrm{m} = 69\,\mathrm{m}$. Reconstruction efficiencies below (above) two muon threshold are $\eta_{\mathrm{rec}}^{K,B} \simeq 0.4(0.7)$. Then, the constraint

will be updated as $N_{\text{dec}} \leq 3$ at 95% C.L., if no signal is detected there. Since the SHiP experiment can detect the decay channels of the mediator into $\pi\pi$ and KK, it will have more sensitivity for a heavy mediator ($\lesssim 4\,\text{GeV}$) than that of the CHARM experiment. We include this future-expected limit to study the future prospects of the minimal WIMP model.

Kaon decay with very-long lived ϕ decay. When the lifetime of the mediator is very long, it is searched through the process, $K^{\pm} \to \pi^{\pm} + \text{missing}$, where the SM process, $K^{\pm} \to \pi^{\pm}\nu\bar{\nu}$, becomes a background against the signal. In addition to the signal channel, $K^{\pm} \to \pi^{\pm}\,(\text{long} - \text{lived}\,\phi)$, another channel, $K^{\pm} \to \pi^{\pm}\phi \to \pi^{\pm}\chi\chi$, also contributes to the signal when the mediator is twice heavier than the WIMP, as in the case of the B meson decay described at the last paragraph of section 3.3.2. At present, the E949 collaboration put a stringent constraint on the branching fraction $P_l\,\text{Br}(K^+ \to \pi^+\phi) + (1 - P_l)\,\text{Br}(K^+ \to \pi^+\phi)\,\text{Br}(\phi \to \chi\chi)$, where P_l is defined in eq. (3.9) with the size of the detector and the boost factor being replaced by $l_{xy} \simeq 145\,\text{cm}$ and $\gamma\beta \simeq 1$, respectively. The constraint on the branching fraction at 90% C.L. is found in figure 18 of ref. [125].

On the other hand, such a very long-lived mediator is also searched by using the neutral Kaon decay, $K_L \to \pi^0 + \text{missing}$. Then, the SM process, $K_L \to \pi^0\nu\bar{\nu}$, becomes a background against the signal. At present, the KEK E391a experiment put a constraint on the branching fraction as $P_l\,\text{Br}(K_L \to \pi^0\phi) + (1 - P_l)\,\text{Br}(K_L \to \pi^0\phi)\,\text{Br}(\phi \to \chi\chi) \leq 2.6 \times 10^{-8}$ with l_{xy} and $\gamma\beta m_\phi$ used in P_l being replaced by $l_{xy} \simeq 1\,\text{m}$ and $\gamma\beta m_\phi \simeq 1\,\text{GeV}$, respectively [130]. We involve the above two constraints from the charged and neutral Kaon decay experiments in our likelihood analysis to investigate the present status of the minimal WIMP model.

In the near future, the constraint from the charged Kaon decay will be improved by the NA62 experiment as $P'_l\,\text{Br}(K^+ \to \pi^+\phi) + (1 - P'_l)\,\text{Br}(K^+ \to \pi^+\phi)\,\text{Br}(\phi \to \chi\chi) \lesssim 10^{-11}$ if no signal is detected, where $P'_l = \exp[-l_z/(\gamma\beta c\tau_\phi)]$ with $l_z = 65\,\text{cm}$ and $\gamma\beta m_\phi = 37.5\,\text{GeV}$ [126, 127]. On the other hand, the constraint from the natural Kaon decay will be improved as $P_l\,\text{Br}(K_L \to \pi^0\phi) + (1 - P_l)\,\text{Br}(K_L \to \pi^0\phi)\,\text{Br}(\phi \to \chi\chi) \lesssim 1.46 \times 10^{-9}$ at the KOTO experiment with P_l being the same as that for the KEK E391a experiment [132], which is close to the so-called Grossman-Nir bound. Since the branching fractions of the decay channels, $\text{Br}(K^+ \to \pi^+\phi)$ and $\text{Br}(K_L \to \pi^0\phi)$, are at the same order, the constraint from the charged Kaon decay is stronger than the neutral one in the most of the parameter region. Despite this fact, we involve both the constraints in our likelihood analysis for the sake of comprehensiveness to investigate the future prospects of the minimal WIMP model.

3.3.4 Higgs decay

The mediator can also be produced from the Higgs decay, $h \to \phi\phi$, and this process is indeed being investigated by measuring the Higgs boson property carefully at the LHC experiment. The latest result of the measurement is consistent with the SM prediction, so that we have various constraints on the decay process depending on the decay length of the mediator.

Higgs decay with prompt ϕ decay. When the mediator promptly decays into two leptons, it is searched for through the Higgs decay channel, $h \to 4\ell$. At present, the

ATLAS collaboration put a constraint on the branching fraction of the four muon process, $(P'_p)^2 \text{Br}(h \to \phi\phi) \times \text{Br}(\phi \to \mu\mu)^2$, where P'_p is the probability that the decay is considered to be a prompt one at the experiment and defined as $P'_p = 1 - \exp[-\sigma/(\gamma\beta c\tau_\phi)]$ with $\sigma = 1\,\text{mm}$ and $\gamma\beta = m_h/(2m_\phi)$, respectively. The limit on the branching fraction at 90% C.L. is found in ref. [134]. On the other hand, the CMS collaboration put constraints on similar branching fractions with the same σ and $\gamma\beta$ by considering various leptonic channels, $h \to 4\mu$, $2\mu2\tau$ and 4τ. Constraint on the branching fraction of each channel is obtained from ref. [133] using the same prefactor P'_p. We involve these constraints in our analysis for the present status of the minimal WIMP model.[22]

In the near future, both the collaborations will update their constraints at the high-luminosity upgrade of the LHC experiment (HL-LHC) [137], if no signal is detected. Since we can expect about a hundred times more data at the HL-LHC than the current one, the sensitivity of the search will be improved by one order of magnitude if the statistical error dominates. For the future prospects of the model, we hence involve the same constraints on the above branching fractions in our analysis with making the limits ten times severer.

Higgs decay with displaced ϕ decay. When the mediator decays with the decay length of 0.1–10 m, it is searched for by the displaced vertex analysis at the LHC experiment. The mediator is produced mainly from the Higgs decay, $pp \to h+X \to \phi\phi+X$, when the mixing angle, $\sin\theta$, is small. Then, two displaced vertices are formed by the mediator decay if it is long-lived, and those are detected via the decays $\phi \to \mu\mu$, ee and $\pi\pi$. Here, the decay products are collimated as the mediator is boosted. At present, the ATLAS collaboration put a constraint on the branching fraction of the Higgs decay with displaced vertices using various decay channels of the mediator [144]. These results are summarized in ref. [135], where an upper limit on the branching fraction, $\text{Br}(h \to \phi\phi)$, is given at 90% C.L. as a function of the mediator mass and the mixing angle (lifetime). Roughly speaking, the region of $\text{Br}(h \to \phi\phi) \gtrsim 30\%$ is excluded when $0.3\,\text{GeV} \lesssim m_\phi \lesssim 60\,\text{GeV}$ and $0.1\,\text{m} \lesssim c\tau_\phi \lesssim 10\,\text{m}$. We involve the constraint in ref. [135] in our analysis for the present status of the minimal WIMP model. Note that this constraint is not applied in the $m_\phi \geq 2m_\chi$ region, as the $\phi \to \chi\chi$ decay was not considered in ref. [135].

Since the systematic error already dominates the statistical one to put the constraint on the branching fraction $\text{Br}(h \to \phi\phi)$ (with displaced vertices) at the present LHC experiment, it is difficult to expect a significant improvement of the sensitivity on this search at the HL-LHC experiment. We therefore do not consider the constraint from the search for the Higgs decay with displaced vertices to study the future prospects of the minimal WIMP model.

Higgs decay with very long-lived ϕ decay. When the mediator is very long-lived, the decay process, $h \to \phi\phi$, contributes to the invisible decay width of the Higgs boson. In addition, the other decay channels exist, which are $h \to \chi\chi$ and $h \to \phi\phi \to 4\chi$, and always contribute to the invisible decay width of the Higgs boson without respect to the

---

[22]Both ATLAS and CMS collaborations assumed in their analyses that the Higgs boson decays into two pseudo-scalars, which means that different branching fractions of Higgs and mediator decays are used. We have corrected those to apply their constraints to our case where the Higgs boson decays into two scalars.

decay length of the mediator. As a result, the new physics contribution to the branching fraction of the invisible Higgs decay is given as follows:

$$\mathrm{Br}(h \to \mathrm{inv.})_{\mathrm{BSM}} = P_{\ell_{30}}^2 \, \mathrm{Br}(h \to \phi\phi) + \mathrm{Br}(h \to \chi\chi) + (1 - P_{\ell_{30}}^2) \, \mathrm{Br}(h \to \phi\phi \to 4\chi), \quad (3.14)$$

where $P_{\ell_{30}} = \exp[-\ell_{30}/(\gamma\beta c\tau_\phi)]$ and $1 - P_{\ell_{30}}$ are the probabilities that the mediator decays outside and inside the detector, respectively, with the size of detector and the boost factor being $\ell_{30} = 30\,\mathrm{m}$ and $\gamma\beta \simeq m_h/(2m_\phi)$. At present, the constraint on the branching fraction is given as $\mathrm{Br}(h \to \mathrm{inv.})_{\mathrm{BSM}} \leq 0.19$ at 90% C.L. [136] from Higgs precision measurements, and we include this in our analysis for the present status of the minimal WIMP model.

The constraint on this branching fraction will be improved at the HL-LHC experiment with $3\,\mathrm{ab}^{-1}$ data. If no signal is detected there [138], we can set $\mathrm{Br}(h \to \mathrm{inv.})_{\mathrm{BSM}} \leq 0.05$ at 90% C.L. We include it in our analysis for the future prospects of the minimal WIMP model.

3.3.5 Direct production

When the mediator is heavier than the B meson and the mixing angle is not very suppressed, the mediator is also efficiently searched for by its direct production at high-energy colliders. The mediator is produced by the Bremsstrahlung process, $f\bar{f} \to V^* \to V\phi$, with f and V being a SM fermion and a weak gauge boson, respectively, and the mediator always decays promptly in the parameter region of our interest. At present, the LEP experiment put the most severe limit on the mixing angle $(\sin\theta)$ as a function of the mediator mass (m_ϕ). To be more precise, the L3 collaboration have used the hadronic decay channel of the mediator associated with Z boson decays, $Z \to \nu\bar{\nu}$, e^-e^+ and $\mu^-\mu^+$, where its result is found in ref. [139]. Similarly, the ALEPH collaboration have also used the hadronic decay channel of the mediator, but only associated with the decay $Z \to \nu\bar{\nu}$. Its result is found in ref. [145], which is slightly weaker than that of the L3 collaboration. On the other hand, the OPAL collaboration have utilized the inclusive Z production with its leptonic decays, $Z \to e^-e^+$ and $\mu^-\mu^+$, where its result is found in ref. [146]. It is, however, applicable for a very light mediator, say as light as $10^{-6}\,\mathrm{GeV}$, and it dose not play an important role in the analysis.

The LHC experiment is also searching for the mediator produced by the above direct production process [147], though it is less sensitive than the LEP experiment. Moreover, the obtained limit on the mixing angle is already dominated by systematic errors, it seems difficult to expect a significant improvement even at the HL-LHC experiment. We therefore involve the limit obtained by the L3 collaboration in our likelihood analysis to investigate the present status of the minimal WIMP model, and do not consider the expected constraint from the direct mediator production for the near future prospects of the WIMP model.

4 Results

We are now in a position to present the result of our likelihood analysis. We first explain the framework of our analysis in some details, as it plays a crucial role in our study. Then, we will present various results obtained in our analysis and discuss their implications to investigate the present status and near-future prospects of the minimal WIMP model.

Likelihood type	Present	Future
Step	Preselection criteria, LHCb, Kinematical equilibrium, BBN	—
Poisson	CHARM, XENON1T, CRESST, Darkside-50	SHiP
Half-Gaussian	CLEO, BABAR, Belle, LHCb, N48/2, KTeV, E949, KEK E391a, LHC, LEP	SuperCDMS-SNOLAB, LZ, NEWS-SNOLAB, Belle II, LHCb NA62, KOTO, HL-LHC
Gaussian	Relic abundance, Plank(ΔN_{eff})	CMB-S4(ΔN_{eff})

Table 4. Summary of likelihood distributions used in our analysis.

4.1 Simulation framework

There are many released limits and data used in this work. Because of lacking discovery of new physics, the majority of them are based on the 90 % upper or lower confidence limit on a one-dimensional physical observable.[23] Nevertheless, for some other constraints such as relic density, because of its clear discovery, it is nature to describe such a likelihood probability by a two-tail Gaussian with a narrow peak. Except above two types of limits, theoretical constraint is used to veto the parameter space whose answer is often physical or not physical. As summarized in table 4, we have used four types of likelihood function in our analysis: (i) Gaussian likelihood, (ii) Half Gaussian likelihood with the central value being fixed to be zero, (iii) Poisson likelihood for counting experiments, and (iv) Step function likelihood. In the following, we will present the usage of these four likelihood functions.

The most powerful advantage of the global analysis is to increase the statistics by combining different data sets which allows us to remove more parameter spaces from different corners. However, in order to conservatively exclude parameter space by adding the statistics, a proper likelihood function is needed and its tail at the exclusion region is particularly important. Once the central value and error bar are given, the Gaussian likelihood is

$$\mathcal{L}_{\text{Gau.}} \propto \exp\left[-\frac{\chi^2}{2}\right], \qquad \text{where} \qquad \chi^2 = \left[\frac{\text{Prediction} - \text{Center value}}{\text{Error bar}}\right]^2. \qquad (4.1)$$

On the other hand, for counting experiments, if expected event number and observed event number are provided, Poisson distribution is usually adopted for its likelihood function,

$$\mathcal{L}_{\text{Pos.}} \propto \frac{e^{-(s+b)}(s+b)^o}{o!}, \qquad (4.2)$$

where s and b are expected signal and background events, while o is observed events.

It is usually having null signal detection in new physics search. In such a search, a lower limit or upper limit of an observable is reported. Such a limit with some information given

---

[23]The terminology 90 % C.L. for $\delta\chi^2 = 2.71$ in one-tail Gaussian likelihood distribution is sometimes used.

by experimental collaboration, one can of course reconstruct and verify some likelihood used in the experimental collaboration. Because of expansive background simulation and likelihood computation time, it will not be realistic to repeat whole procedure to reconstruct such a precise likelihood as used in the experimental collaboration. Therefore, we model the likelihood based on two reasonable assumptions: null signal detection and Gaussian distribution with the alignment of 90 % C.L. The likelihood of such a distribution called half Gaussian is almost identical as eq. (4.1) but with two differences; the center value is set to be zero because of null signal detection and the error-bar-squared can be obtained by the 90 % C.L. limit divided by 2.71 to align 90 % Gaussian one tail limit. Note that such a half Gaussian distribution shall be more conservative than precise one because new physics signal is expected to have an excess than background in the future.

Some experimental upper/lower limits are built based on multi-dimensional variables which are hard to reconstruct their likelihoods. For example, the limits of the LHC Higgs displaced vertex search in section 3.3.4 are based on three dimensional variables, m_ϕ, $\sin\theta$ and the branching fraction of $h \to \phi\phi$. For a sake of simplicity, one may just use a hard cut for such an experimental constraint to answer whether the parameter space is allowed or excluded. Sometimes, one could perform a scan with the constraints described in case (ii) by using a step function, but it is particularly avoided in our analysis because it will lose the advantage of combined analysis as discussed in the previous paragraph.

Finally, when performing two-dimensional contour figures in this paper, we use the method "Profiled Likelihood", namely the minimum Chi-squared method. Like frequentist, such a method allows us to get rid of unwanted/not interesting parameters by taking the maximum likelihood along the direction of other unwanted/not interesting dimensions.

Regarding to the sampling, as seen in appendices A and B, the likelihood function is flat within vast 1sigma allowed region but dramatically changing at the 2sigma tails. Therefore, in our analysis, we adopt an unusual strategy to scan our parameter space. We first scan the parameter space with the range in eq. (3.1) and the conditions in table 1. Note that two dark matter parameters m_χ and c_s are not scanned in this step. After collecting $\mathcal{O}(10^6)$ allowed points, we use it to present the parameter space constrained by the preselection criteria in appendix A. In the second step, based on the former collected data set, we varied m_χ and c_s for each points to fit the relic abundance and kinematical equilibrium conditions. However, the parameter λ_Φ does not affect the dark matter phenomenology at all. In this step, we evaluated $\mathcal{O}(10^8)$ points but only $\sim 5 \times 10^6$ points fulfill the relic abundance and kinematical equilibrium conditions. In the third step, based on the $\mathcal{O}(10^8)$ points collected from the former scan, we evaluate all the likelihoods with the constraints given in tables 2 and 3. Finally, we use the knowledge we learned from previous scans as the new prior distribution to do several more sophisticated scans. We employed two scan tools (emcee [148] and MultiNest [149]) to undertake the sampling. With total $\mathcal{O}(10^8)$ likelihood evaluation done by the tools emcee and MultiNest, we found the coverage is good enough. We combine all the scans from the former steps to draw our figures.

4.2 Present status

Results of our analysis for the present status of the minimal WIMP model projected on the (m_χ, m_ϕ)- and $(m_\phi, |\sin\theta|)$-planes are shown in the left and right panels of figure 3, respectively, while those projected on all planes of input parameters are found in appendix C.1.

(a) In the left panel, the upper limit on the mediator mass m_ϕ comes from the relic abundance condition. As mentioned above, most of parameter regions satisfy the relation $m_\phi \lesssim m_\chi$, while the exception is the s-channel resonance-enhanced region with $m_\phi \sim 2m_\chi$. The latter case appears only for $m_\phi \gtrsim \mathcal{O}(1)\,\text{GeV}$ to be consistent with collider constraints.

(b) The lower limit on the WIMP mass is obtained by the combination of collider constraints and kinematic equilibrium condition. When it is lighter than $\mathcal{O}(10)\,\text{MeV}$, the mixing angle is constrained to be below 10^{-3} due to Kaon experiments. The mixing angle is, however, required to be larger than 10^{-3} to satisfy the kinematical equilibrium condition, as shown in the plot on the $(m_\chi, |\sin\theta|)$-plane in figure 8, which leads to the limit, $m_\chi \gtrsim 10\,\text{MeV}$.

(c) On the other hand, the lower limit on m_ϕ in the range of $m_\chi \lesssim 500\,\text{MeV}$ comes from the ΔN_{eff} constraint discussed in section 3.2.4, while the limit in the range of $m_\chi \gtrsim 3\,\text{GeV}$ is from the direct dark matter detection constraint, for the spin-independent scattering cross section between the dark matter and a nucleon is proportional to m_ϕ^{-4}. The lower limit on m_ϕ in the range of $500\,\text{MeV} \lesssim m_\chi \lesssim 3\,\text{GeV}$ is obtained in a complicated way: it is from the combination of the direct detection constraint and the kinematical equilibrium condition. When the dark matter mass is below a few GeV, the freeze-out temperature becomes lower than the QCD phase transition, so that a mixing angle is required not to be very suppressed in order to maintain the kinematical equilibrium.[24] However, such an unsuppressed mixing angle (as well as a small m_ϕ) leads to a large spin-independent scattering cross section between the dark matter and a nucleon and ruled out by the direct dark matter detection.

(d) In the right panel, the lower limit on the mixing angle is from the BBN constraint discussed in section 3.2.5, $\tau_\phi \leq 1\,\text{s}$ in the range of $m_\phi \geq 2m_\pi$ and $\tau_\phi \leq 10^5\,\text{s}$ in the range of $m_\phi < 2m_\pi$. The spike structure at $m_\phi \sim 1\,\text{GeV}$ comes from the uncertainty on the decay width of the mediator discussed in section 2.4, while another one at $m_\phi \sim 200\,\text{MeV}$ is from the quick change of the decay width due to the threshold of the $\phi \to \mu^-\mu^+$ channel.

(e) On the other hand, the upper limit on the angle comes mainly from collider constraints. For $m_\phi \lesssim 500\,\text{MeV}$, the limit is set by Kaon experiments such as CHARM. For $500\,\text{MeV} \lesssim m_\phi \lesssim 5\,\text{GeV}$, B meson experiments set the limit. The long island at $m_\phi \simeq 1\,\text{GeV}$ and $10^{-3} \lesssim |\sin\theta| \lesssim 10^{-1}$ is again due to the theoretical uncertainty of

---

[24]The process $\phi f \to \phi f$ via the $h - \phi - \phi$ coupling does not work (with 'f' being a SM fermion), for only light SM fermions exist in the universe and their couplings to h are suppressed by small Yukawa couplings.

the ϕ-decay width. The reason why this island region is isolated is that the displaced vertex search of $B \to X_s \phi$ at the BaBar experiment ruled out the parameter region of $0.5\,\mathrm{GeV} \lesssim m_\phi \lesssim 1.5\,\mathrm{GeV}$ and $5 \times 10^{-4} \lesssim |\sin\theta| \lesssim 10^{-3}$. The step-like structure at $m_\phi \sim 2\text{–}4\,\mathrm{GeV}$ is because $\phi \to gg, c\bar{c},\ \tau^-\tau^+$ opens and the branching fraction of the observable channel, e.g. $\phi \to \mu^-\mu^+$, is suppressed.

(f) When the mediator becomes heavier than $5\,\mathrm{GeV}$, the limit on the mixing angle is set by the direct dark matter detection at underground experiments. This is because the dark matter is required to be heavier than the mediator in most of the parameter region, for the relic abundance condition is satisfied by the $\chi\chi \to \phi\phi$ annihilation process, and the direct dark matter detection put a sever limit when $m_\chi \gtrsim 5\,\mathrm{GeV}$. Only the exception is found in extended region at $m_\phi \sim$ several $10\,\mathrm{GeV}$ and $|\sin\theta| \sim 10^{-2}$, where the relic abundance condition is satisfied by the s-channel resonance-enhanced annihilation $\chi\chi \to \phi \to f\bar{f}$.

(g) The SN1987A constraint [52] is over depicted on the $(m_\phi, |\sin\theta|)$-plane as a darker transparent color region at $5 \cdot 10^{-7} \lesssim |\sin\theta| \lesssim 3 \cdot 10^{-5}$ and $m_\phi \lesssim \mathcal{O}(100)\,\mathrm{MeV}$. It is seen that the SN1987A constraint is potentially important, for it restricts the parameter region that is not restricted by other constraints. The exclusion region by the SN1987A constraint can be understood as follows: the mediator interaction is too weak to affect the SN cooling when $|\sin\theta| \lesssim 5 \cdot 10^{-7}$, while the mediator decays or trapped inside the SN when $|\sin\theta| \gtrsim 3 \cdot 10^{-5}$ and does not contribute the cooling. When $m_\phi \gtrsim T_c \simeq 30\,\mathrm{MeV}$ with T_c being the critical core temperature of SN1987A, the mediator cannot be thermally, thus efficiently, produced.

4.3 Future prospects

Results of our analysis for the future prospects of the minimal WIMP model projected on the (m_χ, m_ϕ)- and $(m_\chi, |\sin\theta|)$-planes are shown in the left and right panels of figure 4, respectively, where we have assumed that dark matter signals as well as mediator signals are not detected at any near future experiments/observations discussed in the previous section. Our results projected on all planes of input parameters are again found in appendix C.2.

(h) In the left panel of figure 4, comparing with the one in figure 3, the lower limit on m_ϕ becomes severer as $m_\phi \gtrsim 20\,\mathrm{MeV}$ in the range of $m_\chi \lesssim 300\,\mathrm{MeV}$ due to the future-expected constraint from the ΔN_{eff} measurement. Together with the relic abundance condition, it also gives a lower limit on the WIMP mass. On the other hand, the lower limit on the mediator mass in the range of $m_\chi \gtrsim 300\,\mathrm{MeV}$ becomes stronger than those in figure 3 because the significant upgrade will be expected at the direct dark matter detection in the near future. The void region, which is located at $m_\chi \sim 1\,\mathrm{GeV}$ and $m_\phi \sim$ a few hundred MeV, is because of the constraint from the SHiP experiment. In addition, the mixing angle in this region is required to be enough large from the kinematical equilibrium condition when $m_\chi \sim 1\,\mathrm{GeV}$, while such a mixing angle will be ruled out if no signal is detected at the experiment.
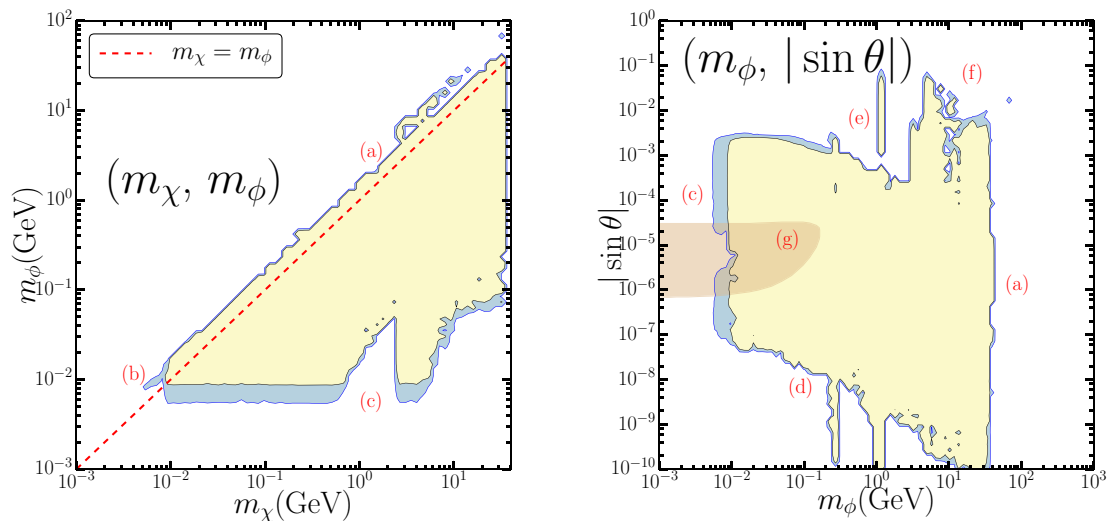
Figure 3. Results of our analysis for the present status of the minimal WIMP model projected on the (m_χ, m_ϕ)- and $(m_\phi, |\sin\theta|)$-planes at 68% C.L. (yellow) and 95% C.L. (blue). Please see figures in appendix C.1 for those who are interested in results projected on all planes of input parameters. The alphabet on each edge of the contour corresponds to each paragraph of the main text.
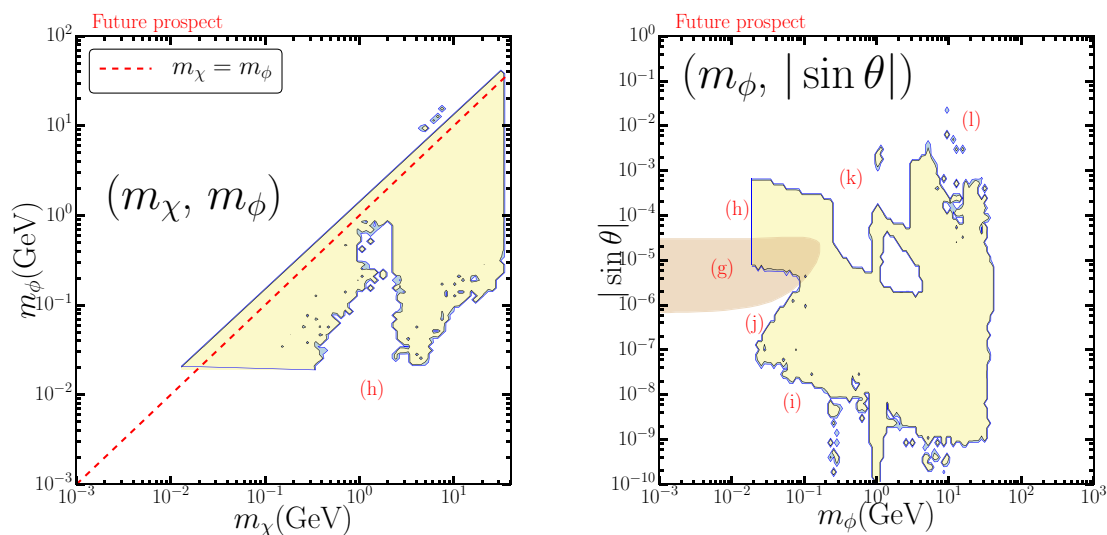

Figure 4. Results of our analysis for the future prospects of the minimal WIMP model projected on the (m_χ, m_ϕ)- and $(m_\chi, |\sin\theta|)$-planes at 68% C.L. (yellow) and 95% C.L. (blue). Please see figures in appendix C.2 for those who are interested in results projected on all planes of input parameters. The alphabet on each edge of the contour corresponds to each paragraph of the main text.

(i) In the right panel of figure 4, the lower limit on the mixing angle $|\sin\theta|$ in the range of $m_\phi \lesssim 10\,\text{GeV}$ is not very much different from the previous one in figure 3. On the other hand, when $m_\phi \gtrsim 10\,\text{GeV}$, the region of $|\sin\theta| \lesssim \mathcal{O}(10^{-9})$, where it was survived in figure 3, is removed in figure 4. This is because the search for the Higgs invisible decay at the HL-LHC experiment rules out the region if no signal of the decay is detected there.

(j) The excluded region at $m_\phi \lesssim 100\,\text{MeV}$ and $|\sin\theta| \sim 10^{-6}$ is from the direct dark matter detection at future underground experiments. This is because, as discussed in appendix C, the dark matter mass must be larger than $200\,\text{MeV}$ to satisfy the kinematical equilibrium condition in this parameter region, and a small mediator mass leads to a large scattering cross section between the dark matter and a nucleon despite of a suppressed mixing angle. The sensitive future direct dark matter detection thus start proving this region.

(k) On the other hand, the upper limit on the mixing angle is also very much improved. The SHiP experiment will change the landscape significantly at the region of $0.3\,\text{GeV} \lesssim m_\phi \lesssim 4\,\text{GeV}$ and $2 \times 10^{-6} \lesssim |\sin\theta| \lesssim 10^{-4}$, if no mediator signal is detected. Moreover, LHCb and Belle II experiments could also put severe constraints on $|\sin\theta|$ in the range of $0.5\,\text{GeV} \lesssim m_\phi \lesssim 5\,\text{GeV}$, while the direct dark matter detection at future underground experiments could put a severer constraint on the mixing angle $|\sin\theta|$ in the range of $m_\phi \gtrsim 5\,\text{GeV}$.

(l) Finally, let us comment on the resonant annihilation region, where the relation $m_\phi \sim 2m_\chi$ holds. As seen in the right panel of figure 4, this region could still survive in the near future at $m_\phi \sim 2m_\chi \sim 10\,\text{GeV}$ and $|\sin\theta| \sim 10^{-2}$, though it obviously shrunk compared to the region in figure 3. This is because that the sensitivity of the direct dark matter detection is significantly improved when the dark matter mass is greater than several GeV.

4.4 Implication of the results

Here, we consider implication of the results discussed in previous two sub-sections. In figure 5, some results projected on various observables are shown, where the region consistent with all present experimental results discussed so far is depicted using the same color code as those in figures 3 and 4. Moreover, the region which will survive (at 95 % C. L.) even if no dark matter and mediator signals are detected in the near future is also over depicted as a red line. We discuss below implication of the results in each panel of figure 5 in some detail.

In the top left panel, the results are projected on the $(m_\chi, \sigma_{\text{SI}})$-plane, where σ_{SI} is the spin-independent scattering cross section between the WIMP and a nucleon, as defined in section 3.2.3. As expected, the direct dark matter detection is effective to directly search for the WIMP as far as σ_{SI} is large enough.[25] On the other hand, it can be also seen that the wide region with a very small value of σ_{SI} remains survived even in future, especially

---

[25]The improvement of the lower limit on m_χ in the near future is because of the provisional ΔN_{eff} constraint.
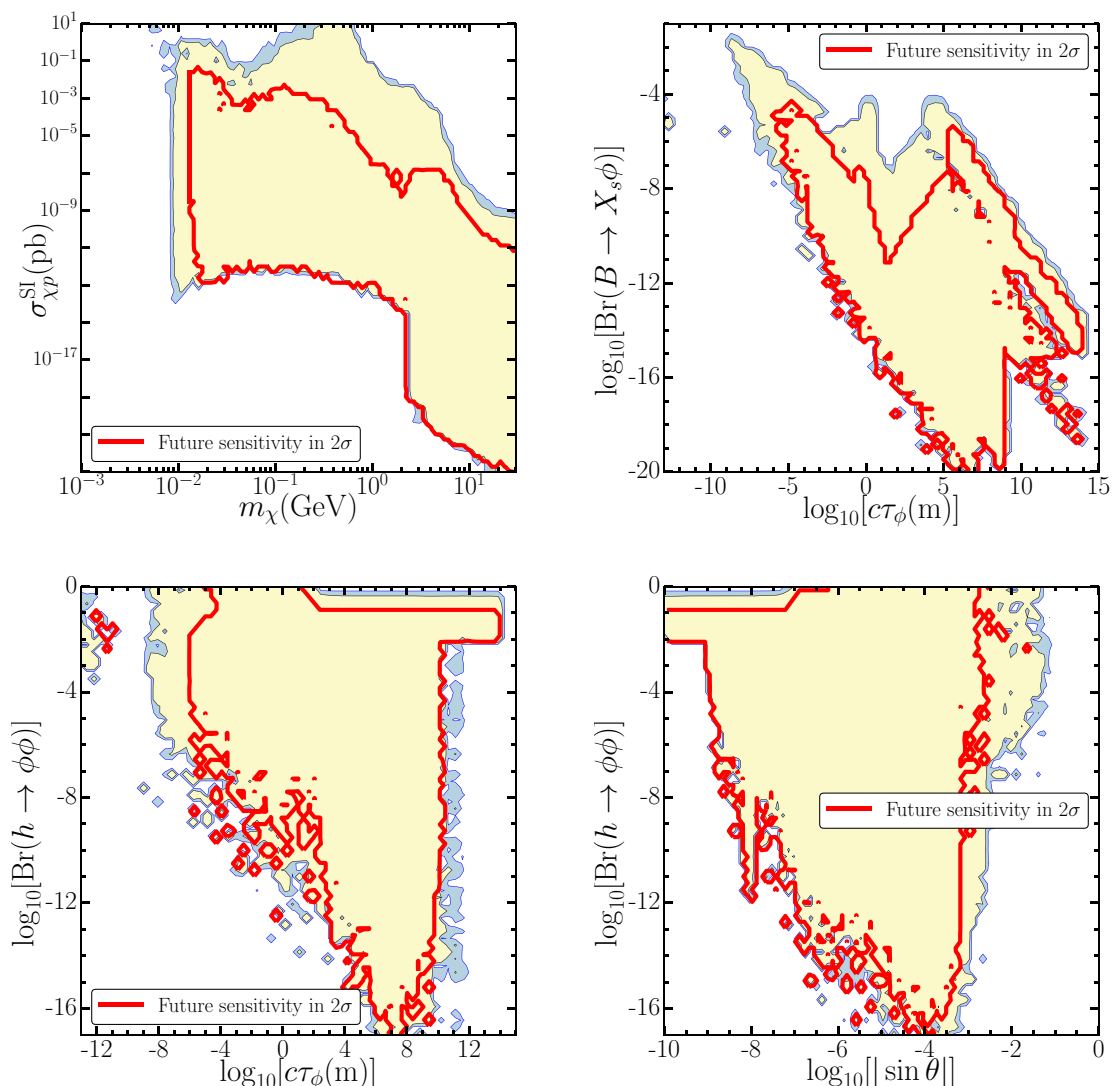
Figure 5. Results of our analysis for the present status of the minimal WIMP model projected on the (m_χ, m_ϕ)- and $(m_\phi, |\sin\theta|)$-planes at 68% C.L. (yellow) and 95% C.L. (blue). Please see figures in appendix C.1 for those who are interested in results projected on all planes of input parameters.

when m_χ is larger than $\mathcal{O}(1)\,\mathrm{GeV}$. This originates in the survived parameter region with a suppressed mixing angle ($\sin\theta \sim 0$), and thus other experiments are required to test it.

In the top right panel, we present the favored regions for $c\tau_\phi$ vs. $\mathrm{Br}(B \to X_s\phi)$ with τ_ϕ and $\mathrm{Br}(B \to X_s\phi)$ being the lifetime of the mediator and the decay branching fraction of the B meson into a mediator and a hadronic system with a strangeness [135], respectively. It is found that the region with $c\tau_\phi \simeq (10^{-3}\text{–}10^3)\,\mathrm{m}$ will be well searched for thanks to the flavor experiments. Belle II and SHiP experiments will play significant roles for the search in regions of $10^{-3}\,\mathrm{m} \lesssim c\tau_\phi \lesssim 1\,\mathrm{m}$ and $1\,\mathrm{m} \lesssim c\tau_\phi \lesssim 10^3\,\mathrm{m}$, respectively. On the other hand, the direct dark matter detection plays an important role to search for the region of

$c\tau_\phi \lesssim 10^{-3}$, for both the WIMP and the mediator are required to be heavy enough to have such a short mediator lifetime. Finally, we found that the direct dark matter detection and BBN constraints will play some roles to search for the region of $c\tau_\phi \gtrsim 10^5\,\mathrm{m}$, though the wide parameter region survives even in the future due to the small mixing angle.

In the bottom left panel, we present the favored regions for $c\tau_\phi$ vs. $\mathrm{Br}(h \to \phi\phi)$, where $\mathrm{Br}(h \to \phi\phi)$ is the branching fraction of the exotic Higgs decay into two mediators. As discussed above, the direct dark matter detection will play a crucial role in the near future, in particular to search for the region of $c\tau_\phi \lesssim 10^{-5}\,\mathrm{m}$. On the other hand, other experiments will also play important roles to search for the region of $c\tau_\phi \gtrsim 10^{-5}\,\mathrm{m}$. For instance, LHC experiment will search for the region by observing the exotic Higgs decay when its branching fraction is large enough, while cosmological observations (ΔN_{eff} measurement, etc.) and flavor experiments (Belle II and SHiP experiments, etc.) will search for the same region but when the branching fraction of the exotic Higgs decay is very suppressed.

It is worth emphasizing here that the constraint from the exotic Higgs decay plays a complemental role to others as shown in the bottom right panel. Magnitude of WIMP and mediator signals is proportional to the mixing angle squared in most of experiments and observations, while that of the exotic Higgs decay does not rely on the mixing angle. This is because the mediator is required to have an interaction to SM particles with enough magnitude to satisfy the kinematical equilibrium condition, and it is achieved by the $\phi - \phi - h$ interaction (originating in the $\Phi^2|H|^2$ operator) when the mixing angle (originating in the $\Phi|H|^2$ operator) is suppressed. As a result, the precise measurement of the nature of the Higgs boson will be mandatory in the future to test the minimal WIMP model, and it could be done by future lepton colliders such as ILC [150], CEPC [151] and FCC-ee [152].

5   Summary

We have studied a minimal (renormalizable) model with a light fermionic WIMP and a light scalar mediator whose decay width is computed with uncertainties from non-perturbative QCD effects properly taken into account. In order to investigate the present status and future prospects of the light WIMP and the light scalar mediator, we have performed a comprehensive likelihood analysis involving all robust constraints obtained so far. In addition, we also discuss those future sensitivities which will be obtained in the near future (if no WIMP signals are detected) from particle physics experiments as well as cosmological and astrophysical observations. We have carefully involved a kinematical equilibrium condition assuming that the (chemical) freeze-out of the light WIMP occurred when it was in kinematically equilibrium with the thermal bath composed of SM particles. We have paid particular attention to a possible case that the light WIMP can be in the kinematical equilibrium through existent mediator particles at the freeze-out epoch even if the WIMP does not have an interaction directly to SM particles with enough magnitude.

A very wide parameter region is still surviving at present in the region of $10\,\mathrm{MeV} \lesssim m_\phi \lesssim m_\chi$, and it is found that many kinds of experiments and observations are required to test the WIMP in the near future. Direct dark matter detection experiments will play a crucial role in particular to search for the WIMP with the mass greater than $\mathcal{O}(100)\,\mathrm{MeV}$, while

flavor experiments will play a significant role to search for the mediator in the wide region of its mass. Moreover, precise cosmological observations such as the ΔN_{eff} measurement are mandatory to search for a very light mediator whose mass is of the order of $10\,\text{MeV}$.

On the other hand, a wide parameter region will remain survived in the near future even if no WIMP/mediator signals are detected in the experiments. In principle, the experiments rely on the mixing angle (originating in the $\Phi|H|^2$ operator) to detect WIMP/mediator signals, while all cosmological conditions (relic abundance and kinematical equilibrium conditions) can be satisfied even if the mixing angle is very suppressed. This is because the annihilation process within the dark sector, the $\chi\chi \to \phi\phi$ process, satisfies the relic abundance, while the kinematical equilibrium condition is satisfied through the other interaction between the mediator and SM particles, namely the $\phi - \phi - h$ interaction (originating in the $\Phi^2|H|^2$ operator). As a result, a future experiment which is sensitive to this interaction is mandatory to test the remaining parameter region, and it can be achieved by measuring the nature of the Higgs boson precisely. In particular, future lepton colliders such as ILC [150], CEPC [151] and FCC-ee [152] will provide an ideal environment for this measurement.

Acknowledgments

A   Preselection criteria

As mentioned in section 3.1, we apply preselection criteria on model parameters as $c_p = 0$, $|\theta| \le \pi/6$ and $V(\eta, \xi) \ge V(v_\Phi, v_H)$ in the range of $|\xi| \le 1\,\text{TeV}$ and $|\eta| \le 1\,\text{TeV}$, where ξ and η are defined as $\Phi = \eta$ and $H = (0, \xi/\sqrt{2})^T$, respectively. The region of the parameters survived after applying the criteria is shown in figure 6. The survived parameter region is further investigated by the subsequent likelihood analysis, as discussed in section 3.

Since the mediator mass is eventually constrained to be less than, or at least the same order of m_χ to satisfy the relic abundance condition, as seen in section B.2, let us focus on the region of $m_\phi \lesssim \mathcal{O}(10)\,\text{GeV}$ and discuss how the preselection criteria work to restrict the model parameter space of the model. First, it can be seen in the result on the (m_ϕ, μ_Φ^2)-plane that the parameter μ_Φ^2 is constrained to be $|\mu_\Phi^2| \lesssim (100\,\text{GeV})^2$, because otherwise m_ϕ would be much heavier than $\mathcal{O}(10)\,\text{GeV}$. Next, the quartic coupling of the field Φ is constrained to be $\lambda_\Phi \gtrsim 0$ as seen in the result on the (m_ϕ, λ_ϕ)-plane to make our vacuum stable, because the contribution from the quadratic term $\mu_\Phi^2 \Phi^2$ is small. Finally, the parameter of
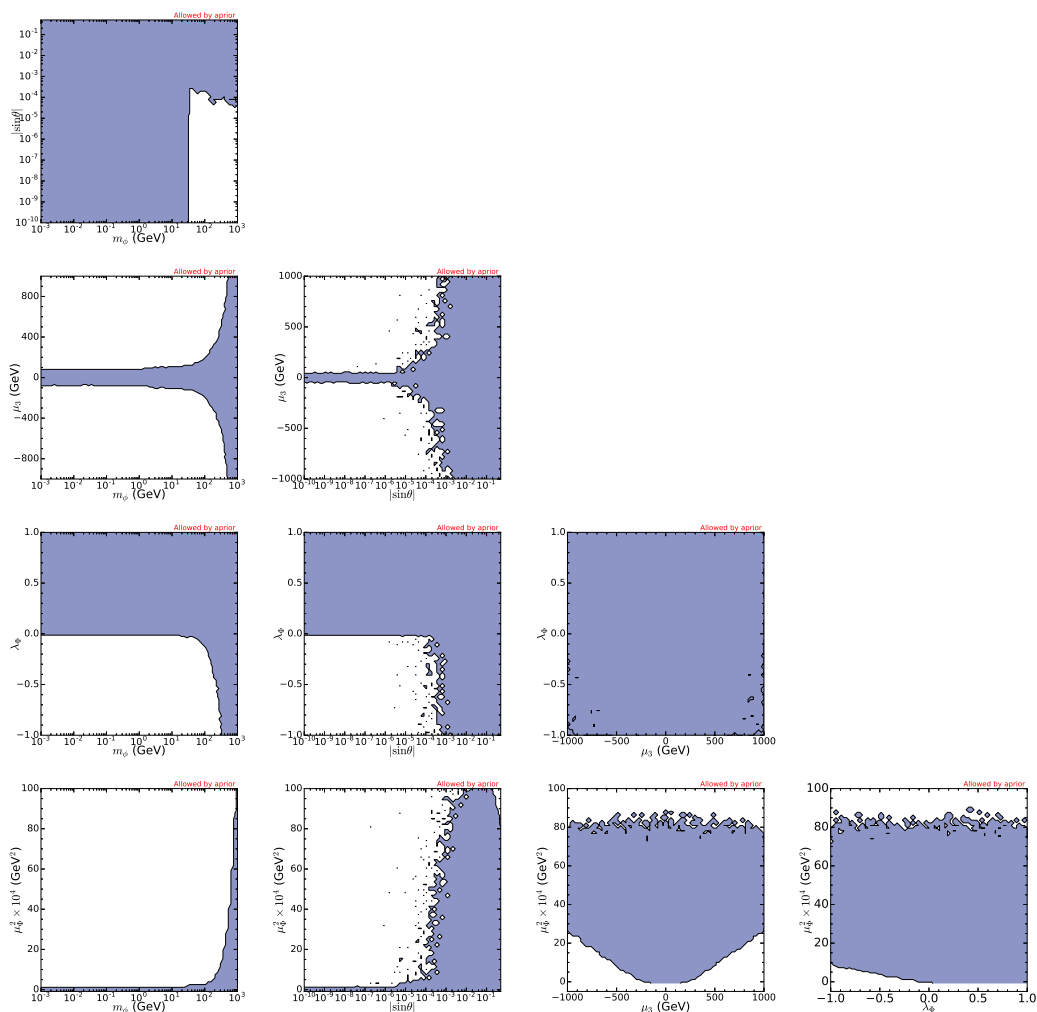
Figure 6. Model parameter region survived after applying preselection criteria in section 3.1.

the cubic term is constrained to be $|\mu_3| \lesssim 100\,\text{GeV}$, as seen in the result on the (m_ϕ, μ_3)-plane, to suppress the negative contribution to the potential in the region of $\Phi = \eta \lesssim 0$.

B Kinematical equilibrium condition

In this appendix, we first write down all the reaction rates $\Gamma_{\chi\text{SM}}$ $\Gamma_{\chi\phi}$ and $\Gamma_{\phi\text{SM}}$ in a concrete form. Then, we present the model parameter region survived after applying the kinematical equilibrium condition as well as the preselection criteria and the relic abundance condition.

B.1 The reaction rates

We first consider the reaction rate between the WIMP and SM particles $\Gamma_{\chi\text{SM}}$. Considering the fact that the WIMP is always non-relativistic while SM particles are relativistic during

the freeze-our process, the reaction rate $\Gamma_{\chi\mathrm{SM}}$ is described by the following formula:

$$\Gamma_{\chi\mathrm{SM}} = \frac{2T_f}{m_\chi} \sum_i \langle \sigma_{\chi\mathrm{SM}_i} v \rangle_{T_f} \, n_{\mathrm{SM}_i}(T_f), \tag{B.1}$$

where $n_{\mathrm{SM}_i}(T_f)$ is the number density of the SM particle 'i' at the freeze-out temperature. Since relativistic SM particles dominantly contribute to the rate, its approximate form is given by $g_i \zeta(3) T_f^3 / \pi^2$ if it is bosonic while $3 g_i \zeta(3) T_f^3 / (4\pi^2)$ if it is fermionic. Here, g_i is the color and spin degrees of freedom of the particle 'i'.[26] The prefactor $2T_f/m_\chi$ comes from the fact that about $m_\chi/(2T_f)$ times collisions are required to maintain the kinematical equilibrium, because the typical momentum transfer in a single collision is estimated to be $\Delta q^2/q^2 \sim 2T_f/m_\chi \ll 1$ in a stochastic process [153–155]. The thermal-averaged scattering cross section $\langle \sigma_{\chi\mathrm{SM}_i} v \rangle_{T_f}$ is calculated according to the following formula [156]:

$$\langle \sigma_{\chi\mathrm{SM}_i} v \rangle_{T_f} = \frac{2\pi^2 T_f \int_{(m_\chi + m_{\mathrm{SM}_i})^2}^{\infty} ds \, s^{3/2} \sigma_{\chi\mathrm{SM}_i} \left(1 - \frac{2(m_\chi^2 + m_{\mathrm{SM}_i}^2)}{s} + \frac{(m_\chi^2 - m_{\mathrm{SM}_i}^2)^2}{s^2} \right) K_1(s^{1/2}/T_f)}{\left[4\pi T_f m_\chi^2 K_2(m_\chi/T_f) \right] \left[4\pi T_f m_{\mathrm{SM}_i}^2 K_2(m_{\mathrm{SM}_i}/T_f) \right]}, \tag{B.2}$$

where $K_n(z)$ is the modified Bessel function of the 2nd kind. When the freeze-out temperature is less than the QCD scale, namely $T_f \lesssim \Lambda_{\mathrm{QCD}} \simeq 155\,\mathrm{MeV}$ [157], the scattering process between the WIMP and an electron or a muon by the exchange of ϕ in the t-channel dominantly contributes to the reaction rate. On the other hand, when $T_f \gtrsim \Lambda_{\mathrm{QCD}}$, scattering processes with various SM particles contribute to the rate. Those are scattering processes of the WIMP with a muon, a tau lepton as well as strange, charm and bottom quarks.

We next consider the reaction rate between the WIMP and the mediator, $\Gamma_{\chi\phi}$. Since the mediator can be either relativistic or non-relativistic at the freeze-out temperature depending on its mass m_ϕ, the rate is given by the formula which is similar to that in eq. (B.1):

$$\Gamma_{\chi\phi} = F\left(\frac{m_\chi}{T_f}, \frac{m_\phi}{T_f} \right) \langle \sigma_{\chi\phi} v \rangle n_\phi(T_f), \tag{B.3}$$

where $n_\phi(T_f)$ is the number density of the mediator at the freeze-out temperature. The prefactor $F(x_1, x_2)$ is the extension of that in eq. (B.1), and it can be estimated based on the following discussion. First, when $x_1 \gg 1$ & $x_2 \ll 1$, or $x_1 \ll 1$ & $x_2 \gg 1$, the prefactor should be the same as the one in eq. (B.1), namely $F(x_1, x_2) = 2/x_1$ or $2/x_2$. Next, when both arguments are small enough, the prefactor $F(x_1, x_2)$ should be $\mathcal{O}(1)$, for the momentum transfer $\Delta q^2/q^2$ between relativistic particles is so large that a single collision is (almost) enough to maintain the kinematical equilibrium. Detailed calculation of the momentum transfer between relativistic particles expects that the prefactor is $F(x_1, x_2) \simeq 1/2$. Finally, when the both arguments are (almost) the same and large enough, the prefactor should be $\mathcal{O}(1)$ again, for the momentum transfer is expected to be efficient between two non-relativistic particles whose masses are (almost) the same. Taking the above discussion

---

[26]The exact formula of the number density, $\int d^3k \, g_i / [\exp(-E_k/T) \mp 1]$, is used in our numerical analysis.

into account, we use the following formula for estimating the prefactor $F(x_1, x_2)$:

$$F(x_1, x_2) = \begin{cases} 1/2 & \text{for } x_1 \leq 4 \; \& \; x_2 \leq 4 \\ 2/x_1 & \text{for } x_1 \geq 4 \; \& \; x_2 \leq 4 \\ 2/x_2 & \text{for } x_1 \leq 4 \; \& \; x_2 \geq 4 \\ \text{NR}(x_1, x_2) & \text{for } x_1 \geq 4 \; \& \; x_2 \geq 4, \end{cases}$$
$$\text{NR}(x_1, x_2) = \begin{cases} x_2/(2x_1) & \text{for } x_1 \geq x_2 \\ x_1/(2x_2) & \text{for } x_2 \geq x_1. \end{cases} \tag{B.4}$$

The scattering process between the WIMP and the mediator ϕ comes from diagrams exchanging the WIMP in the s- and u-channels as well as a diagram exchanging the mediator in the t-channel. Its thermal-averaged scattering cross section, $\langle \sigma_{\chi\phi} v \rangle$, is calculated using the same formula as that in eq. (B.2) with m_{SM_i} being replaced by the mediator mass m_ϕ.

We finally consider the reaction rate between the mediator ϕ and SM particles. Three different processes contribute to the rate: the (inverse) decay process $\Gamma_{\phi\leftrightarrow\text{SMs}}$, the scattering process $\Gamma_{\phi\text{SM}\leftrightarrow\phi\text{SM}}$ and the absorption (emmision) process $\Gamma_{\phi\text{SM}\leftrightarrow\text{SMs}}$. The contribution from *the (inverse) decay process* is given by the thermal-average of the total decay width of the mediator Γ_ϕ that has been discussed in section 2.4. Its explicit form is given as follows:

$$\Gamma_{\phi\leftrightarrow\text{SMs}} = \left\langle \frac{1}{\gamma} \right\rangle \Gamma_\phi = \frac{\int_1^\infty d\gamma\, \gamma^{-1} \left[\gamma(\gamma^2-1)^{1/2} e^{-\gamma m_\phi/T}\right]}{\int_1^\infty d\gamma \left[\gamma(\gamma^2-1)^{1/2} e^{-\gamma m_\phi/T}\right]} \Gamma_\phi, \tag{B.5}$$

where γ is the so-called the Lorentz gamma factor, and the distribution in the square brackets is the Maxwell-Juttner distribution. The contribution from *the scattering process* is given by a similar formula discussed in eq. (B.1). Since the mediator can be non-relativistic or relativistic at the freeze-out temperature T_f, while relativistic SM particles dominantly contribute to the reaction rate, the explicit form of the contribution is given as follows:

$$\Gamma_{\phi\text{SM}\leftrightarrow\phi\text{SM}} = \sum_i F\left(\frac{m_\phi}{T_f}, \frac{m_{\text{SM}_i}}{T_f}\right) \langle \sigma_{\phi\text{SM}_i} v \rangle_{T_f} n_{\text{SM}_i}(T_f), \tag{B.6}$$

When $T_f \leq \Lambda_{\text{QCD}}$, the scattering process between ϕ and an electron or a muon dominantly contributes to the reaction rate. On the other hand, when $T_f \geq \Lambda_{\text{QCD}}$, scattering processes of ϕ with a muon, a tau lepton as well as strange, charm and bottom quarks contribute to the rate. Corresponding thermal-averaged scattering cross section are calculated using the same formula as that in eq. (B.2) with m_χ being replaced by m_ϕ. The contribution from *the absorption (emmision) process* is given by the same formula as that in eq. (B.6) again:

$$\Gamma_{\phi\text{SM}\leftrightarrow\text{SMs}} = \sum_i F\left(\frac{m_\phi}{T_f}, \frac{m_{\text{SM}_i}}{T_f}\right) \langle \sigma'_{\phi\text{SM}_i} v \rangle_{T_f} n_{\text{SM}_i}(T_f), \tag{B.7}$$

where the scattering cross section $\sigma_{\phi\text{SM}_i}$ in eq. (B.6) is replaced by the cross section of the absorption (emmision) process, $\sigma'_{\phi\text{SM}_i}$. After the QCD phase transition, $T_f \leq \Lambda_{\text{QCD}}$, the following three processes contribute to this reaction rate: $\phi\gamma \to f\bar{f}$, $\phi f \to \gamma f$, $\phi\bar{f} \to \gamma\bar{f}$,
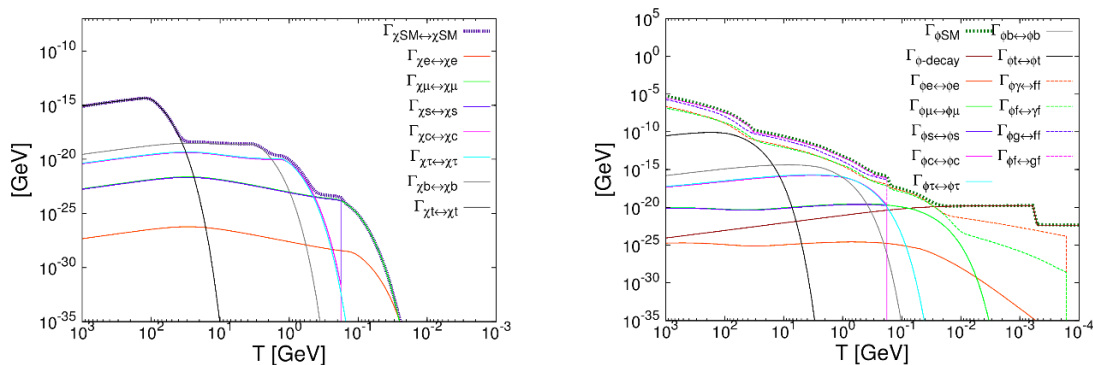
Figure 7. Processes contributing to the rates $\Gamma_{\chi\text{SM}}$ (left panel) and $\Gamma_{\phi\text{SM}}$ (right panel) around the freeze-out temperature T_f. Model parameters are set to be the same as those adopted in figure 2.

where f is an electron or a muon, while $\bar{f}$ is its anti-particle. On the other hand, when $T_f \geq \Lambda_{\text{QCD}}$, in addition to the above processes, other three processes, $\phi g \to q\bar{q}$, $\phi q \to gq$ and $\phi\bar{q} \to g\bar{q}$ also contribute to the rate with q ($\bar{q}$) being a quark (anti-quark). Their corresponding thermal-averaged cross sections are calculated by the same formula as that in eq. (B.6). As a result, the reaction rate between the mediator ϕ and SM particles is given by the sum of all processes mentioned above: $\Gamma_{\phi\text{SM}} = \Gamma_{\phi\leftrightarrow\text{SMs}} + \Gamma_{\phi\text{SM}\leftrightarrow\phi\text{SM}} + \Gamma_{\phi\text{SM}\leftrightarrow\text{SM}s}$.

As a demonstration, we show how each concrete process contributes to the reaction rates $\Gamma_{\chi\text{SM}}$ and $\Gamma_{\phi\text{SM}}$ in the left and the right panels of figure 7, respectively, at around the freeze-out temperature T_f. Model parameters are set to be the same as those adopted in figure 2, namely $(m_\chi, c_s, m_\phi, \sin\theta, \mu_3)$ are fixed to be $(200\,\text{MeV}, 0.022, 100\,\text{MeV}, 10^{-3}, 10\,\text{MeV})$.

B.2 Parameter region after the equilibrium condition applyied

Here, we present the model parameter region survived after applying the kinematical equilibrium condition as well as the preselection criteria and the relic abundance condition. As we mentioned in section 3.1.4, model parameters $(m_\chi, c_s, m_\phi, \theta, \mu_3)$ among seven independent parameters $(m_\chi, c_s, m_\phi, \theta, \mu_3, \mu_\Phi^2, \lambda_\Phi)$ are relevant to the following discussion, so that we show the result in figure 8 for the five parameters. In other words, parameters μ_Φ^2 and λ_Φ become nuisance parameters in the following phenomenological studies in this paper.

First, from the result on the (m_χ, m_ϕ)-plane, the mediator mass shall be at most around the WIMP mass to satisfy the relic abundance condition. It leads to the fact that the mediator is lighter than $\mathcal{O}(10)\,\text{GeV}$ as long as we are discussing the light WIMP scenario. The upper limit on the mediator mass is also seen from the results on other planes spanned by m_ϕ.

Next, as seen from the result on the $(m_\chi, |\sin\theta|)$-plane, the lower limit on $|\sin\theta|$ exists when $m_\chi \lesssim 2\,\text{GeV}$, which is required by the kinematical equilibrium condition. On the other hand, when $m_\chi \gtrsim 2\,\text{GeV}$, the mixing angle is not bounded from below. This is because ϕ can be in a kinematical equilibrium with SM particles not by the mixing
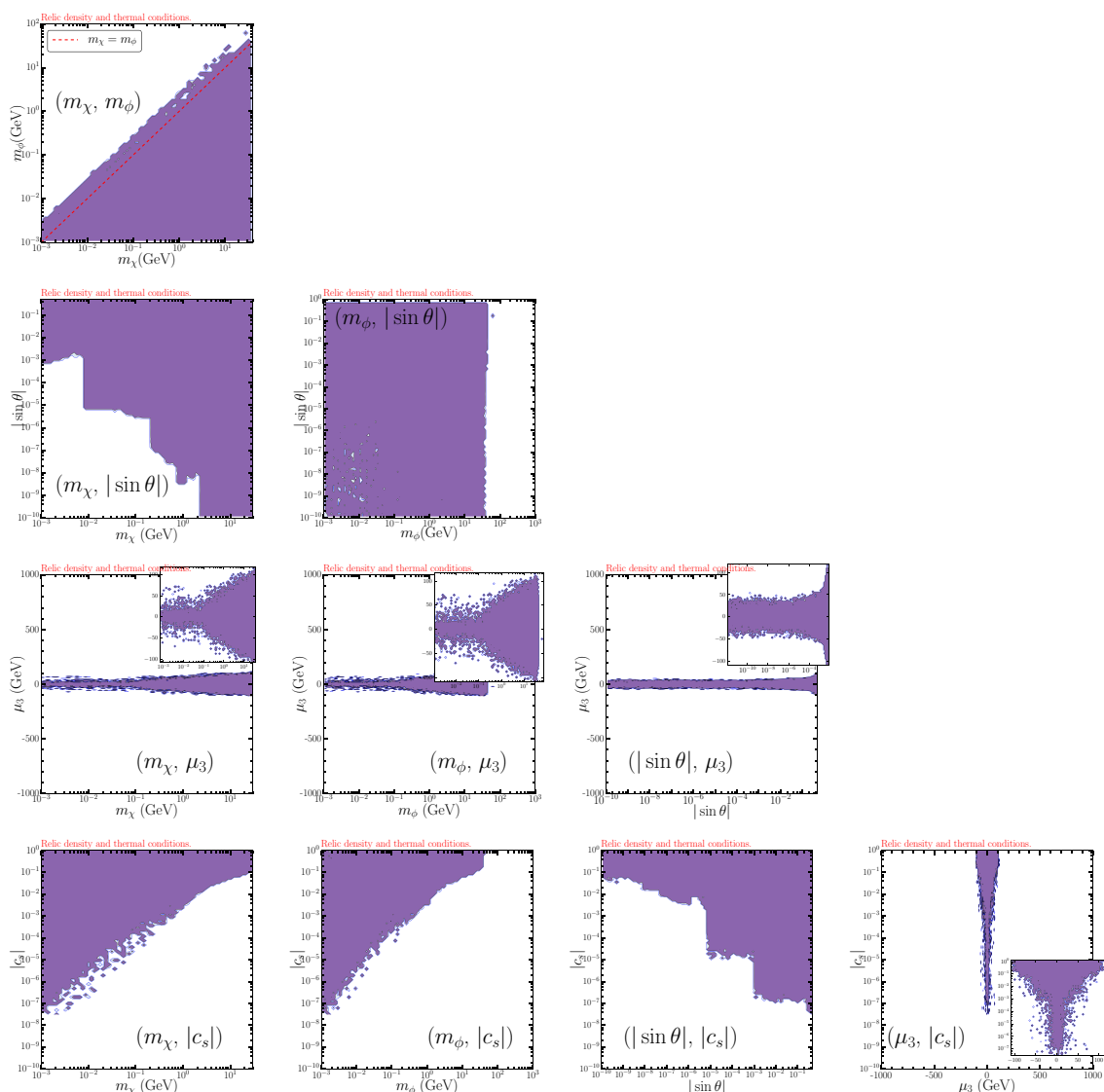
Figure 8. Model parameter region survived after applying relic abundance and kinematical equilibrium conditions discussed in section 3.2 as well as preselection criteria in the previous appendix.

angle but through interactions with an unsuppressed coupling $\lambda_{\Phi H}$ and not-so-suppressed Yukawa couplings.[27]

Third, the result on the planes spanned by the tri-linear coupling parameter μ_3 shows that the parameter is indeed restricted to be around $\mathcal{O}(100)\,\mathrm{GeV}$, as addressed in appendix A.

---

[27]The kinematical equilibrium is maintained by the $\phi f \to \phi f$ process with the Higgs boson being exchanged in the t-channel, where f is a SM fermion. This process is, however, suppressed when the freeze-out temperature is less than the scale of the QCD phase transition, so that we have $m_\chi \sim 20 T_f \gtrsim 20 \Lambda_{\mathrm{QCD}} \sim 2\,\mathrm{GeV}$.

Fourth, the coupling constant between the dark matter and the mediator $|c_s|$ is bounded from below due to the relic abundance condition, as can be seen from the result on the $(m_\phi, |c_s|)$-plane. Here, one might worry about that the relic abundance of the WIMP becomes too small in the region with small m_χ and large $|c_s|$, however this region is satisfied by the case where m_χ is slightly lighter than $2m_\phi$ but enough larger than m_ϕ, namely the relic abundance condition is satisfied by the $\chi\chi \to \phi \to f\bar{f}$ process instead of $\chi\chi \to \phi\phi$.

Fifth, the reason why the result on the $(m_\phi, |c_s|)$-plane is similar to that on the $(m_\chi, |c_s|)$-plane is simply because the relation $m_\phi \leq \mathcal{O}(m_\chi)$ holds in the whole parameter region.

Finally, on the $(|\sin\theta|, |c_s|)$-plane, the reason why the region with small $|\sin\theta|$ and small $|c_s|$ is excluded is as follows. When $|\sin\theta|$ is small, m_χ must be heavy enough to satisfy the kinematical equilibrium condition, as seen from the result on the $(m_\chi, |\sin\theta|)$-plane. On the other hand, m_χ must be light enough when c_s is small to satisfy the relic abundance condition, as seen in the result on the $(m_\chi, |c_s|)$-plane. As a result, small $|\sin\theta|$ and small $|c_s|$ are not simultaneously realized due to the contradiction between the two conditions.

C   Supplemental figures

C.1   Present status

Results of our analysis for the present status of the minimal WIMP model projected on all planes of input parameters $(m_\chi, c_s, m_\phi, \theta, \mu_3)$ are shown in figure 9. Since results on the (m_χ, m_ϕ)- and $(m_\phi, |\sin\theta|)$-planes are already discussed in section 4.2, we will focus mainly on those on other planes, spanned by different combinations of the input parameters.

First, the result on the $(m_\chi, |\sin\theta|)$-plane can be understood from the discussion in section 4.2, because the relic abundance condition requires $m_\chi \gtrsim m_\phi$ in most of parameter region. In fact, the lower limit on m_χ, the lower limit on $|\sin\theta|$ in the range of $m_\chi \gtrsim 2\,\mathrm{GeV}$ and the upper limit on $|\sin\theta|$ are understood in this manner. Only the exception is about the lower limit on $|\sin\theta|$ in the range of $m_\chi \lesssim 2\,\mathrm{GeV}$, where this region is excluded by the kinematical equilibrium condition, as already discussed in the previous appendix B.

Next, as seen from the result on the (m_ϕ, μ_3)-plane, the tri-linear coupling μ_3 is more constrained than the one in the corresponding panel of figure 8 when $m_\phi \lesssim 1\,\mathrm{GeV}$. We have confirmed that this is due to constraints from meson decay experiments as well as the vacuum stability condition which was imposed as one of preselection criteria: the mixing angle $|\sin\theta|$ is suppressed less than $\mathcal{O}(10^{-2})$ because of the collider constraints, so that μ_3 is required to be small enough when $m_\phi \lesssim 1\,\mathrm{GeV}$ in order to stabilize our vacuum. In a similar manner, results on the (m_χ, μ_3)- and $(|\sin\theta|, \mu_3)$-planes can be understood as well.

Third, concerning the result on the $(m_\phi, |c_s|)$-panel, the lower limit on m_ϕ comes mainly from the ΔN_{eff} constraint, though the upper-left corner with $|\sin\theta| \gtrsim 5 \times 10^{-2}$ is further constrained by the direct dark matter detection. The lower bound on the coupling $|c_s|$ in the bulk region is from the relic abundance condition, where it is satisfied by the $\chi\chi \to \phi\phi$ annihilation. The result on the $(m_\chi, |c_s|)$-plane is also understood in the same manner.
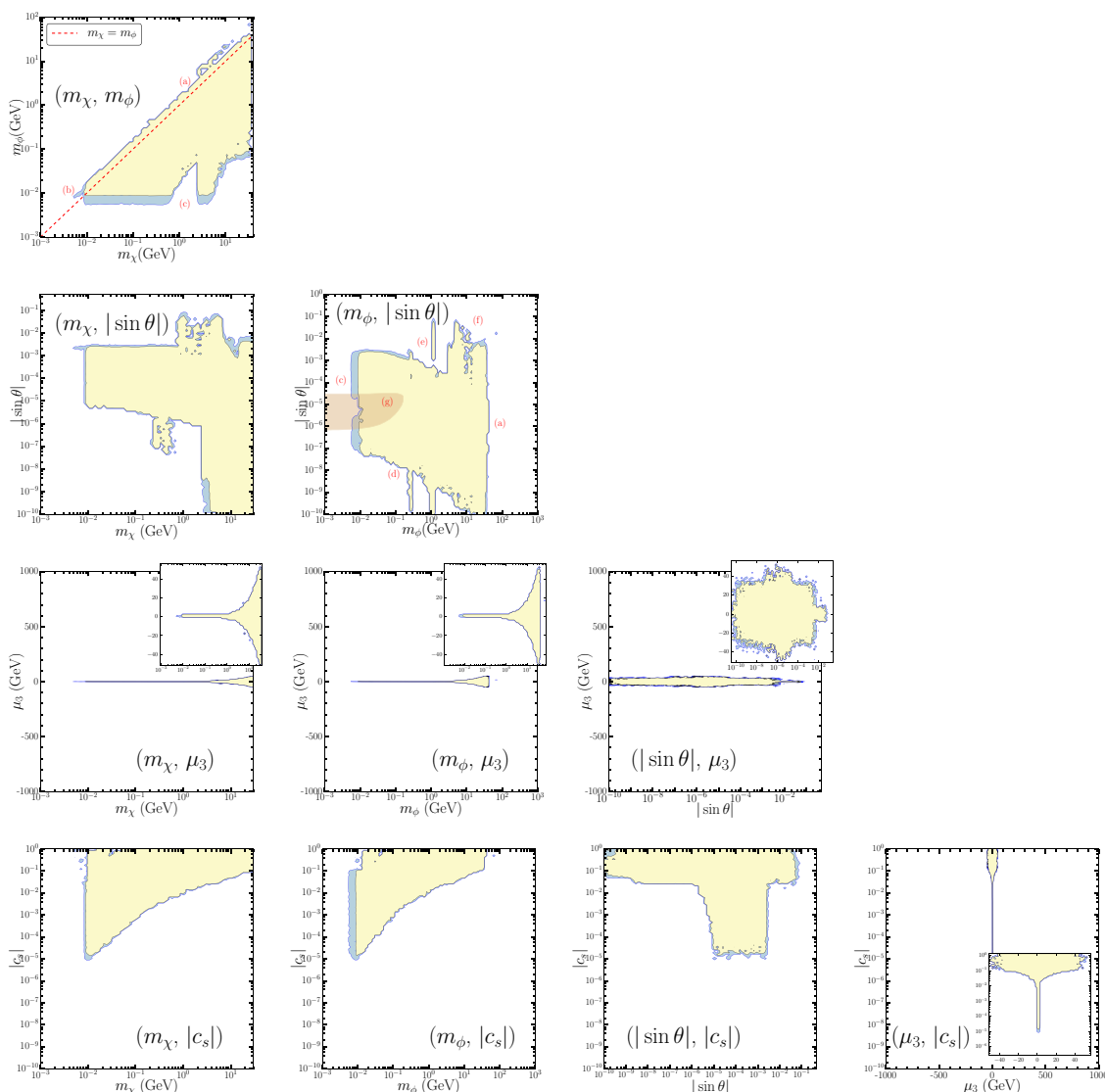
Figure 9. Present status of the minimal WIMP model projected on all planes of input parameters.

Fourth, the result on the $(\mu_3, |c_s|)$-plane can be understood by those on the $(m_\chi, |c_s|)$- and (m_χ, μ_3)-planes. When $|c_s|$ is smaller, a larger m_χ is not allowed due to the relic abundance condition. On the other hand, a smaller m_χ leads to a very restricted tri-linear coupling μ_3.

Finally, the result on the $(|\sin\theta|, |c_s|)$-plane can be understood as follows: the region of $|\sin\theta| \lesssim 10^{-3}$ is not very much different from that in the corresponding panel of figure 8. On the other hand, the region of $10^{-3} \lesssim |\sin\theta| \lesssim 10^{-1}$ is excluded by meson decay experiments, because a smaller $|c_s|$ indicates a smaller m_ϕ, as seen on the $(m_\phi, |c_s|)$-plane. The region of $|\sin\theta| \gtrsim 10^{-1}$ is excluded by collider experiments as well as the direct dark matter detection.

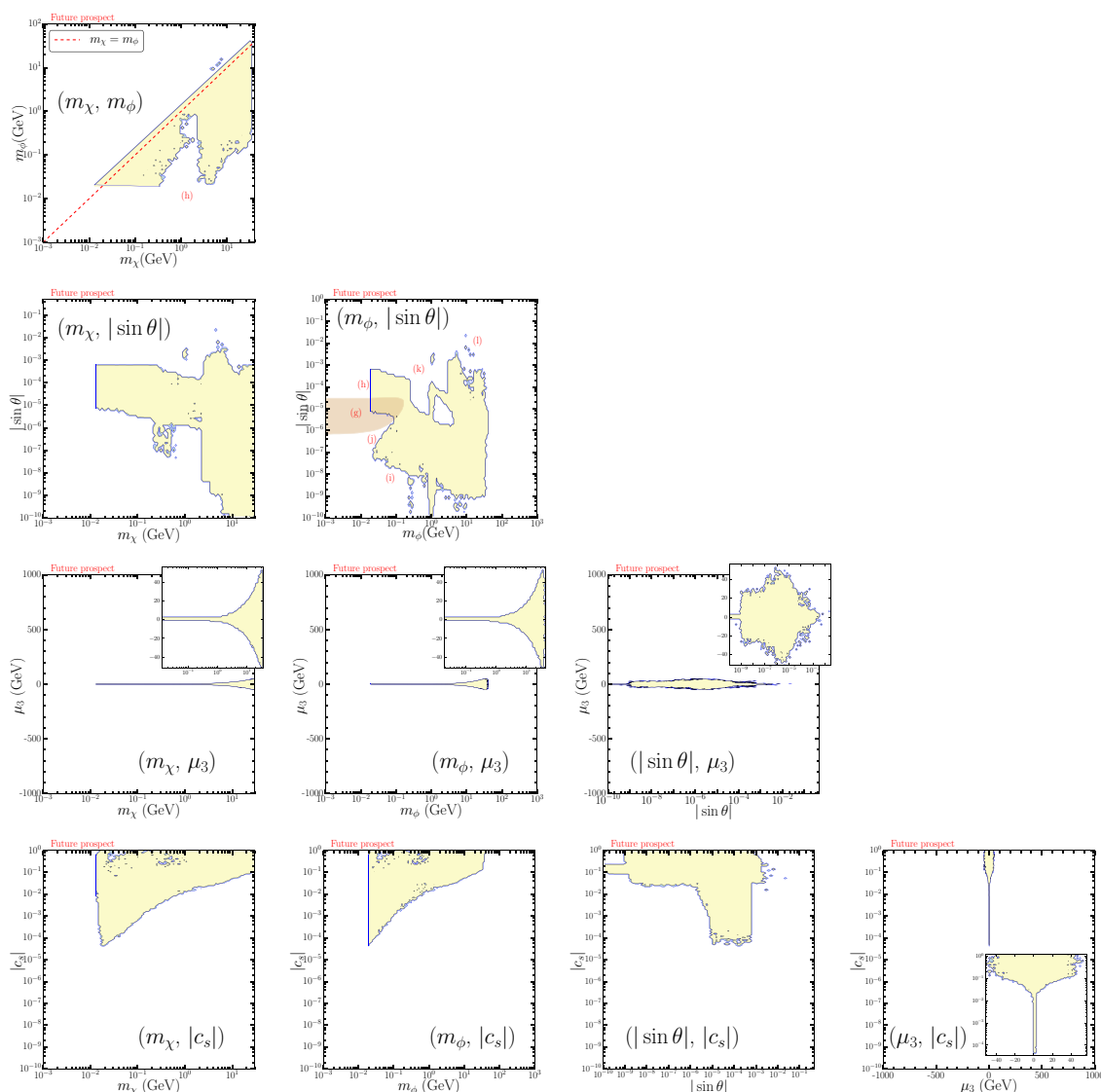**Figure 10**. Future prospects of the minimal WIMP model projected on all planes of input parameters.

C.2 Future prospects

Results of our analysis for the future prospects of the minimal WIMP model projected on all planes of input parameters are shown in figure 10, assuming that no dark matter and mediator signals are detected even in the near future. Since results on the (m_χ, m_ϕ)- and $(m_\phi, |\sin\theta|)$-planes are already discussed in section 4.3, we will focus on those on other planes spanned by different combinations of the input parameters, as in the previous subsection C.1.

First, the result on the $(m_\chi, |\sin\theta|)$-plane can be understood from the discussion in section 4.3: the allowed region shrank compared to the corresponding panel in figure 9 because of the provisional future-update on ΔN_{eff}, direct detection and collider constraints.

Next, the results on (m_ϕ, μ_3)-, (m_χ, μ_3)- and $(|\sin\theta|, \mu_3)$-planes show that the constraint on the tri-linear coupling μ_3 becomes severer than those of figure 9 even at $m_\phi \lesssim m_\chi \lesssim$ a few GeV, because future collider experiments will put a severer constraint on these mass region, if no signal is detected there. Moreover, μ_3 is highly restricted in the range of $m_\phi \gtrsim$ a few ten GeV or $|\sin\theta| \gtrsim 10^{-3}$, but the resonant annihilation region is severely constrained by the provisional direct dark matter detection in the near future, as discussed in section 4.3.

Third, allowed regions on $(m_\chi, |c_s|)$- and $(m_\phi, |c_s|)$-planes are, overall, shrunk compared to those in figure 9. Those lower limits on m_ϕ and m_χ come from the $\Delta N_{\rm eff}$ measurement, while the lower limit on $|c_s|$ is from the relic abundance condition. The small void region at $0.3\,{\rm GeV} \lesssim m_\chi \lesssim 1\,{\rm GeV}$ ($0.3\,{\rm GeV} \lesssim m_\phi \lesssim 1\,{\rm GeV}$) and $|c_s| \gtrsim 0.1$ is due to the constraint from the SHiP experiment with the relic abundance condition being satisfied by the $\chi\chi \to \phi\phi$ annihilation at the threshold $m_\phi \sim m_\chi$. The other void region at $30\,{\rm MeV} \lesssim m_\chi \lesssim 80\,{\rm MeV}$ ($30\,{\rm MeV} \lesssim m_\phi \lesssim 80\,{\rm MeV}$) and $|c_s| \gtrsim 0.1$ is from the direct dark matter detection.

Moreover, the allowed region on the $(\mu_3, |c_s|)$-plane remains similar as that of the present status in figure 9, except the resonant annihilation region at $|c_s| \sim 10^{-2}$ is shrinking.

Last but not least, on the $(|\sin\theta|, |c_s|)$-plane, it is seen that the lower limit on the coupling constant $|c_s|$ is more or less the same as that in figure 9. It is again from the relic abundance condition as seen in the $(m_\phi, |c_s|)$- and $(m_\chi, |c_s|)$-planes. On the other hand, future meson decay experiments and direct dark matter detection make the parameter region of $|\sin\theta| \gtrsim 10^{-3}$ excluded. On the other hand, the shape of the contour at the region of $|\sin\theta| \lesssim 10^{-9}$ is mainly due to the uncertainty of the mediator decay width as seen in the $(m_\phi, |\sin\theta|)$-plan. Since the dark matter mass is almost fixed to be around $10\,{\rm GeV}$ as seen in the $(m_\chi, |\sin\theta|)$-plan, it requires a specific value of c_s to satisfy the relic abundance condition.

D Relaxing kinematic equilibrium condition

In the main text, we imposed the kinematic equilibrium condition at around the freeze-out temperature $T_D \sim T_f$ to figure out the conventional WIMP parameter region. However, it is also acceptable that the dark sector and the SM sector kinematically decoupled at higher temperature above the freeze-out, and then two sectors evolve independently [42].

Note that we adopt the condition $T_D = T_f$ to figure out a very conventional WIMP parameter region in our setup. On the other hand, the condition can be relaxed by requiring that the WIMP is in the equilibrium at some temperature of the universe before the freeze-out, because it still allows us to make a quantitative prediction on its abundance. In this section, we will discuss how the result of our analysis alters by relaxing the condition.

In order to understand how the kinematic equilibrium condition affects the parameter region, we relax the condition by requiring the decouple temperature T_D above the freeze-out temperature such as $T_D = 10T_f$ or $T_D = 100T_f$. Then, we show how the thermal DM parameter region is expanded in the $(m_\chi, |\sin\theta|)$- and $(|\sin\theta|, |c_s|)$-planes in figure 11.

The expansion of the parameter region can be understood as that the higher decoupling temperature T_D increases the light degree of freedom from heavier SM particles, which have
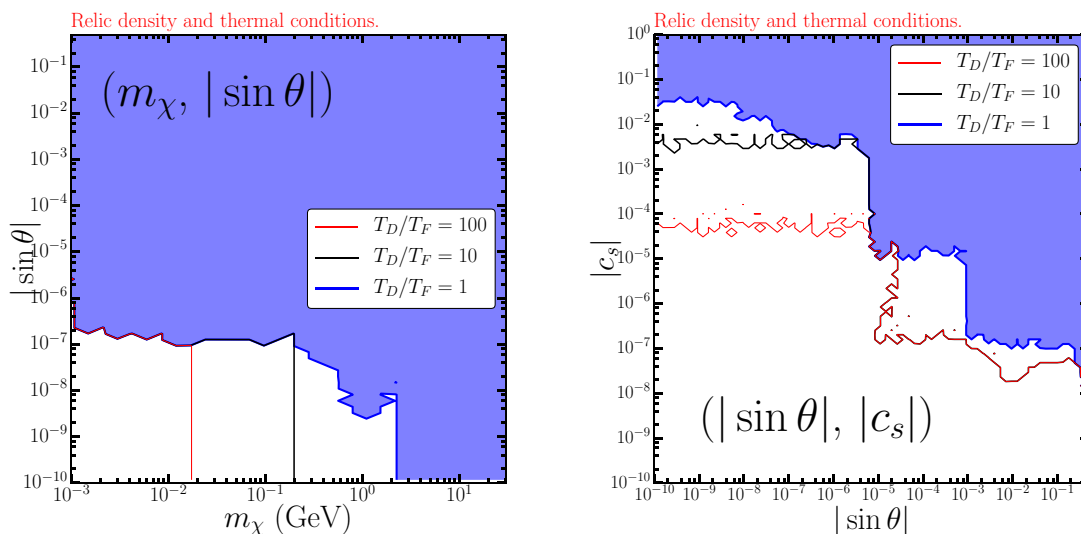
Figure 11. Model parameter regions survived after applying the relic abundance condition and the relaxed kinematical equilibrium condition. The black (red) line shows how the parameter regions extends when the kinematical equilibrium condition is relaxed to be $T_D/T_F = 10$ ($T_D/T_F = 100$) instead of $T_D/T_F = 10$. The blue shaded regions in both panels are the same as those in figure 8.

larger Yukawa couplings to help maintaining the kinematic equilibrium. From another point of view, because the freeze-out condition fixes the relation $T_f \simeq m_\chi/20$, relaxing the decoupling temperature T_D to higher temperature than T_f allows a lighter DM mass region still maintaining the same degree of freedom and keeping the thermal equilibrium.

In the $(m_\chi, |\sin\theta|)$-plane in figure 11, for the $T_D = T_f$ case, the vertical edge of $m_\chi \simeq 2\,\mathrm{GeV}$ is from the pion threshold, which shifts to $m_\chi \simeq 0.2\,\mathrm{GeV}$ and $\simeq 0.02\,\mathrm{GeV}$ for the $T_D = 10 T_f$ and $T_D = 100 T_f$ cases, respectively. We can clearly see how the parameter region is extended to the one with a smaller value of m_χ. The same behavior can be seen in the $(|\sin\theta|, |c_s|)$-plane in figure 11, where the parameter region extends to a smaller value of $|c_s|$ due to the correlation between m_χ and $|c_s|$ seen in the $(m_\chi, |c_s|)$-plane in figure 8.

It is worth pointing out that, once the kinematic equilibrium condition is relaxed, the temperature of the dark sector (both dark matter and mediator) during the freeze-out could be different from the temperature of the SM thermal bath. Since the result in figure 11 is obtained assuming both the temperatures are (almost) equal, above discussions are validated only in such a case.[28] On the other hand, when the temperatures are very different, the relic abundance condition as well as BBN and N_{eff} constraints have to be altered and the survived parameter space will be changed accordingly. A comprehensive study of early decoupled scenarios are indeed interesting but beyond the scope of our current study.

Open Access. This article is distributed under the terms of the Creative Commons Attribution License ([CC-BY 4.0](#)), which permits any use, distribution and reproduction in any medium, provided the original author(s) and source are credited.

---

[28]Such a case is realized when the mediator is relativistic in between the kinematical decoupling and the freeze-out, because the expansion histories of the two sectors are similar though they are independent.

References

[1] J.R. Ellis, K. Enqvist, D.V. Nanopoulos and F. Zwirner, *Observables in low-energy superstring models*, *Mod. Phys. Lett.* **A 1** (1986) 57 [INSPIRE].

[2] R. Barbieri and G.F. Giudice, *Upper bounds on supersymmetric particle masses*, *Nucl. Phys.* **B 306** (1988) 63 [INSPIRE].

[3] J. Bernstein, L.S. Brown and G. Feinberg, *The cosmological heavy neutrino problem revisited*, *Phys. Rev.* **D 32** (1985) 3261 [INSPIRE].

[4] M. Srednicki, R. Watkins and K.A. Olive, *Calculations of relic densities in the early universe*, *Nucl. Phys.* **B 310** (1988) 693 [INSPIRE].

[5] C. Boehm, T.A. Ensslin and J. Silk, *Can annihilating dark matter be lighter than a few GeVs?*, *J. Phys.* **G 30** (2004) 279 [astro-ph/0208458] [INSPIRE].

[6] C. Boehm, D. Hooper, J. Silk, M. Casse and J. Paul, *MeV dark matter: has it been detected?*, *Phys. Rev. Lett.* **92** (2004) 101301 [astro-ph/0309686] [INSPIRE].

[7] H. Murayama and J. Shu, *Topological dark matter*, *Phys. Lett.* **B 686** (2010) 162 [arXiv:0905.1720] [INSPIRE].

[8] T. Hambye and M.H.G. Tytgat, *Confined hidden vector dark matter*, *Phys. Lett.* **B 683** (2010) 39 [arXiv:0907.1007] [INSPIRE].

[9] K. Hamaguchi, E. Nakamura, S. Shirai and T.T. Yanagida, *Low-scale gauge mediation and composite messenger dark matter*, *JHEP* **04** (2010) 119 [arXiv:0912.1683] [INSPIRE].

[10] O. Antipin, M. Redi and A. Strumia, *Dynamical generation of the weak and dark matter scales from strong interactions*, *JHEP* **01** (2015) 157 [arXiv:1410.1817] [INSPIRE].

[11] O. Antipin, M. Redi, A. Strumia and E. Vigiani, *Accidental composite dark matter*, *JHEP* **07** (2015) 039 [arXiv:1503.08749] [INSPIRE].

[12] R. Huo, S. Matsumoto, Y.-L. Sming Tsai and T.T. Yanagida, *A scenario of heavy but visible baryonic dark matter*, *JHEP* **09** (2016) 162 [arXiv:1506.06929] [INSPIRE].

[13] S. Kanemura, S. Matsumoto, T. Nabeshima and N. Okada, *Can WIMP dark matter overcome the nightmare scenario?*, *Phys. Rev.* **D 82** (2010) 055026 [arXiv:1005.5651] [INSPIRE].

[14] L. Lopez-Honorez, T. Schwetz and J. Zupan, *Higgs portal, fermionic dark matter and a Standard Model like Higgs at* 125 *GeV*, *Phys. Lett.* **B 716** (2012) 179 [arXiv:1203.2064] [INSPIRE].

[15] A. Djouadi, A. Falkowski, Y. Mambrini and J. Quevillon, *Direct detection of Higgs-portal dark matter at the LHC*, *Eur. Phys. J.* **C 73** (2013) 2455 [arXiv:1205.3169] [INSPIRE].

[16] K. Cheung, Y.-L.S. Tsai, P.-Y. Tseng, T.-C. Yuan and A. Zee, *Global study of the simplest scalar phantom dark matter model*, *JCAP* **10** (2012) 042 [arXiv:1207.4930] [INSPIRE].

[17] A. Falkowski, C. Gross and O. Lebedev, *A second Higgs from the Higgs portal*, *JHEP* **05** (2015) 057 [arXiv:1502.01361] [INSPIRE].

[18] V. Barger, M. McCaskey and G. Shaughnessy, *Complex scalar dark matter vis-à-vis CoGeNT, DAMA/LIBRA and XENON*100, *Phys. Rev.* **D 82** (2010) 035019 [arXiv:1005.3328] [INSPIRE].

[19] M. Gonderinger, H. Lim and M.J. Ramsey-Musolf, *Complex scalar singlet dark matter: vacuum stability and phenomenology*, *Phys. Rev.* **D 86** (2012) 043511 [arXiv:1202.1316] [inSPIRE].

[20] M. Vogelsberger, J. Zavala and A. Loeb, *Subhaloes in self-interacting galactic dark matter haloes*, *Mon. Not. Roy. Astron. Soc.* **423** (2012) 3740 [arXiv:1201.5892] [inSPIRE].

[21] M. Rocha et al., *Cosmological simulations with self-interacting dark matter I: constant density cores and substructure*, *Mon. Not. Roy. Astron. Soc.* **430** (2013) 81 [arXiv:1208.3025] [inSPIRE].

[22] A.H.G. Peter, M. Rocha, J.S. Bullock and M. Kaplinghat, *Cosmological simulations with self-interacting dark matter II: halo shapes vs. observations*, *Mon. Not. Roy. Astron. Soc.* **430** (2013) 105 [arXiv:1208.3026] [inSPIRE].

[23] M. Pospelov, A. Ritz and M.B. Voloshin, *Secluded WIMP dark matter*, *Phys. Lett.* **B 662** (2008) 53 [arXiv:0711.4866] [inSPIRE].

[24] M. Pospelov and A. Ritz, *Astrophysical signatures of secluded dark matter*, *Phys. Lett.* **B 671** (2009) 391 [arXiv:0810.1502] [inSPIRE].

[25] O. Bertolami and R. Rosenfeld, *The Higgs portal and an unified model for dark energy and dark matter*, *Int. J. Mod. Phys.* **A 23** (2008) 4817 [arXiv:0708.1784] [inSPIRE].

[26] S. Matsumoto et al., *Observing the coupling between dark matter and Higgs boson at the ILC*, in *International Linear Collider Workshop (LCWS10 and ILC10)*, Beijing, China, 26–30 March 2010 [arXiv:1006.5268] [inSPIRE].

[27] S. Kanemura, S. Matsumoto, T. Nabeshima and H. Taniguchi, *Testing Higgs portal dark matter via Z fusion at a linear collider*, *Phys. Lett.* **B 701** (2011) 591 [arXiv:1102.5147] [inSPIRE].

[28] A. Kamada, M. Yamada and T.T. Yanagida, *Self-interacting dark matter with a vector mediator: kinetic mixing with the* $U(1)_{(B-L)_3}$ *gauge boson*, *JHEP* **03** (2019) 021 [arXiv:1811.02567] [inSPIRE].

[29] A. Kamada, K. Kaneta, K. Yanagi and H.-B. Yu, *Self-interacting dark matter and muon* $g-2$ *in a gauged* $U(1)_{L_\mu-L_\tau}$ *model*, *JHEP* **06** (2018) 117 [arXiv:1805.00651] [inSPIRE].

[30] B. Patt and F. Wilczek, *Higgs-field portal into hidden sectors*, hep-ph/0605188 [inSPIRE].

[31] Y.G. Kim and K.Y. Lee, *The minimal model of fermionic dark matter*, *Phys. Rev.* **D 75** (2007) 115012 [hep-ph/0611069] [inSPIRE].

[32] A. Djouadi, O. Lebedev, Y. Mambrini and J. Quevillon, *Implications of LHC searches for Higgs-portal dark matter*, *Phys. Lett.* **B 709** (2012) 65 [arXiv:1112.3299] [inSPIRE].

[33] M. Pospelov and A. Ritz, *Higgs decays to dark matter: beyond the minimal model*, *Phys. Rev.* **D 84** (2011) 113001 [arXiv:1109.4872] [inSPIRE].

[34] S. Baek, P. Ko and W.-I. Park, *Search for the Higgs portal to a singlet fermionic dark matter at the LHC*, *JHEP* **02** (2012) 047 [arXiv:1112.1847] [inSPIRE].

[35] S. Esch, M. Klasen and C.E. Yaguna, *Detection prospects of singlet fermionic dark matter*, *Phys. Rev.* **D 88** (2013) 075017 [arXiv:1308.0951] [inSPIRE].

[36] K. Ghorbani, *Fermionic dark matter with pseudo-scalar Yukawa interaction*, *JCAP* **01** (2015) 015 [arXiv:1408.4929] [inSPIRE].

[37] A. Freitas, S. Westhoff and J. Zupan, *Integrating in the Higgs portal to fermion dark matter*, *JHEP* **09** (2015) 015 [`arXiv:1506.04149`] [INSPIRE].

[38] M. Dutra, C.A. de S. Pires and P.S. Rodrigues da Silva, *Majorana dark matter through a narrow Higgs portal*, *JHEP* **09** (2015) 147 [`arXiv:1504.07222`] [INSPIRE].

[39] K. Ghorbani and L. Khalkhali, *Mono-Higgs signature in a fermionic dark matter model*, *J. Phys.* **G 44** (2017) 105004 [`arXiv:1608.04559`] [INSPIRE].

[40] A. Beniwal, M. Lewicki, M. White and A.G. Williams, *Gravitational waves and electroweak baryogenesis in a global study of the extended scalar singlet model*, *JHEP* **02** (2019) 183 [`arXiv:1810.02380`] [INSPIRE].

[41] A. Kamada, M. Yamada, T.T. Yanagida and K. Yonekura, *SIMP from a strong* U(1) *gauge theory with a monopole condensation*, *Phys. Rev.* **D 94** (2016) 055035 [`arXiv:1606.01628`] [INSPIRE].

[42] J.A. Evans, S. Gori and J. Shelton, *Looking for the WIMP next door*, *JHEP* **02** (2018) 100 [`arXiv:1712.03974`] [INSPIRE].

[43] THE GAMBIT DARK MATTER WORKGROUP collaboration, *DarkBit: a GAMBIT module for computing dark matter observables and likelihoods*, *Eur. Phys. J.* **C 77** (2017) 831 [`arXiv:1705.07920`] [INSPIRE].

[44] GAMBIT collaboration, *Status of the scalar singlet dark matter model*, *Eur. Phys. J.* **C 77** (2017) 568 [`arXiv:1705.07931`] [INSPIRE].

[45] GAMBIT collaboration, *Global analyses of Higgs portal singlet dark matter models using GAMBIT*, *Eur. Phys. J.* **C 79** (2019) 38 [`arXiv:1808.10465`] [INSPIRE].

[46] GAMBIT collaboration, *Global fits of GUT-scale SUSY models with GAMBIT*, *Eur. Phys. J.* **C 77** (2017) 824 [`arXiv:1705.07935`] [INSPIRE].

[47] GAMBIT collaboration, *A global fit of the MSSM with GAMBIT*, *Eur. Phys. J.* **C 77** (2017) 879 [`arXiv:1705.07917`] [INSPIRE].

[48] P. Athron, J.M. Cornell, F. Kahlhoefer, J. McKay, P. Scott and S. Wild, *Impact of vacuum stability, perturbativity and XENON1T on global fits of Z_2 and Z_3 scalar singlet dark matter*, *Eur. Phys. J.* **C 78** (2018) 830 [`arXiv:1806.11281`] [INSPIRE].

[49] S. Banerjee, S. Matsumoto, K. Mukaida and Y.-L.S. Tsai, *WIMP dark matter in a well-tempered regime: a case study on singlet-doublets fermionic WIMP*, *JHEP* **11** (2016) 070 [`arXiv:1603.07387`] [INSPIRE].

[50] S. Matsumoto, S. Mukhopadhyay and Y.-L.S. Tsai, *Singlet Majorana fermion dark matter: a comprehensive analysis in effective field theory*, *JHEP* **10** (2014) 155 [`arXiv:1407.1859`] [INSPIRE].

[51] S. Matsumoto, S. Mukhopadhyay and Y.-L.S. Tsai, *Effective theory of WIMP dark matter supplemented by simplified models: singlet-like Majorana fermion case*, *Phys. Rev.* **D 94** (2016) 065034 [`arXiv:1604.02230`] [INSPIRE].

[52] G. Krnjaic, *Probing light thermal dark-matter with a Higgs portal mediator*, *Phys. Rev.* **D 94** (2016) 073009 [`arXiv:1512.04119`] [INSPIRE].

[53] H. Leutwyler and M.A. Shifman, *Goldstone bosons generate peculiar conformal anomalies*, *Phys. Lett.* **B 221** (1989) 384 [INSPIRE].

[54] A. Djouadi, J. Kalinowski and M. Spira, *HDECAY: a program for Higgs boson decays in the Standard Model and its supersymmetric extension*, [*Comput. Phys. Commun.* **108** (1998) 56](https://doi.org) [[hep-ph/9704448](https://arxiv.org/abs/hep-ph/9704448)] [INSPIRE].

[55] J.F. Gunion, H.E. Haber, G.L. Kane and S. Dawson, *The Higgs hunter's guide*, *Front. Phys.* **80** (2000) 1 [INSPIRE].

[56] J.F. Donoghue, J. Gasser and H. Leutwyler, *The decay of a light Higgs boson*, [*Nucl. Phys.* **B 343** (1990) 341](https://doi.org) [INSPIRE].

[57] M.W. Winkler, *Decay and detection of a light scalar boson mixing with the Higgs boson*, [*Phys. Rev.* **D 99** (2019) 015018](https://doi.org) [[arXiv:1809.01876](https://arxiv.org/abs/1809.01876)] [INSPIRE].

[58] J.D. Clarke, R. Foot and R.R. Volkas, *Phenomenology of a very light scalar* $(100\,\mathrm{MeV} < m_h < 10\,\mathrm{GeV})$ *mixing with the SM Higgs*, [*JHEP* **02** (2014) 123](https://doi.org) [[arXiv:1310.8042](https://arxiv.org/abs/1310.8042)] [INSPIRE].

[59] E. Duchovni, E. Gross and G. Mikenberg, *Motivation and technique for light Higgs boson search*, [*Phys. Rev.* **D 39** (1989) 365](https://doi.org) [INSPIRE].

[60] T.N. Truong and R.S. Willey, *Branching ratios for decays of light Higgs bosons*, [*Phys. Rev.* **D 40** (1989) 3635](https://doi.org) [INSPIRE].

[61] T.R. Slatyer, *Indirect dark matter signatures in the cosmic dark ages. I. Generalizing the bound on s-wave dark matter annihilation from Planck results*, [*Phys. Rev.* **D 93** (2016) 023527](https://doi.org) [[arXiv:1506.03811](https://arxiv.org/abs/1506.03811)] [INSPIRE].

[62] ATLAS and CMS collaborations, *Measurements of the Higgs boson production and decay rates and constraints on its couplings from a combined ATLAS and CMS analysis of the LHC pp collision data at* $\sqrt{s} = 7$ *and 8 TeV*, [*JHEP* **08** (2016) 045](https://doi.org) [[arXiv:1606.02266](https://arxiv.org/abs/1606.02266)] [INSPIRE].

[63] PLANCK collaboration, *Planck 2015 results VII. High frequency instrument data processing: time-ordered information and beams*, [*Astron. Astrophys.* **594** (2016) A7](https://doi.org) [[arXiv:1502.01586](https://arxiv.org/abs/1502.01586)] [INSPIRE].

[64] XENON collaboration, *Dark matter search results from a one ton-year exposure of XENON1T*, [*Phys. Rev. Lett.* **121** (2018) 111302](https://doi.org) [[arXiv:1805.12562](https://arxiv.org/abs/1805.12562)] [INSPIRE].

[65] CRESST collaboration, *First results on low-mass dark matter from the CRESST-III experiment*, in 15th *International Conference on Topics in Astroparticle and Underground Physics (TAUP 2017)*, Sudbury, ON, Canada, 24–28 July 2017 [[arXiv:1711.07692](https://arxiv.org/abs/1711.07692)] [INSPIRE].

[66] G. Gerbier et al., *NEWS: a new spherical gas detector for very low mass WIMP detection*, [arXiv:1401.7902](https://arxiv.org/abs/1401.7902) [INSPIRE].

[67] *NEWS-G collaboration webpage*, https://news-g.org/.

[68] PANDAX-II collaboration, *Dark matter results from first 98.7 days of data from the PandaX-II experiment*, [*Phys. Rev. Lett.* **117** (2016) 121303](https://doi.org) [[arXiv:1607.07400](https://arxiv.org/abs/1607.07400)] [INSPIRE].

[69] SUPERCDMS collaboration, *New results from the search for low-mass weakly interacting massive particles with the CDMS low ionization threshold experiment*, [*Phys. Rev. Lett.* **116** (2016) 071301](https://doi.org) [[arXiv:1509.02448](https://arxiv.org/abs/1509.02448)] [INSPIRE].

[70] SUPERCDMS collaboration, *Projected sensitivity of the SuperCDMS SNOLAB experiment*, [*Phys. Rev.* **D 95** (2017) 082002](https://doi.org) [[arXiv:1610.00006](https://arxiv.org/abs/1610.00006)] [INSPIRE].

[71] NEWS-G collaboration, *First results from the NEWS-G direct dark matter search experiment at the LSM*, *Astropart. Phys.* **97** (2018) 54 [`arXiv:1706.04934`] [ɪɴSPIRE].

[72] DARKSIDE collaboration, *Low-mass dark matter search with the DarkSide-50 experiment*, *Phys. Rev. Lett.* **121** (2018) 081307 [`arXiv:1802.06994`] [ɪɴSPIRE].

[73] LZ collaboration, *LUX-ZEPLIN (LZ) conceptual design report*, `arXiv:1509.02910` [ɪɴSPIRE].

[74] LUX, LZ collaboration, *The present and future of searching for dark matter with LUX and LZ*, `PoS(ICHEP2016)220` (2016) [`arXiv:1611.05525`] [ɪɴSPIRE].

[75] PLANCK collaboration, *Planck 2013 results. XVI. Cosmological parameters*, *Astron. Astrophys.* **571** (2014) A16 [`arXiv:1303.5076`] [ɪɴSPIRE].

[76] CMB-S4 collaboration, *CMB-S4 science book, first edition*, `arXiv:1610.02743` [ɪɴSPIRE].

[77] G. Bélanger, F. Boudjema and A. Pukhov, *MicrOMEGAs: a code for the calculation of dark matter properties in generic models of particle interaction*, in *The Dark Secrets of the Terascale: proceedings, TASI* 2011, Boulder, CO, U.S.A., 6 June–11 July 2011, World Scientific, Singapore (2013), pg. 739 [`arXiv:1402.0787`] [ɪɴSPIRE].

[78] M. Drees, F. Hajkarim and E.R. Schmitz, *The effects of QCD equation of state on the relic density of WIMP dark matter*, *JCAP* **06** (2015) 025 [`arXiv:1503.03513`] [ɪɴSPIRE].

[79] J. Hisano, S. Matsumoto and M.M. Nojiri, *Explosive dark matter annihilation*, *Phys. Rev. Lett.* **92** (2004) 031303 [`hep-ph/0307216`] [ɪɴSPIRE].

[80] J. Hisano, S. Matsumoto, M.M. Nojiri and O. Saito, *Non-perturbative effect on dark matter annihilation and γ ray signature from galactic center*, *Phys. Rev.* **D 71** (2005) 063528 [`hep-ph/0412403`] [ɪɴSPIRE].

[81] J. Hisano, S. Matsumoto, M. Nagai, O. Saito and M. Senami, *Non-perturbative effect on thermal relic abundance of dark matter*, *Phys. Lett.* **B 646** (2007) 34 [`hep-ph/0610249`] [ɪɴSPIRE].

[82] S. Tulin, H.-B. Yu and K.M. Zurek, *Resonant dark forces and small scale structure*, *Phys. Rev. Lett.* **110** (2013) 111301 [`arXiv:1210.0900`] [ɪɴSPIRE].

[83] S. Tulin, H.-B. Yu and K.M. Zurek, *Beyond collisionless dark matter: particle physics dynamics for dark matter halo structure*, *Phys. Rev.* **D 87** (2013) 115007 [`arXiv:1302.3898`] [ɪɴSPIRE].

[84] M. Kaplinghat, S. Tulin and H.-B. Yu, *Direct detection portals for self-interacting dark matter*, *Phys. Rev.* **D 89** (2014) 035009 [`arXiv:1310.7945`] [ɪɴSPIRE].

[85] K. Kainulainen, K. Tuominen and V. Vaskonen, *Self-interacting dark matter and cosmology of a light scalar mediator*, *Phys. Rev.* **D 93** (2016) 015016 [*Erratum ibid.* **D 95** (2017) 079901] [`arXiv:1507.04931`] [ɪɴSPIRE].

[86] F. Kahlhoefer, K. Schmidt-Hoberg and S. Wild, *Dark matter self-interactions from a general spin-0 mediator*, *JCAP* **08** (2017) 003 [`arXiv:1704.02149`] [ɪɴSPIRE].

[87] T. Binder, T. Bringmann, M. Gustafsson and A. Hryczuk, *Early kinetic decoupling of dark matter: when the standard way of calculating the thermal relic density fails*, *Phys. Rev.* **D 96** (2017) 115010 [`arXiv:1706.07433`] [ɪɴSPIRE].

[88] PANDAX-II collaboration, *Dark matter results from 54-ton-day exposure of PandaX-II experiment*, *Phys. Rev. Lett.* **119** (2017) 181302 [`arXiv:1708.06917`] [ɪɴSPIRE].

[89] Z. Liu, Y. Su, Y.-L. Sming Tsai, B. Yu and Q. Yuan, *A combined analysis of PandaX, LUX and XENON1T experiments within the framework of dark matter effective theory*, *JHEP* **11** (2017) 024 [arXiv:1708.04630] [INSPIRE].

[90] A.D. Dolgov, *Neutrinos in cosmology*, *Phys. Rept.* **370** (2002) 333 [hep-ph/0202122] [INSPIRE].

[91] M. Ibe, A. Kamada, S. Kobayashi and W. Nakano, *Composite asymmetric dark matter with a dark photon portal*, *JHEP* **11** (2018) 203 [arXiv:1805.06876] [INSPIRE].

[92] PLANCK collaboration, *Planck 2018 results. VI. Cosmological parameters*, arXiv:1807.06209 [INSPIRE].

[93] J. Berger, K. Jedamzik and D.G.E. Walker, *Cosmological constraints on decoupled dark photons and dark Higgs*, *JCAP* **11** (2016) 032 [arXiv:1605.07195] [INSPIRE].

[94] M. Hufnagel, K. Schmidt-Hoberg and S. Wild, *BBN constraints on MeV-scale dark sectors. Part II. Electromagnetic decays*, *JCAP* **11** (2018) 032 [arXiv:1808.09324] [INSPIRE].

[95] A. Fradette and M. Pospelov, *BBN for the LHC: constraints on lifetimes of the Higgs portal scalars*, *Phys. Rev.* **D 96** (2017) 075033 [arXiv:1706.01920] [INSPIRE].

[96] W. Hu and J. Silk, *Thermalization and spectral distortions of the cosmic background radiation*, *Phys. Rev.* **D 48** (1993) 485 [INSPIRE].

[97] E. Masso and R. Toldra, *New constraints on a light spinless particle coupled to photons*, *Phys. Rev.* **D 55** (1997) 7967 [hep-ph/9702275] [INSPIRE].

[98] KAMIOKANDE-II collaboration, *Observation of a neutrino burst from the supernova SN 1987A*, *Phys. Rev. Lett.* **58** (1987) 1490 [INSPIRE].

[99] J.H. Chang, R. Essig and S.D. McDermott, *Revisiting supernova 1987A constraints on dark photons*, *JHEP* **01** (2017) 107 [arXiv:1611.03864] [INSPIRE].

[100] J.H. Chang, R. Essig and S.D. McDermott, *Supernova 1987A constraints on sub-GeV dark sectors, millicharged particles, the QCD axion and an axion-like particle*, *JHEP* **09** (2018) 051 [arXiv:1803.00993] [INSPIRE].

[101] C. Mahoney, A.K. Leibovich and A.R. Zentner, *Updated constraints on self-interacting dark matter from supernova 1987A*, *Phys. Rev.* **D 96** (2017) 043018 [arXiv:1706.08871] [INSPIRE].

[102] T. Fischer, S. Chakraborty, M. Giannotti, A. Mirizzi, A. Payez and A. Ringwald, *Probing axions with the neutrino signal from the next galactic supernova*, *Phys. Rev.* **D 94** (2016) 085012 [arXiv:1605.08780] [INSPIRE].

[103] H. Tu and K.-W. Ng, *Supernovae and Weinberg's Higgs portal dark radiation and dark matter*, *JHEP* **07** (2017) 108 [arXiv:1706.08340] [INSPIRE].

[104] A. Sung, H. Tu and M.-R. Wu, *New constraint from supernova explosions on light particles beyond the Standard Model*, *Phys. Rev.* **D 99** (2019) 121305 [arXiv:1903.07923] [INSPIRE].

[105] D.H. Weinberg, J.S. Bullock, F. Governato, R. Kuzio de Naray and A.H.G. Peter, *Cold dark matter: controversies on small scales*, *Proc. Nat. Acad. Sci.* **112** (2015) 12249 [arXiv:1306.0913] [INSPIRE].

[106] S. Tulin and H.-B. Yu, *Dark matter self-interactions and small scale structure*, *Phys. Rept.* **730** (2018) 1 [arXiv:1705.02358] [INSPIRE].

[107] CLEO collaboration, *Search for very light CP-odd Higgs boson in radiative decays of* $\Upsilon(1S)$, *Phys. Rev. Lett.* **101** (2008) 151802 [arXiv:0807.1427] [INSPIRE].

[108] BABAR collaboration, *Search for di-muon decays of a low-mass Higgs boson in radiative decays of the* $\Upsilon(1S)$, *Phys. Rev.* **D 87** (2013) 031102 [*Erratum ibid.* **D 87** (2013) 059903] [arXiv:1210.0287] [INSPIRE].

[109] BABAR collaboration, *Search for a low-mass scalar Higgs boson decaying to a tau pair in single-photon decays of* $\Upsilon(1S)$, *Phys. Rev.* **D 88** (2013) 071102 [arXiv:1210.5669] [INSPIRE].

[110] BELLE collaboration, *Measurement of the differential branching fraction and forward-backword asymmetry for* $B \to K^{(*)}\ell^+\ell^-$, *Phys. Rev. Lett.* **103** (2009) 171801 [arXiv:0904.0770] [INSPIRE].

[111] BELLE collaboration, *Search for* $B \to h^{(*)}\nu\bar{\nu}$ *decays at Belle*, *Phys. Rev. Lett.* **99** (2007) 221802 [arXiv:0707.0138] [INSPIRE].

[112] LHCb collaboration, *Differential branching fraction and angular analysis of the* $B^+ \to K^+\mu^+\mu^-$ *decay*, *JHEP* **02** (2013) 105 [arXiv:1209.4284] [INSPIRE].

[113] LHCb collaboration, *Search for hidden-sector bosons in* $B^0 \to K^{*0}\mu^+\mu^-$ *decays*, *Phys. Rev. Lett.* **115** (2015) 161802 [arXiv:1508.04094] [INSPIRE].

[114] LHCb collaboration, *Search for long-lived scalar particles in* $B^+ \to K^+\chi(\mu^+\mu^-)$ *decays*, *Phys. Rev.* **D 95** (2017) 071101 [arXiv:1612.07818] [INSPIRE].

[115] T. Aushev et al., *Physics at super B factory*, arXiv:1002.5012 [INSPIRE].

[116] E. Manoni, *Studies of missing energy decays of B meson at Belle II*, presented at *EPS HEP 2017*, Venice, Italy, July 2017.

[117] BABAR collaboration, *Search for long-lived particles in* e^+e^- *collisions*, *Phys. Rev. Lett.* **114** (2015) 171801 [arXiv:1502.02580] [INSPIRE].

[118] BABAR collaboration, *Direct CP, lepton flavor and isospin asymmetries in the decays* $B \to K^{(*)}\ell^+\ell^-$, *Phys. Rev. Lett.* **102** (2009) 091803 [arXiv:0807.4119] [INSPIRE].

[119] BABAR collaboration, *Search for the rare decay* $B \to K\nu\bar{\nu}$, *Phys. Rev.* **D 82** (2010) 112002 [arXiv:1009.1529] [INSPIRE].

[120] BABAR collaboration, *Search for* $B \to K^{(*)}\nu\bar{\nu}$ *and invisible quarkonium decays*, *Phys. Rev.* **D 87** (2013) 112005 [arXiv:1303.7465] [INSPIRE].

[121] J. Albrecht, F. Bernlochner, M. Kenzie, S. Reichert, D. Straub and A. Tully, *Future prospects for exploring present day anomalies in flavour physics measurements with Belle II and LHCb*, arXiv:1709.10308 [INSPIRE].

[122] NA48/2 collaboration, *New measurement of the* $K^\pm \to \pi^\pm\mu^+\mu^-$ *decay*, *Phys. Lett.* **B 697** (2011) 107 [arXiv:1011.4817] [INSPIRE].

[123] KTEV collaboration, *Search for the decay* $K_L \to \pi^0\mu^+\mu^-$, *Phys. Rev. Lett.* **84** (2000) 5279 [hep-ex/0001006] [INSPIRE].

[124] KTEV collaboration, *Search for the rare decay* $K_L \to \pi^0 e^+e^-$, *Phys. Rev. Lett.* **93** (2004) 021805 [hep-ex/0309072] [INSPIRE].

[125] BNL-E949 collaboration, *Study of the decay* $K^+ \to \pi^+\nu\bar{\nu}$ *in the momentum region* $140 < P_\pi < 199\, MeV/c$, *Phys. Rev.* **D 79** (2009) 092004 [arXiv:0903.0030] [INSPIRE].

[126] S. Martellotti, *The NA62 experiment at CERN*, in *Proceedings*, 12th *Conference on the Intersections of Particle and Nuclear Physics (CIPANP* 2015*)*, Vail, CO, U.S.A., 19–24 May 2015 [arXiv:1510.00172] [INSPIRE].

[127] NA62 collaboration, *Results and perspectives from the NA*62 *experiment at CERN*, *Nuovo Cim.* **C 39** (2016) 322 [INSPIRE].

[128] CHARM collaboration, *Search for axion like particle production in* 400 *GeV proton-copper interactions*, *Phys. Lett.* **B 157** (1985) 458 [INSPIRE].

[129] F. Bezrukov and D. Gorbunov, *Light inflaton hunter's guide*, *JHEP* **05** (2010) 010 [arXiv:0912.0390] [INSPIRE].

[130] E391A collaboration, *Experimental study of the decay* $K_L^0 \to \pi^0 \nu \bar{\nu}$, *Phys. Rev.* **D 81** (2010) 072004 [arXiv:0911.4789] [INSPIRE].

[131] S. Alekhin et al., *A facility to search for hidden particles at the CERN SPS: the SHiP physics case*, *Rept. Prog. Phys.* **79** (2016) 124201 [arXiv:1504.04855] [INSPIRE].

[132] KOTO collaboration, *Present status of the search for the* $K_L^0 \to \pi^0 \nu \bar{\nu}$ *decay with the KOTO detector at J-PARC*, in *Proceedings, Meeting of the APS Division of Particles and Fields (DPF* 2017*)*, Fermilab, Batavia, IL, U.S.A., 31 July–4 August 2017 [arXiv:1710.01412] [INSPIRE].

[133] CMS collaboration, *Search for light bosons in decays of the* 125 *GeV Higgs boson in proton-proton collisions at* $\sqrt{s} = 8$ *TeV*, *JHEP* **10** (2017) 076 [arXiv:1701.02032] [INSPIRE].

[134] ATLAS collaboration, *Search for Higgs boson decays to beyond-the-Standard-Model light bosons in four-lepton events with the ATLAS detector at* $\sqrt{s} = 13$ *TeV*, *JHEP* **06** (2018) 166 [arXiv:1802.03388] [INSPIRE].

[135] J.D. Clarke, *Constraining portals with displaced Higgs decay searches at the LHC*, *JHEP* **10** (2015) 061 [arXiv:1505.00063] [INSPIRE].

[136] K. Cheung, J.S. Lee and P.-Y. Tseng, *Higgs precision analysis updates* 2014, *Phys. Rev.* **D 90** (2014) 095009 [arXiv:1407.8236] [INSPIRE].

[137] CMS collaboration, *Projected performance of an upgraded CMS detector at the LHC and HL-LHC: contribution to the Snowmass process*, in *Proceedings*, 2013 *Community Summer Study on the Future of U.S. Particle Physics: Snowmass on the Mississippi (CSS*2013*)*, Minneapolis, MN, U.S.A., 29 July–6 August 2013 [arXiv:1307.7135] [INSPIRE].

[138] P. Bechtle, S. Heinemeyer, O. Stål, T. Stefaniak and G. Weiglein, *Probing the Standard Model with Higgs signal rates from the Tevatron, the LHC and a future ILC*, *JHEP* **11** (2014) 039 [arXiv:1403.1582] [INSPIRE].

[139] L3 collaboration, *Search for neutral Higgs boson production through the process* $e^+ e^- \to Z^* H^0$, *Phys. Lett.* **B 385** (1996) 454 [INSPIRE].

[140] PARTICLE DATA GROUP collaboration, *Review of particle physics*, *Chin. Phys.* **C 38** (2014) 090001 [INSPIRE].

[141] M.J. Dolan, F. Kahlhoefer, C. McCabe and K. Schmidt-Hoberg, *A taste of dark matter: flavour constraints on pseudoscalar mediators*, *JHEP* **03** (2015) 171 [*Erratum ibid.* **07** (2015) 103] [arXiv:1412.5174] [INSPIRE].

[142] A. Ali, E. Lunghi, C. Greub and G. Hiller, *Improved model independent analysis of semileptonic and radiative rare B decays*, *Phys. Rev.* **D 66** (2002) 034002 [hep-ph/0112300] [INSPIRE].

[143] W.J. Marciano and Z. Parsa, *Rare kaon decays with "missing energy"*, *Phys. Rev.* **D 53** (1996) R1 [INSPIRE].

[144] ATLAS collaboration, *Search for long-lived neutral particles decaying into lepton jets in proton-proton collisions at $\sqrt{s} = 8$ TeV with the ATLAS detector*, *JHEP* **11** (2014) 088 [arXiv:1409.0746] [INSPIRE].

[145] ALEPH collaboration, *Search for a nonminimal Higgs boson produced in the reaction $e^+e^- \to hZ^*$*, *Phys. Lett.* **B 313** (1993) 312 [INSPIRE].

[146] OPAL collaboration, *Decay mode independent searches for new scalar bosons with the OPAL detector at LEP*, *Eur. Phys. J.* **C 27** (2003) 311 [hep-ex/0206022] [INSPIRE].

[147] CMS collaboration, *Measurements of inclusive and differential Z boson production cross sections in pp collisions at $\sqrt{s} = 13$ TeV*, CMS-PAS-SMP-15-011, CERN, Geneva, Switzerland (2015).

[148] D. Foreman-Mackey, D.W. Hogg, D. Lang and J. Goodman, *emcee: the MCMC hammer*, *Publ. Astron. Soc. Pac.* **125** (2013) 306 [arXiv:1202.3665] [INSPIRE].

[149] F. Feroz, M.P. Hobson and M. Bridges, *MultiNest: an efficient and robust Bayesian inference tool for cosmology and particle physics*, *Mon. Not. Roy. Astron. Soc.* **398** (2009) 1601 [arXiv:0809.3437] [INSPIRE].

[150] K. Fujii et al., *Physics case for the 250 GeV stage of the International Linear Collider*, arXiv:1710.07621 [INSPIRE].

[151] M. Ahmad et al., *CEPC-SPPC preliminary conceptual design report. 1. Physics and detector*, IHEP-CEPC-DR-2015-01, (2015) [IHEP-TH-2015-01] [IHEP-EP-2015-01] [INSPIRE].

[152] D. d'Enterria, *Physics case of FCC-ee*, *Frascati Phys. Ser.* **61** (2016) 17 [arXiv:1601.06640] [INSPIRE].

[153] C. Boehm, M.J. Dolan and C. McCabe, *A lower bound on the mass of cold thermal dark matter from Planck*, *JCAP* **08** (2013) 041 [arXiv:1303.6270] [INSPIRE].

[154] P. Gondolo, J. Hisano and K. Kadota, *The effect of quark interactions on dark matter kinetic decoupling and the mass of the smallest dark halos*, *Phys. Rev.* **D 86** (2012) 083523 [arXiv:1205.1914] [INSPIRE].

[155] T. Binder, L. Covi, A. Kamada, H. Murayama, T. Takahashi and N. Yoshida, *Matter power spectrum in hidden neutrino interacting dark matter models: a closer look at the collision term*, *JCAP* **11** (2016) 043 [arXiv:1602.07624] [INSPIRE].

[156] P. Gondolo and G. Gelmini, *Cosmic abundances of stable particles: improved analysis*, *Nucl. Phys.* **B 360** (1991) 145 [INSPIRE].

[157] T. Bhattacharya et al., *QCD phase transition with chiral quarks and physical quark masses*, *Phys. Rev. Lett.* **113** (2014) 082001 [arXiv:1402.5175] [INSPIRE].